

Theory of Anomalous Floquet Higher-Order Topology: Classification, Characterization, and Bulk-Boundary Correspondence

Rui-Xing Zhang^{1,2,*} and Zhi-Cheng Yang^{2,3}

¹*Condensed Matter Theory Center, Department of Physics,
University of Maryland, College Park, Maryland 20742-4111, USA*

²*Joint Quantum Institute, University of Maryland, College Park, MD 20742, USA*

³*Joint Center for Quantum Information and Computer Science,
University of Maryland, College Park, MD 20742, USA*

(Dated: January 20, 2022)

Periodically-driven or Floquet systems can realize anomalous topological phenomena that do not exist in any equilibrium states of matter, whose classification and characterization require new theoretical ideas that are beyond the well-established paradigm of static topological phases. In this work, we provide a general framework to understand anomalous Floquet higher-order topological insulators (AFHOTIs), the classification of which has remained a challenging open question. In two dimensions (2D), such AFHOTIs are defined by their robust, symmetry-protected corner modes pinned at special quasienergies, even though all their Floquet bands feature trivial band topology. The corner-mode physics of an AFHOTI is found to be generically indicated by 3D Dirac/Weyl-like topological singularities living in the phase spectrum of the bulk time-evolution operator. Physically, such a phase-band singularity is essentially a “footprint” of the topological quantum criticality, which separates an AFHOTI from a trivial phase adiabatically connected to a static limit. Strikingly, these singularities feature unconventional dispersion relations that cannot be achieved on any static lattice in 3D, which, nevertheless, resemble the surface physics of 4D topological crystalline insulators. We establish the above higher-order bulk-boundary correspondence through a dimensional reduction technique, which also allows for a systematic classification of 2D AFHOTIs protected by point group symmetries. We demonstrate applications of our theory to two concrete, experimentally feasible models of AFHOTIs protected by C_2 and D_4 symmetries, respectively. Our work paves the way for a unified theory for classifying and characterizing Floquet topological matters.

CONTENTS

I. Introduction	2	C. Topological singularity protected by a single mirror symmetry: D_1 group	16
II. Preliminaries and summary of results	4	D. A list of possible topological charges for D_n	18
A. Basic notions	4	E. A case study: D_2 group	19
B. Anomalous Floquet higher-order topology	5	1. $D_{2,+,-}^+$	19
C. Phase-band singularities for 2D class AIII Floquet systems	5	2. $D_{2,-,-}^-$	20
D. Connection to 4D topological crystalline insulators	7	F. Classification of D_n -protected topological singularities	20
E. From phase-band singularities to higher-order topology	8	VI. Bulk-boundary correspondence & higher-order topological indices	21
III. Revisiting 1D anomalous Floquet topology	9	A. Classification of C_n -protected AFHOTIs	21
A. Winding number and phase-band singularity	10	1. Dimensional reduction	21
B. Model	11	2. Bulk-boundary correspondence & topological indices	23
IV. C_n -protected phase-band singularity	12	B. Classification of D_1 -protected AFHOTIs	24
V. D_n -protected phase-band singularity	14	1. Dimensional reduction	24
A. Constraining C_n topological charges with a mirror symmetry	14	2. Bulk-boundary correspondence & topological indices	25
B. Dynamical Dirac point and its doublet	15	C. D_2 -protected AFHOTIs	26
		1. $D_{2,+,\pm}^+$	26
		2. $D_{2,-,-}^-$	26
		D. Classifying general D_n -protected AFHOTIs	26
		1. Guidelines for classifying D_n -protected AFHOTIs	26
		2. Higher-order topological indices for D_n -protected AFHOTIs	27

* ruixing@umd.edu

3. Boundary geometry for observing all symmetry-protected corner modes	28
VII. Model realizations and experimental detections	29
A. C_2 -symmetric AFHOTI	29
B. D_4 -symmetric AFHOTI	29
C. Experimental realization and detection of phase-band singularities	30
VIII. Discussions	31
Acknowledgments	31
A. C_2 -protected 4D topological crystalline insulators	32
1. Minimal model and rotation Chern number	32
2. Surface state and C_2 -velocity locking	32
B. Topological charges of D_n single groups with $(C_n)^n = 1$	33
C. Angular momentum basis and mirror symmetry	33
D. Fragility of dynamical Weyl quadrupole in Ref. [1]	34
E. Phase diagram of the C_2 -symmetric model	34
F. Analytical details of D_4 -symmetric AFHOTI	35
1. Analytical expression of $U(\mathbf{k}, t)$	35
2. Condition for DDP	35
3. Effective Hamiltonian of D_4 -protected DDP	36
References	36

I. INTRODUCTION

The recognition of the role of topology in band theory has spawned a systematic classification and identification of topological band insulators that are distinct from atomic ones [2–10]. The nontrivial bulk band topology manifests itself as robust gapless states residing on lower-dimensional boundaries. Such bulk-boundary correspondence constitutes a hallmark of topological band theory, and plays an essential role in both experimental probe and theoretical characterization. Apart from internal symmetries (time reversal, particle-hole, and chiral symmetries), the ubiquitous crystalline symmetries in solids furnish a much richer set of topological crystalline insulators (TCIs) [11–17] that were previously overlooked in the tenfold-way topological classification. A well-known example is the three-dimensional (3D) mirror-protected TCI phase in bulk SnTe [18], whose topological Dirac

surface states have been experimentally observed using angle-resolved photoemission spectroscopy (ARPES) [19].

Remarkably, crystalline symmetries can sometimes support a novel *higher-order* bulk-boundary correspondence [20–42], which is generally not possible in any internal-symmetry-protected topological insulators. Namely, for some TCIs, the bulk topology enforces gapless modes to live on boundary manifolds with codimension $d > 1$, for example, 1D hinge modes on the surface of a bulk-3D system, and 0D corner modes on the edge of a bulk-2D system. Such TCIs are generally termed “higher-order topological insulators” (HOTIs). Researchers have introduced various symmetry-based indicators [43, 44] (i.e. functions of crystalline symmetry eigenvalues at high symmetry momenta) to achieve a simple and feasible topological diagnosis for HOTIs. So far, materialization of HOTI physics has been predicted in bismuth [45] (experimentally supported by scanning tunneling microscopy studies), EuIn_2As_2 [46], MoTe_2 [47], Cd_3As_2 [48], $\text{MnBi}_{2n}\text{Te}_{3n+1}$ [49], etc.

More recently, motivated by the experimental progress in synthetic photonic and cold atomic systems, such topological ideas have been extended beyond static electronic materials and apply to out-of-equilibrium systems as well, in particular, Floquet systems that are subject to time-periodic drives [50–61]. For instance, the quasienergy Floquet bands of a periodically driven system can carry their own topological indices, analogous to the energy bands in a static system. However, such topological theory of Floquet bands is incapable of capturing *anomalous* Floquet topological phenomena. Specifically, Ref. [62] first pointed out the possibility of a 2D anomalous Floquet topological insulator (AFTI) in class A, which hosts robust chiral edge modes even when all of its bulk Floquet bands carry trivial Chern numbers. In fact, the topological nature of such anomalous chiral edge mode configuration is encoded in the full time-evolution operator $U(\mathbf{k}, t)$ *within* one period T , instead of its Floquet band Hamiltonian. Following this seminal work, a complete classification of AFTIs from the ten Altland-Zirnbauer symmetry classes in all dimensions has been achieved [63, 64].

Following the breakthroughs of static HOTIs, it is natural to extend the concept of AFTIs to a higher-order version, i.e. anomalous Floquet higher-order topological insulators (AFHOTIs) [1, 65–70]. In 2D, such an AFHOTI, by definition, features robust 0D modes bound to the system’s geometric corners, which are further energetically pinned at both quasienergies 0 and π/T ¹. However, theoretical proposals for AFHOTIs have so far been restricted to case-by-case studies, and the corresponding topological indices are also designed in a model-specific manner with limited generality. Moreover, the majority of AFHOTI proposals are in fact *not* bulk higher-order topological in the conventional sense. Namely, the corner modes of such a Floquet system can be symmetrically eliminated via closing the boundary quasienergy

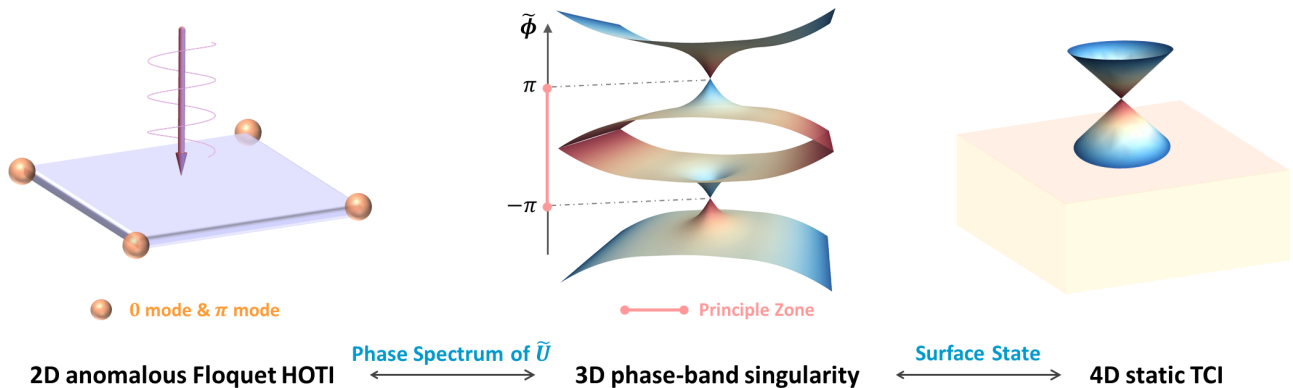


FIG. 1. A 2D AFHOTI features Floquet corner modes at both quasienergies 0 and π . It is characterized by the emergence of topological singularity on the principle zone boundary of the 3D phase band $\tilde{\phi}(\mathbf{k}, t)$, i.e. the eigenspectrum of the periodized return map $\tilde{U}(\mathbf{k}, t)$. Such a phase-band singularity is further linked to the gapless surface state of a 4D static topological crystalline insulator.

gap, instead of a bulk one. Following the convention in static HOTIs, one can call such Floquet systems *extrinsic* AFHOTIs, in sharp contrast to the *intrinsic* AFHOTIs which do feature a higher-order bulk-boundary correspondence. A typical example of an extrinsic AFHOTI is shown in Ref. [1], which introduced a 2D quantum walk model as a Floquet version of a quadrupole insulator [20, 21]. Despite the phenomenological resemblance to an intrinsic AFHOTI, however, the crystalline symmetries (i.e. D_2 symmetry) in their model are insufficient to protect corner modes against generic adiabatic, D_2 -preserving perturbations. Despite being inherently different, the crucial distinctions between extrinsic and intrinsic AFHOTIs have not been explored in depth in the literature. Specifically, lacking a general theory, the intrinsic AFHOTIs have so far remained far less well-understood than both their first-order cousins (i.e. AF-TIs) and their static analogs (i.e. HOTIs). How to systematically characterize and classify higher-order anomalous Floquet topological phases remains an intriguing, crucial, and challenging open question in the fields of both topological phases and non-equilibrium dynamics.

In this work, we fill in this gap by providing a theoretical framework that allows for a systematic classification and characterization of general AFHOTIs. Unless otherwise stated, the AFHOTIs considered in this work always refer to the intrinsic ones. As a demonstration, in this work we focus on 2D AFHOTIs protected by both point group symmetries and chiral symmetry. The presence of chiral symmetry is necessary for all 2D AFHOTIs and is responsible for pinning their topological corner modes at quasienergies 0 and π/T . A key stepping stone in our

theoretical framework is the deep connection between 2D anomalous Floquet higher-order topology and irremovable topological singularities in the 3D phase bands of the time-evolution operator. Such topological singularities live in the 3D (\mathbf{k}, t) parameter space and generally take the form of stable 3D Weyl or Dirac points across the principal zone boundary of the phase band. It is the very existence of such phase-band singularities that prohibits the AFHOTIs from being adiabatically deformed to any static system, making our AFHOTIs intrinsically dynamical phases of matter. Strikingly, all of the robust phase-band singularities exhibit unconventional dispersion relations that *cannot* be achieved in a 3D static lattice. Rather, such exotic 3D singularities resemble the boundary physics of static TCIs in 4D.

Specifically, our classification scheme for 2D AFHOTIs consists of two steps: (i) a classification of symmetry-protected topological phase-band singularities; (ii) a mapping from bulk phase-band singularities to boundary topological modes. For the first step, we start by exploring phase-band singularities protected by n -fold rotation groups C_n . We find that a stable C_n -protected singularity generically takes the form of a “dynamical Weyl pair” (DWP), which is a pair of chiral-related Weyl points with a vanishing net monopole charge. We prove that such a single DWP is stable *iff* C_n anticommutes with chiral symmetry. This further allows us to define a set of C_n *topological charges* that fully classify all stable DWPs for a given Floquet system with C_n symmetry.

We then move on to classify the phase-band singularities protected by a dihedral group D_n , which is generated by a C_n rotation and a mirror reflection M_x . The mirror symmetry in the D_n group not only constrains the C_n topological charges, but is also capable of protecting new type of singularities on their own. We identify a set of *mirror topological charges* to fully characterize mirror-protected singularities, which are well-defined only if mirror and chiral symmetries commute with one another.

¹ The AFHOTIs should also be distinguished from conventional Floquet HOTIs [71–74], where the corner modes only show up at *either* 0 *or* π/T . Such corner modes can be diagnosed from the topological indices of the bulk Floquet bands.

Combining the rotation and mirror topological charges, we obtain a complete classification of phase-band singularities for general class AIII D_n -symmetric Floquet systems in 2D. In particular, we emphasize that the D_2 -symmetric Floquet quadrupole insulator model proposed in Ref. [1] is *singularity-free* (see Appendix D) and carries *none* of the above crystalline topological charges, consistent with its extrinsic topological nature.

However, phase-band singularities *do not* necessarily imply higher-order topology. Therefore, the second part of our results aims to establish the higher-order bulk boundary correspondence, i.e. the mapping between bulk singularities and Floquet corner modes. This is achieved by introducing a new theoretical technique dubbed “phase-band dimensional reduction” (PBDR). Physically, PBDR maps a 2D Floquet system with phase-band singularities to a set of lower-dimensional building blocks, in this case, 1D class AIII AFTIs [75, 76] with end modes. If the end modes of the resulting 1D AFTIs are both symmetry protected and topology enforced, they will correspond to robust corner modes in the original 2D Floquet system before the PBDR mapping. In this way, we succeed in establishing the higher-order bulk-boundary correspondence and defining the associated higher-order topological indices, which thus completes our classification for 2D AFHOTIs with point group symmetries. In particular, we find that C_n -protected AFHOTIs generally admit a \mathbb{Z}_2 classification, while those protected by D_n groups can admit a \mathbb{Z} or $\mathbb{Z} \times 2\mathbb{Z}$ classification, depending on their specific symmetry properties.

The rest of the paper is organized as follows. Sec. II is a summary of our main results in this paper, which also contains a brief review of basic notions that are important to our theory. In Sec. III, we revisit the theory of 1D AFTIs in class AIII and demonstrate how the anomalous Floquet topology in these 1D systems is encoded in their phase-band singularities. Sec. IV and V classify C_n and D_n -protected phase-band singularities in 2D class AIII Floquet systems, respectively. We introduce the PBDR technique in Sec. VI, where we also establish the higher-order bulk-boundary correspondence for each symmetry class, and conclude the classifications for 2D AFHOTIs with point group symmetries. As demonstrations, we apply our topological diagnostic to two concrete AFHOTI models in Sec. VII: one with C_2 symmetry and the other with D_4 symmetry. Finally, we close with discussions for future directions in Sec. VIII.

II. PRELIMINARIES AND SUMMARY OF RESULTS

In this section, we start with some basic notions for general Floquet systems and further introduce the concept of phase-band topological singularities as an indicator of anomalous Floquet topological phenomena. We then define the concept of AFHOTIs in 2D and further specify the crucial role of both spectral and crystalline

symmetries in protecting those exotic phases. Our key result in this work, the topological classification of 2D AFHOTIs with point group symmetries, is summarized in the last part.

A. Basic notions

The quantum dynamics of a time-periodic Bloch Hamiltonian $H(\mathbf{k}, t) = H(\mathbf{k}, t + T)$ is described by its time-evolution operator

$$U(\mathbf{k}, t) = \mathcal{T} e^{-i \int_0^t H(\mathbf{k}, t') dt'}, \quad (1)$$

where \mathcal{T} denotes time ordering. At stroboscopic times, the Floquet operator $U(\mathbf{k}, T)$ defines the Floquet Hamiltonian via

$$H_F^{(\varepsilon)}(\mathbf{k}) \equiv \frac{i}{T} \log_\varepsilon U(\mathbf{k}, T), \quad (2)$$

whose eigenvalues $\{\epsilon_n(\mathbf{k})\}$ define the quasienergy or Floquet bands. Here ε labels the branch cut of the logarithmic function, with

$$\log_\varepsilon(e^{i\alpha}) = i\alpha, \text{ for } \varepsilon - 2\pi < \alpha < \varepsilon. \quad (3)$$

For our purpose, we take $\varepsilon = \pi$ throughout our discussion and hence the superscript in $H_F^{(\varepsilon)}(\mathbf{k})$ will be omitted for simplicity. It is easy to see that $\{\epsilon_n(\mathbf{k})\}$, the quasienergy spectrum of H_F , is periodic in units of $2\pi/T$, leading to a series of Floquet Brillouin zones. Therefore, we can restrict the quasienergies of H_F within the principle zone $(-\frac{\pi}{T}, \frac{\pi}{T}]$. Below we will drop the factor of $1/T$ in the quasienergies. Similarly to conventional electronic bands in static systems, a Floquet band can carry its own topological index. For example, a monolayer graphene can be turned into a Floquet Chern insulator in the presence of circularly polarized light [57], which features both a nonzero Chern number in its bulk Floquet bands and a chiral edge mode in the quasienergy spectrum of a finite system with open boundary.

An anomalous Floquet topological system, however, features exotic boundary topological phenomena in its quasienergy spectrum, despite the triviality of all its Floquet bands. A known example is the 2D anomalous Floquet topological insulator (AFTI) in class A with chiral edge modes on the boundary, while each of its Floquet bands carries a vanishing Chern number [62]. Such an anomalous Floquet topological phase, by definition, has no static analogs. Hence, its topological information is, in principle, encoded in the full time evolution process (e.g. $U(\mathbf{k}, t)$ for $t \in (0, T]$), but not in a single Floquet operator $U(\mathbf{k}, T)$.

To understand the general anomalous Floquet topological physics, it is instructive to consider the eigenvalue spectrum of $U(\mathbf{k}, t)$:

$$U(\mathbf{k}, t) |\phi_n(\mathbf{k}, t)\rangle = e^{-i\phi_n(\mathbf{k}, t)} |\phi_n(\mathbf{k}, t)\rangle, \quad (4)$$

where $|\phi_n(\mathbf{k}, t)\rangle$ denotes an eigenstate of the evolution operator, and $\{\phi_n(\mathbf{k}, t)\}$ are known as the “phase bands” in (\mathbf{k}, t) space [77]. When $t = T$, the phase band $\phi_n(\mathbf{k}, T)$ is exactly the Floquet band $\epsilon_n(\mathbf{k})$ (i.e. eigenvalues of H_F) up to a factor of T . Similarly to the Floquet bands, $\{\phi_n(\mathbf{k}, t)\}$ are well-defined modulo 2π , and can thus be restricted within the principal zone $(-\pi, \pi]$. Usually, it is convenient to define the return map (or the “micromotion” operator)

$$\tilde{U}(\mathbf{k}, t) \equiv U(\mathbf{k}, t)e^{iH_F(\mathbf{k})t}, \quad (5)$$

which is periodic in time

$$\tilde{U}(\mathbf{k}, t) = \tilde{U}(\mathbf{k}, t + T), \quad (6)$$

and contains the same information as $U(\mathbf{k}, t)$ [62]. The phase band $\{\tilde{\phi}_n(\mathbf{k}, t)\}$ for \tilde{U} can be defined similarly.

In particular, a *phase-band singularity* occurs when (i) the phase band manifold $\phi_n(\mathbf{k}, \mathbf{t})$ or $\tilde{\phi}_n(\mathbf{k}, t)$ is gapless across its principal zone boundary (e.g. $\phi_n = \pm\pi$); (ii) the gaplessness has a topological origin and is irremovable without closing the bulk Floquet gap. We emphasize that the phase-band singularities generally serve as an indicator of general anomalous Floquet topological phenomena, including both AFTIs and AFHOTIs, which can manifest itself as point nodes, line nodes, etc. For example, the anomalous chiral edge modes of a 2D class A AFTI are determined by the net monopole charge of Weyl nodes in the phase band [77]. As we will show later, the concept of phase-band singularity also plays a crucial role in our theory of AFHOTIs.

B. Anomalous Floquet higher-order topology

We define a 2D Floquet system as a symmetry-protected AFHOTI if the following conditions are satisfied:

- (i) its bulk Floquet spectrum is gapped around quasienergies 0 and π ;
- (ii) the bulk Floquet bands are topologically trivial;
- (iii) it has no 1D anomalous (e.g. chiral or helical) edge modes penetrating the bulk Floquet gaps;
- (iv) it hosts robust 0D localized modes at quasienergies 0 and π ;
- (v) both 0 and π modes are protected symmetrically and topologically, which cannot be eliminated without breaking the symmetry or closing the bulk Floquet gap at 0 and π .

Let us make a few remarks on the above definition. First of all, a spectral symmetry (e.g. chiral symmetry S) is required for pinning the 0D modes at the special quasienergies, without which the 0D modes can move

freely in energy and merge with the bulk Floquet bands. We note that for some static obstructed atomic insulators with no chiral symmetry, one can still measure the fractional electron charge accumulated around each sample corner as a signature of the corner-mode physics [36, 37], even when the corner localized eigenstates are shifted away from zero energy. However, such a fractional corner charge relies on a good definition of electron filling, which is somewhat tricky in periodically driven systems. In this case, only corner modes that are energetically pinned by chiral symmetry will be considered as higher-order topological in our theory.

Secondly, the higher-order bulk-boundary correspondence of an AFHOTI is *only* possible with the protection of certain spatial or space-time crystalline symmetry G . The symmetry protection guarantees the robustness of 0D modes against any adiabatic perturbations that respect G , i.e., smooth deformations to $U(\mathbf{k}, t)$ that keep the bulk quasienergy gap open at 0 and π . In contrast, without G , one can always attach additional 1D Floquet topological states with 0 and π end modes to the system’s boundary, which can hybridize with the original 0D modes and shift them away from quasienergies 0 and π . The robustness against any symmetry-allowed perturbation is an important factor that distinguishes our definition of (intrinsic) AFHOTIs from the aforementioned extrinsic ones.

In addition, the triviality of bulk Floquet bands guarantees that the number of robust zero modes equals to that of the π modes. In reality, both the zero and π modes will simultaneously appear around certain geometric corners of a system with open boundary. Therefore, while we only mention explicitly one set of corner modes hereafter, the readers should always have in mind that there are two copies of such corner modes in the system at quasienergies 0 and π , respectively.

Lastly, we note that an AFHOTI, by definition, cannot be diagnosed by any known topological index that is defined for static systems. This motivates us to establish a new theoretical framework for describing general AFHOTI phenomena, which is briefly summarized in the following subsections.

C. Phase-band singularities for 2D class AIII Floquet systems

In this work, we focus on the topological classification and characterization of 2D AFHOTIs protected by both chiral symmetry S and 2D point group symmetries. Namely, we will take the crystalline group G as either a rotation group C_n or a dihedral group D_n , for $n \in \{1, 2, 3, 4, 6\}$. Similar to 2D AFTIs, the topological nature of a 2D AFHOTI is generally encoded in certain types of singularities in the 3D phase-band manifold. This yields a simple and intuitive interpretation: the singularities are essentially a “footprint” of the topological quantum criticality that separates an AFHOTI from

a trivial phase connected to a static limit.

To see this, let us first assume that an AFHOTI hosts a singularity in its phase bands $\phi(\mathbf{k}, t)$, as shown in Fig. 2. It is easy to see that by gradually increasing the driving frequency ω of this AFHOTI, we are effectively pushing the singularity away from $t = 0$ along the time axis. In particular, at some critical frequency ω_c the singularity exactly sits at $t = T$ and closes the Floquet gap at quasienergy π . When $\omega > \omega_c$, the system remains singularity-free until it reaches the static limit with $\omega \rightarrow \infty$. In this case, all phases with $\omega > \omega_c$ (or $\omega > \omega_c$) are topologically and dynamically equivalent, since they are all connected to one another along the frequency path with no π -gap closing. As a result, the phase-band singularity at $\omega = \omega_c$ manifests itself as a topological phase transition between the AFHOTI and the static limit. Therefore, an AFHOTI, being statically impossible, must host phase-band singularities as an obstruction to the static limit. In other words,

- classifying the phase-band singularity is equivalent to classifying the quantum criticality that separates our target system from a static limit.

It should be emphasized that the presence of singularities is a *necessary yet insufficient* condition for AFHOTIs. In other words, not all π -gap-closing quantum criticalities indicate a transition from the static limit to an AFHOTI. Below, we will start from a systematic classification for phase-band singularities in general 2D class AIII Floquet systems with point-group symmetries, and leave discussions on their topological implications to Sec. II E.

First of all, the phase-band singularities for 2D class AIII Floquet systems generically manifest themselves as collections of 3D Weyl nodes,² whose locations and monopole charges are compatible with the crystalline symmetry group $G = C_n$ or D_n as well as the chiral symmetry \mathcal{S} . In general, such a Weyl node can appear anywhere within the phase band Brillouin zone. However, for anomalous Floquet topology, we only need to focus on Weyl nodes across the *principal zone boundary* at $\tilde{\phi} = \pm\pi$, which completely determine the boundary modes at quasienergy π and cannot be removed without closing the Floquet gap at π [77]. That all Floquet bands are topologically trivial requires the same number of boundary modes at quasienergy zero. Generically, the effective Hamiltonian of a 3D phase-band Weyl node can be written as:

$$h_w \equiv i \log \tilde{U}(\mathbf{k}, t) \approx \pi \mathbb{1}_2 + v_x k_x \sigma_x - v_y k_y \sigma_y + v_t t \sigma_z, \quad (7)$$

where $\sigma_{x,y,z}$ are Pauli matrices, and the constant $\pi \mathbb{1}_2$ indicates that the Weyl node resides at the principal zone boundary.

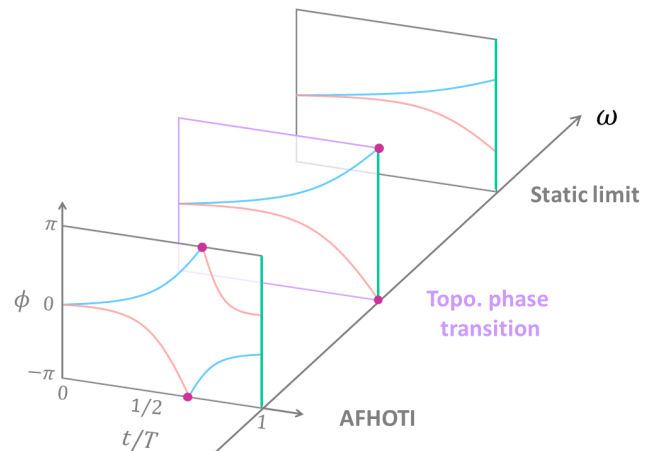


FIG. 2. By gradually increasing the driving frequency ω , an AFHOTI with phase-band singularity (the red dots) undergoes a topological phase transition with π -gap closing in the quasienergy spectrum, before turning into a static, singularity-free system. Note that the Floquet bands are the intersections between the phase band $\phi(\mathbf{k}, t)$ and the green line at $t = T$. Therefore, at the topological transition point, the gapless Floquet bands around the π -gap is exactly the phase-band singularity in the original AFHOTI.

To gain some intuitions of the symmetry constraints imposed on the phase-band Weyl node, we first note that chiral symmetry \mathcal{S} acts as a *unitary time-reflection symmetry* on the return map:

$$\mathcal{S} \tilde{U}(\mathbf{k}, t) \mathcal{S}^{-1} = \tilde{U}(\mathbf{k}, T - t), \quad (8)$$

Thus, starting with a Weyl node carrying a Weyl charge q at (\mathbf{k}, t) , \mathcal{S} will map it to another Weyl node with charge $-q$ at $(\mathbf{k}, T - t)$. As a result, the phase-band Weyl nodes always come in chiral-related pairs, which guarantees a vanishing net Weyl charge and thus the absence of chiral edge modes. We dub such a chiral-related Weyl pair a *dynamical Weyl pair* (DWP).

Naively, without any additional symmetry being imposed, such a pair of Weyl nodes can annihilate one another when brought together and hence is unstable. Nevertheless, when there is an additional n -fold rotation symmetry C_n anticommuting with \mathcal{S} , a novel mechanism can be activated to prevent pair annihilation of certain DWPs on the rotation-invariant axes. Specifically, an on-axis Weyl node can be effectively viewed as a pair of counter-propagating 1D modes dispersing along t -direction. Then the right-moving and left-moving modes must transform as irreducible representations under C_n ,

such nodal loops are either contractible, in which case they can be shrunk to a point; or noncontractible (going around the entire Brillouin zone), which are generically unstable when translation symmetry is absent. Therefore, in this work, it suffices to consider point-like singularities (i.e. Weyl/Dirac nodes in 3D). An example of a contractible nodal loop is also considered in Sec. V.

² In general, nodal loop singularities are also possible. However,

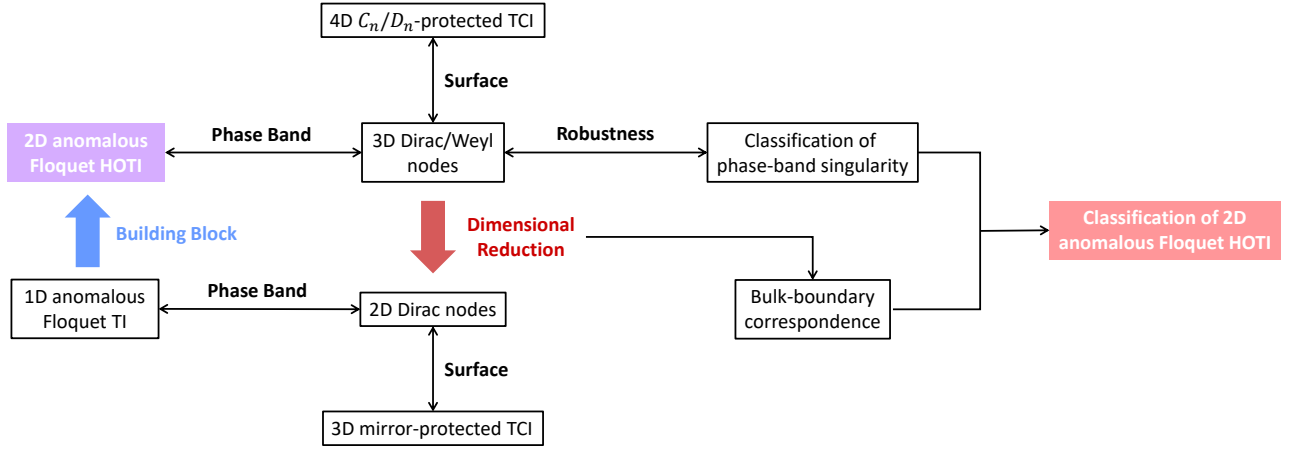


FIG. 3. Logic flow of our classification scheme for 2D anomalous Floquet higher-order topology.

which can thus be labeled by the z -component angular momentum $j_z = J$ and $j_z = J + 1$, respectively. We note that bands with distinct j_z values cannot hybridize to anticross on a rotation axis. This inspires us to define an *irrep-dependent Weyl charge* q_J for an on-axis Weyl node. While the value of q_J still characterizes the monopole charge, the additional subscript J originates from the quantum number j_z carried by the bands and thus provides the necessary symmetry information. In particular, two on-axis Weyl nodes carrying q_{J_1} and q_{J_2} can annihilate each other only if both $q_{J_1} = -q_{J_2}$ and $J_1 = J_2$ are satisfied.

As we show in Sec. IV, when $[C_n, \mathcal{S}] = 0$, the chiral-related Weyl pair always carries opposite values of Weyl charges with the same J -label: q_J and $-q_J$, thus they can always be trivialized as a whole. When $\{C_n, \mathcal{S}\} = 0$, we find that such a DWP carries opposite Weyl charges with distinct J -labels: $q_J = -q_{J+\frac{n}{2}}$, and hence is stable by itself. Notably, this implies that robust DWPs do not exist for C_3 -symmetric systems, as $\frac{n}{2}$ must be an integer. The net topological singularities in the phase band is characterized by a set of C_n topological charges $\{Q_J^{(n)}\}$, which counts the net Weyl charge labeled by J for all C_n -invariant axes. Further taking into account constraints from chiral symmetry, we find $\frac{n}{2}$ independent C_n topological charges, leading to a $\mathbb{Z}^{\frac{n}{2}}$ classification for the C_n -protected topological singularities, as shown in Table I.

A dihedral group D_n is generated by both a C_n rotation and an additional mirror symmetry \mathcal{M} . Thus, the rotation charges $Q_J^{(n)}$ remain well-defined for dihedral groups. However, mirror symmetry imposes additional constraints on the rotation charges that further reduce the number of independent $Q_J^{(n)}$'s for each n . Moreover, we demonstrate in Sec. V that a mirror symmetry \mathcal{M} can protect robust singularities by itself if $[\mathcal{M}, \mathcal{S}] = 0$, which defines a \mathbb{Z} -type mirror topological charge $Q_{\mathcal{M}}$. Such a mirror-protected singularity instead takes the form of a 3D fourfold-degenerate Dirac node living on

the 1D intersection between the \mathcal{S} -invariant plane and the \mathcal{M} -invariant plane. For example, a \mathcal{M}_x -protected Dirac node can move freely along the k_y axis at either $(k_x, t) = (0, \frac{T}{2})$ or $(k_x, t) = (\pi, \frac{T}{2})$. Notably, such a \mathcal{M} -protected Dirac singularity can be deformed into an exotic nodal loop upon symmetric perturbations, as will be discussed in details in Sec. V.

Since the dihedral groups contain both rotation and mirror symmetries, it is possible that both $Q_J^{(n)}$ and $Q_{\mathcal{M}}$ are nontrivial in D_n -symmetric systems. For example, it is actually rather common that a phase-band singularity simultaneously carries both rotation and mirror charges. Moreover, when multiple mirror planes are present, a distinct mirror charge $Q_{\mathcal{M}'}$ can be defined for each set of inequivalent mirror plane \mathcal{M}' , as long as it commutes with chiral symmetry. However, not all these topological charges are independent. We find that the total number of independent topological charges sensitively depends on the commutation relations among rotation, mirror, and chiral symmetries. After carefully disentangling the complex relations among various topological charges, we achieve a complete classification of D_n -protected phase-band singularities, which is elaborated in Sec. V and summarized in Table I.

D. Connection to 4D topological crystalline insulators

We point out that a C_n or D_n -protected phase-band topological singularity necessarily features anomalous band connectivity that does not exist in any electronic band structure of 3D static lattice systems. However, such phase-band singularities do resemble exotic surface state physics of 4D TCIs.

For example, we show in Sec. IV that a C_2 -protected DWP exhibits a C_2 -velocity locking effect. Namely, both right (left) movers along the t -axis carry the same C_2 eigenvalues. This obviously violates the energy band

Rotation Group	C_1	C_2	C_3	C_4	C_6
$C_{n,-}^+$	0	0	0	0	0
$C_{n,-}^-$	0	0	0	0	0
$C_{n,+}^+$	0	\mathbb{Z}	0	\mathbb{Z}^2	\mathbb{Z}^3
$C_{n,+}^-$	0	\mathbb{Z}	0	\mathbb{Z}^2	\mathbb{Z}^3
Dihedral Group	D_1	D_2	D_3	D_4	D_6
$D_{n,-,-}^+$	\mathbb{Z}	0	\mathbb{Z}	0	0
$D_{n,-,+}^+$	0	0	0	0	0
$D_{n,+,-}^+$	/	$\mathbb{Z} \times 2\mathbb{Z}$	/	\mathbb{Z}	$\mathbb{Z}^2 \times 2\mathbb{Z}$
$D_{n,+,+}^+$	/	$\mathbb{Z} \times 2\mathbb{Z}$	/	\mathbb{Z}	$\mathbb{Z}^2 \times 2\mathbb{Z}$
$D_{n,-,-}^-$	\mathbb{Z}	$\mathbb{Z} \times 2\mathbb{Z}$	\mathbb{Z}	$\mathbb{Z} \times 2\mathbb{Z}$	$\mathbb{Z} \times 2\mathbb{Z}$
$D_{n,-,+}^-$	0	0	0	0	0
$D_{n,+,-}^-$	/	0	/	$\mathbb{Z} \times 2\mathbb{Z}$	\mathbb{Z}
$D_{n,+,+}^-$	/	0	/	$\mathbb{Z} \times 2\mathbb{Z}$	\mathbb{Z}

TABLE I. Classification of phase-band topological singularities protected by 2D point groups. We label different classes of C_n and D_n groups as $C_{n,\eta_{C_n}}^s$ and $D_{n,\eta_{C_n},\eta_{M_x}}^s$, respectively. $s = +(-)$ when $(C_n)^n = +1(-1)$, i.e. single versus double group; $\eta_{C_n} = -(+)$ when C_n commutes (anticommutes) with chiral symmetry; $\eta_{M_x} = -(+)$ when M_x commutes (anticommutes) with chiral symmetry.

connectivity in a static lattice system, where the number of right movers and left movers carrying the same C_2 eigenvalue must be the same, due to the periodicity of the Brillouin zone. Such a locking between the velocity and some good quantum number can only occur on the boundary of a static topological system living in one higher dimension, and a well-known example is the spin-momentum locking for the helical edge states circulating around a quantum spin Hall insulator [4, 5]. Indeed, we show explicitly in Appendix A that the surface states of a 4D C_2 -protected TCI are 3D Weyl nodes exhibiting the same C_2 -velocity locking effect [78].

In fact, the intrinsic relation between a phase-band topological singularity and a 4D TCI surface state is not accidental. Note that if a phase-band singularity can be realized on a static lattice, the fermion doubling theorem always requires the existence of another singularity with exactly the opposite topological characteristics. Then such a pair of singularities can always be eliminated as a whole, while preserving both the symmetries and the bulk Floquet gaps. Therefore, a phase-band singularity *should violate the fermion doubling theorem* to guarantee its robustness. Such a violation is possible for the phase band since it does not correspond to the energy spectrum of a local Hamiltonian, and the phases $\tilde{\phi}(\mathbf{k}, t)$ are periodic in 2π . Alternatively, in a static system, one can go around the fermion doubling theorem by considering the 3D boundary of a topological system living in four dimensions.

Rotation Group	C_1	C_2	C_3	C_4	C_6
$C_{n,-}^+$	0	0	0	0	0
$C_{n,-}^-$	0	0	0	0	0
$C_{n,+}^+$	0	\mathbb{Z}_2	0	\mathbb{Z}_2	\mathbb{Z}_2
$C_{n,+}^-$	0	\mathbb{Z}_2	0	\mathbb{Z}_2	\mathbb{Z}_2
Dihedral Group	D_1	D_2	D_3	D_4	D_6
$D_{n,-,-}^+$	\mathbb{Z}	0	\mathbb{Z}	0	0
$D_{n,-,+}^+$	0	0	0	0	0
$D_{n,+,-}^+$	/	\mathbb{Z}	/	0	\mathbb{Z}
$D_{n,+,+}^+$	/	\mathbb{Z}	/	0	\mathbb{Z}
$D_{n,-,-}^-$	\mathbb{Z}	$\mathbb{Z} \times 2\mathbb{Z}$	\mathbb{Z}	$\mathbb{Z} \times 2\mathbb{Z}$	$\mathbb{Z} \times 2\mathbb{Z}$
$D_{n,-,+}^-$	0	0	0	0	0
$D_{n,+,-}^-$	/	0	/	\mathbb{Z}	0
$D_{n,+,+}^-$	/	0	/	\mathbb{Z}	0

TABLE II. Classification of anomalous Floquet higher-order topology protected by 2D point groups. The definitions of different classes labeled as $C_{n,\eta_{C_n}}^s$ and $D_{n,\eta_{C_n},\eta_{M_x}}^s$ are the same as Table I.

E. From phase-band singularities to higher-order topology

As we have mentioned, the anomalous chiral edge mode of an AFTI in class A is indicated by the bulk Weyl singularities in its return map operator $\tilde{U}(\mathbf{k}, t)$. This is simply because the net phase-band Weyl charge exactly equals to the topological winding number for \tilde{U} , which counts the total number of anomalous chiral edge modes [62]. Therefore, it is natural to expect that the C_n or D_n -protected phase-band singularities dictate the number of robust corner modes in AFHOTIs. However, lacking a topological invariant characterization of AFHOTIs as well as a higher-order bulk-boundary correspondence based on which, new approaches are needed to relate the phase-band singularities to higher-order topology.

In Sec. VI, we establish such a higher-order bulk-boundary correspondence and identify the corresponding higher-order topological indices for all C_n and D_n -protected AFHOTIs, by developing a *phase-band dimensional reduction* (PBDR) method. Such a method was inspired by the dimensional reduction approach that has been applied to classifying TCIs by reducing the problem to classifying TIs in lower dimensions [79, 80]. Similarly, our PBDR approach reduces the problem of classifying 2D AFHOTIs to that of 1D AFTIs in class AIII (see Fig. 4), for which the classification and bulk-boundary correspondence have been fully established. While 2D AFHOTIs host corner localized 0 and π modes, a 1D AFTI with chiral symmetry hosts 0 and π modes localized at its endpoints. Such end modes in 1D class AIII AFTIs can be classified by the chiral winding number defined for \tilde{U} [see Eq. (11)], which we prove is equivalent

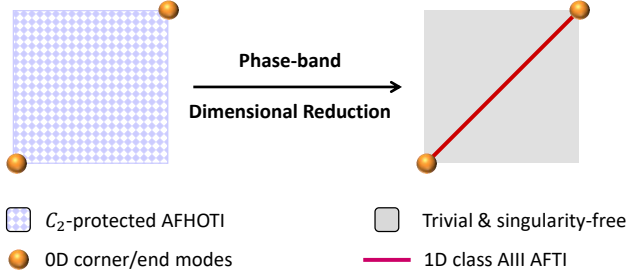


FIG. 4. An example of dimensional reduction applied to C_2 -protected AFHOTTI. The dimensional reduction procedure adiabatically connects a 2D C_2 -protected AFHOTTI harboring corner modes with a 1D AFTI in class AIII harboring end modes.

lent to the phase-band singularity characterization [see Eq. (16)]. Different from the 3D Weyl/Dirac singularities in 2D AFHOTTIs, the phase-band singularities for 1D AFTIs are 2D Dirac nodes in (k, t) space.

More precisely, we divide our target C_n/D_n -symmetric system into symmetry-related patches, as well as a “skeleton” sandwiched in between. In Fig. 4, we give a schematic example for an AFHOTTI with C_2 symmetry. The singularities living on the patches can be adiabatically eliminated by coupling them to a mass term for the phase band. To preserve the crystalline symmetries, such a mass term cannot be spatially uniform, but rather takes the form of a set of symmetry-preserving mass domain walls, which exactly sits on top of the skeleton to respect symmetries. This necessarily leads to chiral-protected 2D Dirac modes localized around each domain wall, which are exactly the defining singularities for 1D AFTIs. Since the singularity-free patches are topologically trivial for our purpose, we have thereby mapped the original 2D system to a collection of symmetry-related 1D AFTIs, completing the PBDR procedure.

After the PBDR, some end modes of the resulting 1D AFTIs may be able to gap out one another and get trivialized. The survivors, however, correspond to robust corner modes in the original 2D system. This allows us to establish the higher-order bulk-boundary correspondence for 2D AFHOTTIs protected by point group symmetries. After a careful analysis, we conclude that

- a 2D C_n -protected AFHOTTI is characterized by a \mathbb{Z}_2 topological index ν_n , where

$$\nu_n \equiv \sum_J |Q_J^{(n)}| \mod 2; \quad (9)$$

- a 2D D_n -protected AFHOTTI is characterized by the set of inequivalent mirror topological charges $\{Q_M\}$, which admits a higher-order topological classification of \mathbb{Z} when there is only one nontrivial mirror charge, or $\mathbb{Z} \times 2\mathbb{Z}$ when there are two inequivalent mirror charges.

We now briefly summarize the boundary features of AFHOTTIs indicated by the above classification. First of all, D_n -protected corner modes can only live on mirror-invariant corners of the system. In particular, AFHOTTIs with a \mathbb{Z} classification is characterized by only one nontrivial mirror charge Q_{M_x} . The value of $|Q_{M_x}|$ corresponds to the number of corner modes on each M_x -preserving corner. Notably, systems with $Q_{M_x} = N$ and $Q_{M_x} = -N$ ($N \in \mathbb{Z}$) are topologically distinct from one another, since their corner modes carry different mirror and chiral eigenvalues.

Secondly, a $\mathbb{Z} \times 2\mathbb{Z}$ classification occurs when a D_n -symmetric system has two inequivalent mirror topological charges Q_M and $Q_{M'}$. We find that in this case they must obey: $Q_M = Q_{M'} \pmod{2}$. Therefore, the number of corner modes at M -invariant corners must equal to that at M' -invariant corners, modulo 2.

In contrast, C_n -protected corner modes can exist on an arbitrary collection of C_n -related corners. However, the \mathbb{Z}_2 classification indicates that only an odd number of corner modes are topologically stable in this case.

In Table II, we summarize our topological classification of 2D AFHOTTIs protected by point group symmetries. This classification, along with the associated higher-order topological indices and the bulk-boundary correspondence, constitutes the key result of this work.

III. REVISITING 1D ANOMALOUS FLOQUET TOPOLOGY

As a warm up, we start by revisiting the theory of 1D anomalous Floquet topological insulator (AFTI) in class AIII, the defining boundary feature of which is the robust end modes pinned at both quasienergies 0 and π/T . Although such systems are not higher-order topological, they demonstrate in a simple way the general idea which carries along to 2D AFHOTTIs, that their anomalous Floquet topology is indicated by phase-band singularities. Moreover, 1D AFTIs provide an elementary building block for establishing the higher-order bulk-boundary correspondence in 2D AFHOTTIs via phase-band dimensional reduction (see Sec. VI).

1D AFTIs in class AIII are known to be characterized by a topological invariant, namely, the chiral winding number [75]. Below we shall first recast this winding number in terms of phase-band singularities (in this case 2D Dirac points), which clarifies the physical meaning of the topological invariant from a new perspective. As we have mentioned earlier, such a 2D Dirac singularity, when appearing at $t = T$, is precisely the topological critical point between the AFTI phase and the trivial phase. We also illustrate our singularity-based topological diagnostic using a simple concrete model, which is a quantum walk analog of the Su-Schrieffer-Heeger model.

A. Winding number and phase-band singularity

Let us first introduce the winding number invariant for characterizing class AIII AFTIs in one spatial dimension. Recall from Eq. (8) that chiral symmetry acts as a time-reflection symmetry on the return map $\tilde{U}(k, t)$. This leads to

$$\left[\mathcal{S}, \tilde{U} \left(k, \frac{T}{2} \right) \right] = 0, \quad (10)$$

which further implies that the return map $\tilde{U}(k, t)$ at the chiral-invariant point $t_0 = \frac{T}{2}$ block diagonalizes according to the chiral eigenvalues $\mathcal{S} = \pm 1$. The topological invariant is thus given by the difference of the winding numbers of the $\mathcal{S} = \pm 1$ blocks of the return map $\tilde{U}(k, \frac{T}{2})$:

$$\mathcal{N}_\mathcal{S} = \int_{-\pi}^{\pi} \frac{dk}{4\pi} \text{Tr} \left[\mathcal{S} \tilde{U}^\dagger \left(k, \frac{T}{2} \right) i \partial_k \tilde{U} \left(k, \frac{T}{2} \right) \right], \quad (11)$$

where the trace is taken over all eigenstates of \tilde{U} . The chiral winding number $\mathcal{N}_\mathcal{S}$ also classifies the number of edge-localized modes at both quasienergies 0 and π via bulk-boundary correspondence.

Written explicitly in the eigenbasis of $\tilde{U}(k, T/2)$ with phase-band eigenvalues $\{\tilde{\phi}_n(k, T/2)\}$, the chiral winding number in Eq. (11) takes the following form:

$$\mathcal{N}_\mathcal{S} = \frac{\mathcal{W}_+ - \mathcal{W}_-}{2}, \quad (12)$$

where for each chiral sector we have

$$\mathcal{W}_\pm = \int_{-\pi}^{\pi} \frac{dk}{2\pi} \sum_{n_\pm} \frac{\partial \tilde{\phi}_{n_\pm}(k, T/2)}{\partial k}. \quad (13)$$

Here n_\pm labels phase-band eigenstates with chiral eigenvalues ± 1 , respectively. Physically, \mathcal{W}_\pm indicates the winding of phase bands at $t = T/2$ around the principle zone for each chiral sector $\mathcal{S} = \pm$. As pointed out in Ref. [75], there exists a compatibility condition that forces the net winding number to vanish:

$$\mathcal{W}_+ + \mathcal{W}_- = 0. \quad (14)$$

We therefore arrive at

$$\mathcal{N}_\mathcal{S} = \mathcal{W}_+. \quad (15)$$

Apparently, a non-zero winding number implies the existence of irremovable phase-band singularities across the principal zone boundary. In 2D (\mathbf{k}, t) space, such a zone-boundary singularity is essentially a 2D Dirac point living on the chiral-invariant line (i.e. $t = \frac{T}{2}$).

The robustness of a single $\mathcal{N}_\mathcal{S}$ -indicated 2D Dirac point is guaranteed by chiral symmetry \mathcal{S} . Since $\mathcal{W}_+ = -\mathcal{W}_-$, a 2D Dirac point with $\mathcal{N}_\mathcal{S} = 1$ is by definition a phase-band crossing between a right-moving channel with $\mathcal{S} = 1$ and a left-moving channel with $\mathcal{S} = -1$, along the chiral-invariant axis. It is then impossible to couple and gap out

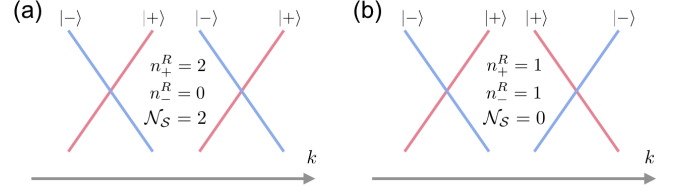


FIG. 5. A pair of 2D Dirac nodes on the chiral symmetric line $t_0 = \frac{T}{2}$. The chiral eigenvalue of each band is labeled as $|\pm\rangle$. (a) The two right (left) movers have the same chiral eigenvalue (“chiral-velocity locking”), hence the two Dirac nodes are stable. The corresponding $\mathcal{N}_\mathcal{S} = 2$. (b) The two right (left) movers have opposite chiral eigenvalues, hence the two Dirac nodes can be gapped out. The corresponding $\mathcal{N}_\mathcal{S} = 0$.

these two counterpropagating branches without violating the chiral symmetry.

The stability of multiple Dirac points is then determined by the chiral winding pattern of each singularity, since two counterpropagating modes along k can only gap out each other when carrying the same chiral index. This inspires us to define n_\pm^R as the number of right-movers carrying a chiral index $\mathcal{S} = \pm$, which will contribute positively (negatively) to the chiral winding number $\mathcal{N}_\mathcal{S}$, respectively. We can then rewrite $\mathcal{N}_\mathcal{S}$ in a physically more intuitive way

$$\mathcal{N}_\mathcal{S} = n_+^R - n_-^R \in \mathbb{Z}, \quad (16)$$

which exactly indicates the net number of robust Dirac points on the zone boundary. For example, when the right-moving modes (along k) of two Dirac points are both within the “+” chiral sector, such a pair of Dirac points carry $\mathcal{N}_\mathcal{S} = 2$ and cannot annihilate each other without breaking \mathcal{S} [see Fig. 5(a)]. Nevertheless, two Dirac points with opposite chiral winding patterns (i.e. $\mathcal{N}_\mathcal{S} = 0$) are always unstable, as shown in Fig. 5(b).

One may wonder whether Dirac nodes are still robust singularities if they live away from the chiral-invariant line. We note that for a Dirac node at (k_0, t_0) with $t_0 \neq \frac{T}{2}$, \mathcal{S} enforces the existence of another Dirac point at $(k_0, T - t_0)$. When bringing such a chiral-related Dirac pair to meet at $t_0 = \frac{T}{2}$, it is easy to show that they necessarily carry $\mathcal{N}_\mathcal{S} = 0$ as a whole. To be specific, since \mathcal{S} switches between the two right-moving modes of the Dirac points, we can always superpose the two channels to form a bonding (symmetric) state (with $\mathcal{S} = 1$) and an anti-bonding (anti-symmetric) state (with $\mathcal{S} = -1$), leading to a trivial chiral winding pattern. Therefore, the “off-line” Dirac nodes can always annihilate with their chiral partners and are thus not robust topological singularities.

Finally, we emphasize on the *chiral-velocity locking* effect of the $\mathcal{N}_\mathcal{S}$ -indicated Dirac nodes, where all right (left) movers carry the same chiral eigenvalue, as shown in Fig. 5(a). This is similar to the well-known spin-momentum locking effect on the edge of a 2D quantum

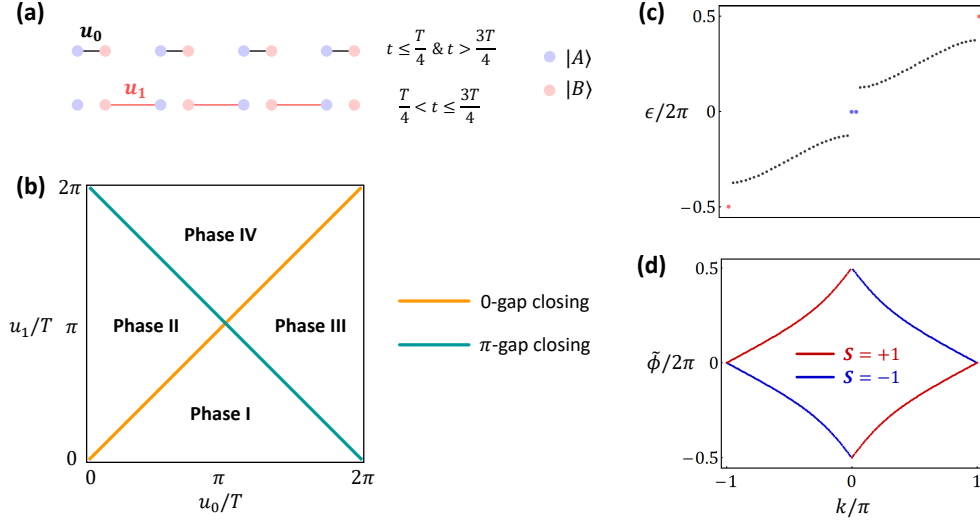


FIG. 6. (a) Schematics of the intra-cell u_0 and inter-cell u_1 couplings for the Hamiltonian H_{1D} in Eq. (17). Each unit cell contains two sublattices labeled by A and B . (b) Phase diagram of H_{1D} . (c) In an open chain geometry, the Floquet spectrum for the phase IV of H_{1D} displays both 0 and π modes at each end of the chain, confirming the system as a 1D AFTI. We have chosen $u_0 = \pi/T$ and $u_1 = 3\pi/(2T)$. (d) Phase bands of the AFTI phase at $t = \frac{T}{2}$ show a nontrivial winding pattern along k , confirming the nontrivial chiral winding number $\mathcal{N}_S = 1$. This agrees with the end-mode physics shown in (c).

spin Hall insulator [6, 7], implying such Dirac nodes cannot be realized in a 2D static lattice system. However, since \mathcal{S} behaves as a mirror symmetry for time, the phase-band Dirac nodes are exactly the same as those on the surface of a 3D mirror-protected topological crystalline insulator [18], if we view t as a crystal momentum orthogonal to k_x . Such a correspondence between a phase-band topological singularity and the boundary mode of a higher-dimensional topological state is a *generic feature for anomalous Floquet topological phases*, as we will show

in Sec. IV and V.

B. Model

We shall now give a concrete example to illustrate our general discussions above. Consider a 1D chain subject to the following time-periodic drive:

$$H_{1D}(k, t) = \begin{cases} u_0 \sum_{\mathbf{r}} c_{\mathbf{r},A}^\dagger c_{\mathbf{r},B} + \text{h.c.} & 0 < t \leq \frac{T}{4} \quad \text{and} \quad \frac{3T}{4} < t \leq T; \\ u_1 \sum_{\mathbf{r}} c_{\mathbf{r}+\mathbf{a}_x,A}^\dagger c_{\mathbf{r},B} + \text{h.c.} & \frac{T}{4} < t \leq \frac{3T}{4}, \end{cases} \quad (17)$$

where A, B denote the two sublattices within a unit cell, as shown in Fig. 6 (a). Under the basis $(|A\rangle, |B\rangle)^T$, chiral symmetry is implemented by $\mathcal{S} = \sigma_z$, and Hamiltonian (17) is invariant under chiral symmetry. Notice that this model is in fact a Floquet version of the well-known Su-Schrieffer-Heeger model [76, 81, 82], where the intra-cell and inter-cell hoppings, i.e. u_0 and u_1 , are periodically switched on and off.

The phase diagram of Hamiltonian (17) is analytically tractable by solving for the vanishing conditions of Floquet bulk gap at quasienergies 0 and π . We find that the phase boundaries are determined by:

$$u_0 \pm u_1 = \frac{2m\pi}{T}, \quad m \in \mathbb{Z}, \quad (18)$$

which separate four topologically distinct phases, as shown in Fig. 6(b). By numerically calculating the Floquet quasienergy spectrum on a finite-size open chain, we find that the four distinct phases can be characterized by the presence of 0 or π end modes: (i) phase I has no boundary modes and is thus topologically trivial; (ii) phase II has robust 0 end mode; (iii) phase III has robust π end mode; (iv) phase IV has both 0 and π end modes [see Fig. 6(c)], and thus realizes our expected AFTI phase.

To calculate \mathcal{N}_S in Eq. (16), we plot the phase band dispersion at $t = \frac{T}{2}$ for phase IV. As shown in Fig. 6 (d), the phase band manifold does host a topological singularity crossing the principle-zone boundary. In particu-

lar, this singularity features our expected chiral-velocity locking effect. Namely, the $\mathcal{S} = +1$ (-1) branch serves as the right (left) mover along the k axis, which directly leads to $\mathcal{N}_S = 1$. The nontrivial value of the chiral winding number thus explains the existence of end modes in Fig. 6(c).

IV. C_n -PROTECTED PHASE-BAND SINGULARITY

Armed with our discussions of 1D driven class AIII systems, we now proceed to consider phase-band singularities in 2D class AIII Floquet systems that are invariant under a n -fold rotation symmetry C_n . Since the generalized Brillouin zone (\mathbf{k}, t) for phase bands is three dimensional, it is natural to consider dynamical Weyl nodes as the elementary building block for understanding singular behaviors in the time-evolution process. As we have pointed out in Sec. II C, the chiral symmetry \mathcal{S} , a unitary time-reflection operation, guarantees that Weyl nodes must come in pairs (i.e. dynamical Weyl pairs or DWPs for short), leading to a vanishing net Weyl charge. This is in contrast with the 2D dynamical Dirac points discussed in Sec. III, where there can be an odd number of Dirac points in total. The DWPs classified in this section are inherently the quantum criticality separating a C_n -protected dynamical phase from a static limit.

Let us start with a dynamical Weyl node at (\mathbf{k}_0, t_0) . If $C_n \mathbf{k}_0 \neq \mathbf{k}_0$ (i.e. the Weyl node living off an rotation-invariant axis), there will be $(n - 1)$ additional Weyl points that are rotation-related. Since there is no symmetry protection, such a group of Weyl points along with their chiral-related partners can always be brought together and adiabatically eliminated as a whole. Therefore, it is sufficient to only consider Weyl points on the t -axis intersecting the rotation-invariant momentum \mathbf{k}_0 .

To describe a Weyl node at (\mathbf{k}_0, t_0) , we start by defining the Weyl basis

$$\psi_J = (|J\rangle, |J+1\rangle)^T, \quad (19)$$

under which the corresponding Weyl charge is labeled as $q_J(\mathbf{k}_0, t_0)$. Here $j_z = J$ or $J+1$ is the z -component angular momentum

$$C_n |J\rangle = e^{i\frac{2\pi}{n}J} |J\rangle, \quad (20)$$

which is defined mod n and takes integer (half-integer) values for spinless (spinful) fermions. The effective Weyl Hamiltonian near (\mathbf{k}_0, t_0) can be written as

$$h_w(t_0) = \pi \mathbb{1}_2 + v_x k_x \sigma_x - v_y k_y \sigma_y + v_t t \sigma_z, \quad (21)$$

where $v_x = v_y$ is required for $n > 2$. The Weyl monopole charge q_J of h_w is thus defined as

$$q_J = -\text{sgn}(v_x v_y v_t). \quad (22)$$

and is further simplified as $q_J = -\text{sgn}(v_t)$ when $n > 2$. We emphasize that our definition of q_J as well as its J

label depends on our choice of basis in Eq. (19), where the j_z eigenvalues are rank-ordered in ascending order. Such a notation is helpful in defining the annihilation rule of Weyl points under C_n . For example, a Weyl node with q_{J_1} can annihilate with another Weyl node with q_{J_2} only if (i) $J_1 = J_2$ and (ii) $q_{J_1} = -q_{J_2}$.

When $[C_n, \mathcal{S}] = 0$, we have

$$\begin{aligned} C_n (\mathcal{S} |J, \mathbf{k}_0, t_0\rangle) &= e^{i\frac{2\pi}{n}J} (\mathcal{S} |J, \mathbf{k}_0, t_0\rangle) \\ &= e^{i\frac{2\pi}{n}J} |J, \mathbf{k}_0, T - t_0\rangle, \end{aligned} \quad (23)$$

up to an unimportant global phase factor. Thus, chiral symmetry maps a phase-band state with $j_z = J$ at (\mathbf{k}_0, t_0) to another state at $(\mathbf{k}_0, T - t_0)$ with the same j_z . Therefore, the chiral-related partner of $h_w(t_0)$ is also formed by the crossing of two phase bands with $j_z = J$ and $J+1$ at $T - t_0$, as schematically shown in Fig. 7(a). Since this Weyl pair now has Weyl charges

$$q_J(\mathbf{k}_0, t_0) = -q_J(\mathbf{k}_0, T - t_0), \quad (24)$$

they can annihilate one another. To see this, we move this pair of Weyl nodes along t -axis while respecting chiral symmetry, such that they coincide at $t_0 = \frac{T}{2}$ and form a fourfold degenerate Dirac point. Under the basis

$$\Psi_{d,-} = (|J\rangle, |J+1\rangle, |J\rangle, |J+1\rangle)^T, \quad (25)$$

the effective Hamiltonian for this Dirac point near $(\mathbf{k}_0, \frac{T}{2})$ is

$$h_d = \pi \mathbb{1}_4 + v_x k_x \gamma_1 - v_y k_y \gamma_2 + v_t t \gamma_5. \quad (26)$$

Again, $v_x = v_y$ is required for $n > 2$. For convenience, we define the 4×4 γ matrices as $\gamma_1 = \tau_0 \otimes \sigma_x$, $\gamma_2 = \tau_0 \otimes \sigma_y$, $\gamma_3 = \tau_x \otimes \sigma_z$, $\gamma_4 = \tau_y \otimes \sigma_z$, $\gamma_5 = \tau_z \otimes \sigma_z$, based on which $\gamma_{jl} = [\gamma_j, \gamma_l]/(2i)$ can be generated for $j, l \in \{1, 2, 3, 4, 5\}$ and $j < l$. We find that

$$\mathcal{S} = \tau_x \otimes \sigma_0 \equiv \gamma_{45}, \quad C_n = e^{i\frac{2\pi}{n}\mathcal{J}_z} \quad (27)$$

with $\mathcal{J}_z = \text{diag}(J, J+1, J, J+1)$. Clearly, we can introduce a mass term proportional to γ_3 that gaps out this DWP without breaking C_n and \mathcal{S} , since $[\gamma_3, C_n] = [\gamma_3, \mathcal{S}] = 0$. We thus conclude that

- there is no stable DWP when $[C_n, \mathcal{S}] = 0$.

When $\{C_n, \mathcal{S}\} = 0$, we have

$$\begin{aligned} C_n (\mathcal{S} |J, \mathbf{k}_0, t_0\rangle) &= -e^{i\frac{2\pi}{n}J} (\mathcal{S} |J, \mathbf{k}_0, t_0\rangle) \\ &= e^{i\frac{2\pi}{n}(J+\frac{n}{2})} |J, \mathbf{k}_0, T - t_0\rangle, \end{aligned} \quad (28)$$

up to a phase factor. Thus, \mathcal{S} maps a phase-band state with $j_z = J$ at (\mathbf{k}_0, t_0) to another state at $(\mathbf{k}_0, T - t_0)$ with a different $j_z = J + \frac{n}{2}$. Since the change of angular momentum $\frac{n}{2}$ can only be an integer, n must be even. This immediately implies that

- C_3 symmetry cannot protect a DWP.

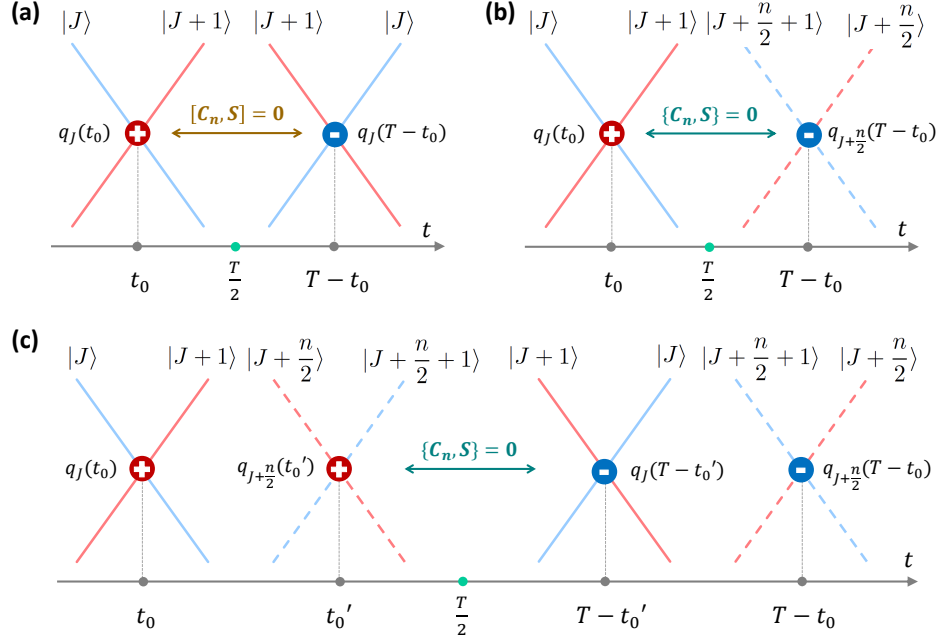


FIG. 7. (a) Pair annihilation of dynamical Weyl nodes when $[C_n, S] = 0$. (b) Stable dynamical Weyl pair when $\{C_n, S\} = 0$. (c) Annihilation of two DWPs when $\{C_n, S\} = 0$.

For $n = 2, 4, 6$, the chiral partner of $h_w(t_0)$ is now a Weyl node formed by two phase bands with $j_z = J + \frac{n}{2}$ and $J + \frac{n}{2} + 1$, which carries a Weyl charge

$$q_{J+\frac{n}{2}}(\mathbf{k}_0, T - t_0) = -q_J(\mathbf{k}_0, t_0), \quad (29)$$

as shown in Fig. 7(b). To check the stability of such DWP, we again make them coincide at $\frac{T}{2}$ and form a Dirac point described by Eq. (26). However, the new basis is now

$$\Psi_{d,+} = \left(|J\rangle, |J+1\rangle, |J + \frac{n}{2}\rangle, |J + \frac{n}{2} + 1\rangle \right)^T, \quad (30)$$

which is distinct from $\Psi_{d,-}$. When $n = 4, 6$, the four phase bands of this 3D Dirac point belong to four different one dimensional irreducible representations (irreps) of $C_{4,6}$. Therefore, this Dirac point cannot be gapped out along the rotation-invariant t -axis, since $C_{4,6}$ symmetry strictly prohibits any coupling between the DWP. The robustness of this DWP is also encoded in their distinct J indices of Weyl charges q_J and $q_{J+\frac{n}{2}}$ [see Fig. 7(c)].

C_2 symmetry, however, has only two distinct irreps and thus the above protection mechanism does not seem to apply. Interestingly, in this case we find

$$C_2 = e^{i\pi J} \gamma_5 \quad (31)$$

under the Dirac-point basis

$$\Psi_{d,+} = (|J\rangle, |J+1\rangle, |J+1\rangle, |J\rangle)^T, \quad (32)$$

which is proportional to the t -linear term of h_d in Eq. (26). Therefore, any C_2 -preserving perturbation,

which must commute with the t -linear term in h_d , can only split the Weyl nodes along the t -axis, but is incapable of gapping them out. Physically, the two phase bands with $C_2 = (-1)^J$ propagate along the same direction on t -axis, while the other two with $C_2 = (-1)^{J+1}$ propagate along the opposite direction. Similar to the chiral-velocity locking effect discussed in Sec. III, here the stable DWP features a locking between C_2 eigenvalue and the velocity along t direction. As we have mentioned before, this locking phenomena between the band dispersion and certain quantum numbers are generally anomalous in the band theory, and cannot be realized in any static 3D lattice system. Nevertheless, we show in Appendix A that such C_2 -velocity locking effect in DWP is exactly the defining characteristic for the surface physics of a 4D C_2 -protected TCI. In fact, a C_n -protected phase-band singularity is generally related to the surface state of a 4D C_n -protected TCI characterized by a rotation Chern number [78]. To conclude, we have proved in general that

- A pair of chiral-related dynamical Weyl points cannot annihilate each other *iff* $\{C_n, S\} = 0$.

When multiple DWPs coexist on the \mathbf{k}_0 -axis, Weyl nodes from *different* chiral-related pairs may annihilate one another, although each pair by itself is stable. Fig. 7(c) gives an example where two DWPs can be gapped out altogether. This inspires us to define

$$q_J^{(n)}(\mathbf{k}_0) = \sum_{t_i \in (0, T)} q_J(\mathbf{k}_0, t_i), \quad (33)$$

which counts the net Weyl charge along the t -axis at momentum \mathbf{k}_0 labeled by J . Crucially, since the Weyl

nodes come in chiral-related pairs, these $q_J^{(n)}$ satisfy the following constraint:

$$q_J^{(n)}(\mathbf{k}_0) = -q_{J+\frac{n}{2}}^{(n)}(\mathbf{k}_0). \quad (34)$$

Then for each rotation-invariant axis at momentum \mathbf{k}_0 , we find the following set of independent net monopole charges for each J ,

$$\{q_{\frac{\alpha}{2}}^{(n)}(\mathbf{k}_0), q_{\frac{\alpha}{2}+1}^{(n)}(\mathbf{k}_0), \dots, q_{\frac{n+\alpha}{2}-1}^{(n)}(\mathbf{k}_0)\} \in \mathbb{Z}^{\frac{n}{2}}, \quad (35)$$

which captures all stable DWPs. Here $\alpha = 0$ for spinless fermion with $(C_n)^n = 1$ and $\alpha = 1$ for spinful fermion with $(C_n)^n = -1$. One can easily check that the example shown in Fig. 7(c) precisely has vanishing J -dependent net monopole charges.

We notice that the definition of $q_J^{(n)}(\mathbf{k}_0)$ relies on well-defined translation symmetries. For example, a Weyl node with $q_J(\mathbf{k}_0, t_i) = 1$ is generally incapable of annihilating with another Weyl node with $q_J(\mathbf{k}'_0, t_i) = -1$ if $\mathbf{k}_0 \neq \mathbf{k}'_0$. However, when translation symmetry is broken, \mathbf{k}_0 and \mathbf{k}'_0 are folded to the same point and thus the two Weyl nodes can be gapped out. For our purpose, we shall focus on the “strong classification” of topological singularities that does not rely any translation symmetry. Such a classification for DWPs is characterized by the C_n -topological charge,

$$Q_J^{(n)} = \sum_{\mathbf{k}_0} q_J^{(n)}(\mathbf{k}_0), \quad (36)$$

where $J \in \{\frac{\alpha}{2}, \frac{\alpha}{2}+1, \dots, \frac{n+\alpha}{2}-1\}$ for $(C_n)^n = (-1)^\alpha$, and \mathbf{k}_0 runs over all rotation-invariant momenta. Systems with different $Q_J^{(n)}$ s cannot be adiabatically connected to each other without breaking the symmetries, and are hence topologically distinct.

V. D_n -PROTECTED PHASE-BAND SINGULARITY

We now proceed to classify phase-band singularities protected by dihedral group symmetries in 2D class AIII Floquet systems. Besides n -fold rotations, a dihedral group D_n has n additional in-plane mirror symmetries. The physical significance of a mirror symmetry \mathcal{M} is twofold:

- (1) when $\{C_n, \mathcal{S}\} = 0$, \mathcal{M} imposes additional constraints on the relationship among various rotation topological charges $Q_J^{(n)}$;
- (2) \mathcal{M} by itself is capable of protecting new types of topological singularity that are indicated by a mirror topological charge $Q_{\mathcal{M}}$, distinct from $Q_J^{(n)}$.

As will be shown later, it is both the rotation and mirror topological charges, as well as the interplay among them, that together determines the classification of D_n -protected phase-band singularities.

The structure of this section is organized as follows. In Sec. VA and Sec. VB, we first discuss the constraints on the rotation topological charges $Q_J^{(n)}$ imposed by mirror symmetry. In Sec. VC, we explore the topological singularities protected by mirror symmetry alone (i.e. D_1 group) and define the corresponding mirror topological charge. This allows us to list all possible topological charges for a general D_n group in Sec. VD. However, through a comprehensive case study of D_2 group in Sec. VE, we find that there exists a complex interplay among rotation and mirror topological charges. Namely, not all charges are independent from one another. In Sec. VF, we outline the general rules that determine a complete set of independent topological charges for all D_n groups, which finalizes the classification of topological phase-band singularities protected by two-dimensional point groups.

A. Constraining C_n topological charges with a mirror symmetry

The constraints on $Q_J^{(n)}$ imposed by mirror symmetry can be understood as follows. When $[C_n, M_x] \neq 0$, the mirror symmetry will “glue” certain one-dimensional irreps of C_n into two-dimensional irreps, thereby imposing additional relations that rotation topological charges with different J must satisfy. In particular, since $C_n M_x = M_x C_n^{-1}$, we have

$$\begin{aligned} C_n (M_x |J, \mathbf{k}_0, t_0\rangle) &= e^{-i\frac{2\pi}{n}J} (M_x |J, \mathbf{k}_0, t_0\rangle) \\ &= e^{-i\frac{2\pi}{n}J} |-J, \mathbf{k}_0, t_0\rangle, \end{aligned} \quad (37)$$

up to a phase factor, where \mathbf{k}_0 is a rotation and mirror symmetric momentum. Namely, M_x maps a phase-band state with $j_z = J$ at (\mathbf{k}_0, t_0) to another state at the same location with $j_z = -J$. In what follows, we shall focus on D_n double groups with $(C_n)^n = -1$, which only has 2d irreps. A discussion for D_n single groups with $(C_n)^n = 1$ is detailed in Appendix B.

Consider a phase-band Weyl node at (\mathbf{k}_0, t_0) under the basis $\psi_J = (|J\rangle, |J+1\rangle)^T$ that carries a charge $q_J(\mathbf{k}_0, t_0)$. M_x will enforce the existence of another Weyl node at the same location with a charge

$$q_{-J-1}(\mathbf{k}_0, t_0) = -q_J(\mathbf{k}_0, t_0) \quad (38)$$

under the basis $\psi_{-J-1} = (|-J-1\rangle, |-J\rangle)^T$. This mirror-enforced Weyl pair forms a 4-fold degenerate *dynamical Dirac point* (DDP). Such a DDP is unstable *only if* $J+1 = -J \pmod{n}$, where the two mirror-related Weyl nodes carry opposite monopole charges with exactly the same J label. In other words, there is no protected singularity if $J = -\frac{1}{2}$ or $\frac{n-1}{2}$, leading to

$$Q_{\frac{n-1}{2}}^{(n)} = 0 \quad \text{for any } D_n \text{ group.} \quad (39)$$

In particular, the D_2 double group always has trivial topological charges and hence no stable topological singularity. For $n = 4, 6$, this indicates that $Q_{\frac{3}{2}}^{(4)} = 0$, and

$Q_{\frac{5}{2}}^{(6)} = 0$. Furthermore, we notice that \mathcal{S} and M_x together impose

$$Q_J^{(n)} = -Q_{-J-1}^{(n)} = -Q_{-J-1+n}^{(n)} = Q_{-J-1+\frac{n}{2}}^{(n)}, \quad (40)$$

which requires

$$Q_{\frac{1}{2}}^{(6)} = Q_{\frac{3}{2}}^{(6)}. \quad (41)$$

Taken together, the nontrivial rotation topological charges under the constraint of mirror symmetry for each D_n double group are:

$$\begin{aligned} D_2 : 0, \\ D_4 : Q_{\frac{1}{2}}^{(4)} \in \mathbb{Z}, \\ D_6 : Q_{\frac{1}{2}}^{(6)} \in \mathbb{Z}. \end{aligned} \quad (42)$$

As shown in Appendix B, the mirror-constrained rotation topological charges for D_n single groups are

$$\begin{aligned} D_2 : Q_0^{(2)} \in \mathbb{Z}, \\ D_4 : Q_0^{(4)} \in \mathbb{Z}, \\ D_6 : \{Q_0^{(6)}, Q_1^{(6)}\} \in \mathbb{Z}^2. \end{aligned} \quad (43)$$

B. Dynamical Dirac point and its doublet

In this part, we will further elaborate on the properties of DDPs defined in the previous subsection. First of all, we emphasize that the existence of DDPs does not rely on the rotation topological charges. Namely, even when $[C_n, \mathcal{S}] = 0$ with vanishing $Q_J^{(n)}$, it is possible to have similar DDPs that are protected by mirror symmetries themselves. Nevertheless, in the current subsection, we will only derive the conditions for such DDPs to exist for various D_n groups when the rotation charges are trivial, and leave their explicit topological characterizations (i.e. the mirror topological charges) to the coming subsections.

Secondly, unlike the case for C_n groups, the mirror-constrained C_n topological charges in Eqs. (42) and (43) indicate either the number of DDPs or that of *DDP doublets* (i.e. chiral-related pairs of DDPs). The formation of a DDP doublet versus that of a single DDP can be understood as follows. Starting from a dynamical Weyl node W_1 and its mirror partner W_2 at (\mathbf{k}_0, t_0) , we denote their chiral partners at $(\mathbf{k}_0, T - t_0)$ as W_3 and W_4 , respectively. Generally, $W_{1,2}$ and $W_{3,4}$ will form two chiral-related DDPs, which we call a DDP doublet. However, in some special cases, the mirror partner of a Weyl node is identical to its chiral partner, e.g. $W_1 = W_4$ and $W_2 = W_3$, leading to a single DDP pinned at $t_0 = T/2$. As we will see in the next subsection, differentiating between a DDP and a DDP doublet is essential for our general classification of D_n -protected singularities. Below, we shall systematically clarify for which D_n groups can a single DDP exist.

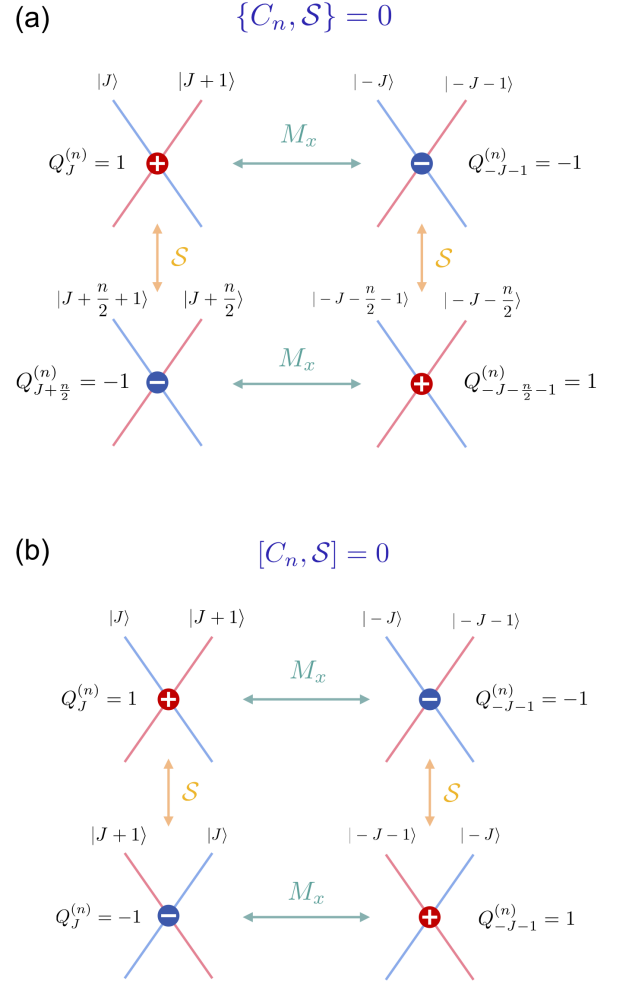


FIG. 8. Commutative diagrams for the Weyl node partners under the action of M_x and \mathcal{S} . (a) $\{C_n, \mathcal{S}\} = 0$. A single DDP is possible when $2J + 1 = \frac{n}{2} \pmod{n}$. (b) $[C_n, \mathcal{S}] = 0$. A single DDP is possible when $2J + 1 = 0 \pmod{n}$. When the above conditions are not satisfied, one will instead have a pair of DDPs (i.e. a DDP doublet).

The situation where $\{C_n, \mathcal{S}\} = 0$ is generally captured by the commutative diagram shown in Fig. 8(a). We start from a single Weyl node under the basis ψ_J , with rotation charge $Q_J^{(n)} = 1$. In Fig. 8(a) we explicitly show its partners under the action of M_x and \mathcal{S} . Indeed, generically M_x and \mathcal{S} will give rise to a doublet of Dirac cones, unless the mirror and chiral partners of the original Weyl node coincide. When this happens, it is possible to have a single DDP sitting at $t_0 = \frac{T}{2}$. From Fig. 8(a), one can immediately see that the condition for this to happen is:

$$J + \frac{n}{2} + 1 = -J \pmod{n}, \quad \text{i.e.,} \quad 2J + 1 = \frac{n}{2} \pmod{n}. \quad (44)$$

More specifically, the above condition can be satisfied when

1. $(C_n)^n = 1$ (spinless): $n = 2, 6$;

2. $(C_n)^n = -1$ (spinful): $n = 4$.

Recall that C_3 cannot anticommute with \mathcal{S} and hence does not appear on the list above. Therefore, we conclude that *when $\{C_n, \mathcal{S}\} = 0$, a single DDP is possible only for spinless D_2 and D_6 groups, and spinful D_4 group.* Otherwise, we generally expect DDP doublets as the phase-band singularities.

Similarly, the situation where $[C_n, \mathcal{S}] = 0$ is shown in Fig. 8(b). One can read off from this commutative diagram that the condition for the existence of a single DDP in this case is given by:

$$J+1 = -J \pmod n, \quad \text{i.e.,} \quad 2J+1 = 0 \pmod n. \quad (45)$$

We first note that a single DDP can always exist in a D_1 group, where all angular momentum irreps are equivalent. In addition, the above condition can be satisfied when

1. $(C_n)^n = 1$ (spinless): $n = 3$;
2. $(C_n)^n = -1$ (spinful): all n .

Therefore, we conclude that *when $[C_n, \mathcal{S}] = 0$, a single DDP is possible for spinless and spinful D_1 groups, spinless D_3 group and all spinful D_n groups.* Fig. 8(b) also shows that the rotation charge in this case must be trivial, as expected from our discussions in the previous section. Nonetheless, it is mirror symmetry that is responsible for protecting the above DDPs, which we will show next.

C. Topological singularity protected by a single mirror symmetry: D_1 group

Besides constraining rotation topological charges, mirror symmetry by itself can protect robust dynamical singularities. Let us consider a single mirror symmetry M_x , which constitutes the D_1 group. We will show that the topological singularity protected by M_x generically takes the form of a nodal loop, which can be shrunk to a single DDP. Furthermore, we will also demonstrate that a DDP doublet related by both chiral and mirror symmetries always has a trivial mirror charge. Hence, the condition for the existence of a single DDP derived previously will become important when we discuss mirror charges for D_n groups in general.

Combining with chiral symmetry, there are now two mirror planes in the 3D (\mathbf{k}, t) space: the $k_x = 0$ plane and the $t_0 = \frac{T}{2}$ plane. The line along k_y direction with $k_x = 0$ and $t_0 = \frac{T}{2}$ is thus invariant under both mirror symmetries. Therefore, topological singularities residing on the k_y -axis can appear as a single DDP that is invariant under M_x and \mathcal{S} symmetries. Alternatively, a DDP doublet on the t -axis (or k_x -axis) is also allowed by symmetry.

Let us first consider a DDP on the mirror symmetric line. If there is only one mirror plane M_x , the DDP can

appear anywhere on the mirror symmetric line, and we can thus always place it at the origin (we have redefined $t - \frac{T}{2}$ as t). The DDP can again be described by the effective Hamiltonian (26). However, the action of chiral and mirror symmetry remains to be determined. By a direct enumeration, we find that there are two possible representations for the chiral and mirror symmetries that are consistent with their actions on Hamiltonian (26):

$$\begin{aligned} \mathcal{S} &= \gamma_{35}, \quad \text{or} \quad \mathcal{S} = \gamma_{45}; \\ M_x &= \gamma_{13}, \quad \text{or} \quad M_x = \gamma_{14}. \end{aligned} \quad (46)$$

One can easily check that out of the 4 combinations of \mathcal{S} and M_x , two of which satisfy $[\mathcal{S}, M_x] = 0$, and the other two satisfy instead $\{\mathcal{S}, M_x\} = 0$. We shall now examine the stability of the DDP for each situation separately; namely, whether or not such a DDP can be gapped out by a symmetric mass term.

When $\{\mathcal{S}, M_x\} = 0$, we have $\mathcal{S} = \gamma_{35}$, $M_x = \gamma_{13}$; or $\mathcal{S} = \gamma_{45}$, $M_x = \gamma_{14}$. Apparently a mass term $h_m \propto \gamma_4$ in the former case, or $h_m \propto \gamma_3$ in the latter case gaps out the DDP while respecting both symmetries: $[\mathcal{S}, h_m] = 0$, $[M_x, h_m] = 0$. We thus conclude that

- there is no stable mirror-protected DDP when $\{\mathcal{S}, M_x\} = 0$.

When $[\mathcal{S}, M_x] = 0$, we have $\mathcal{S} = \gamma_{45}$, $M_x = \gamma_{13}$; or $\mathcal{S} = \gamma_{35}$, $M_x = \gamma_{14}$. Let us take the second case as an example. Similarly to our previous discussions, we are again looking for perturbations that commute with both \mathcal{S} and M_x . In the current situation, there are only two such perturbations: $h_m \propto \gamma_{35}$, or $h_m \propto \gamma_{14}$. However, neither of them is capable of gapping out the DDP in this case, since neither γ_{35} nor γ_{14} anticommutes with the full kinetic terms in Hamiltonian (26). For example, the phase band spectrum of Hamiltonian (26) in the presence of $h_m = m_1 \gamma_{35}$ is given by:

$$\tilde{\phi}(\mathbf{k}, t) = \pi \pm \sqrt{t^2 + \left(\sqrt{k_x^2 + k_y^2} \pm m_1 \right)^2}, \quad (47)$$

which simply corresponds to shifting the two Weyl nodes up and down symmetrically in energy, yielding a nodal loop at:

$$t = 0, \quad k_x^2 + k_y^2 = m_1^2, \quad (48)$$

as depicted in Fig. 9(a). On the other hand, in the presence of $h_m = m_2 \gamma_{14}$, the phase band spectrum takes the form:

$$\tilde{\phi}(\mathbf{k}, t) = \pi \pm \sqrt{k_x^2 + \left(\sqrt{k_y^2 + t^2} \pm m_2 \right)^2}, \quad (49)$$

which now corresponds to shifting the two Weyl nodes symmetrically along the k_y axis, yielding a nodal loop at:

$$k_x = 0, \quad k_y^2 + t^2 = m_2^2, \quad (50)$$

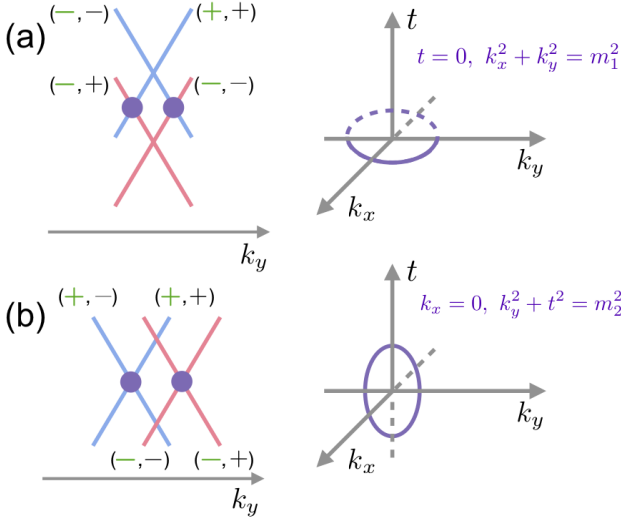


FIG. 9. A DDP in the presence of perturbations respecting both \mathcal{S} and M_x symmetries. (a) The first allowed perturbation moves the Weyl nodes up and down symmetrically in energy, yielding a nodal loop as indicated by the purple dots and line. (b) The second allowed perturbation moves the location of the Weyl nodes symmetrically along k_y axis, yielding a nodal loop as indicated by the purple dots and line. The green and black “ \pm ” label the \mathcal{S} and M_x eigenvalues of each band: (\mathcal{S}, M_x) , respectively.

as depicted in Fig. 9(b). However, neither of the perturbations is able to remove the topological singularity in the phase band, due to the combination of \mathcal{S} and M_x symmetries.

To understand the protection mechanism for the above DDP, we first label every phase band dispersing along the k_y axis with both its chiral and mirror eigenvalues as (\mathcal{S}, M_x) . We then find that a general mirror-preserving DDP with $[\mathcal{S}, M_x] = 0$ always features the following properties:

- (i) it consists of four branches along the k_y axis that are labeled by $(\mathcal{S}, M_x) = (+, +), (+, -), (-, +), (-, -)$;
- (ii) the $(+, +)$ and $(-, -)$ branches disperse along the same direction, while the $(+, -)$ and $(-, +)$ branches disperse along the other direction.

With this pattern of symmetry indices, one immediately finds that all crossings of the DDP are protected by both chiral and mirror symmetries. Namely, any two bands that cross necessarily have either opposite \mathcal{S} or M_x eigenvalues. For example, as shown in Fig. 9(a), the perturbation $m_1\gamma_{35}$ shifts the two Weyl nodes up and down in phase band energy, yielding two crossings labeled by purple dots in Fig. 9(a). While the two bands crossings at the purple dots have identical M_x eigenvalues, they cannot be gapped out for sharing the opposite \mathcal{S} eigenvalues. An analysis of all other cases can be carried out

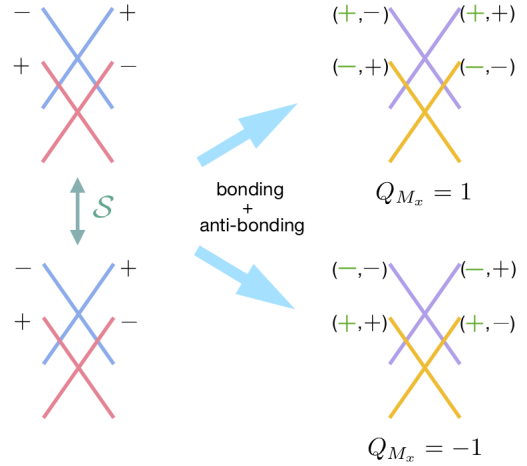


FIG. 10. Mirror charge of a DDP doublet. A DDP doublet consists of two Dirac nodes related by chiral symmetry, as shown on the left. The black \pm labels the M_x eigenvalue of each branch. Chiral eigenstates are bonding (symmetric) and anti-bonding (antisymmetric) superpositions of the two left / right movers. The resultant chiral eigenvalues of each branch are labeled by green \pm on the right. Such a DDP doublet apparently has $Q_{M_x} = 0$.

in a similar fashion, and leads to the same result. We thus conclude that

- A single mirror symmetry M_x can protect stable phase band topological singularities *iff* $[\mathcal{S}, M_x] = 0$. The generic topological singularities in this case are nodal loops, which can be shrunk to DDPs but can never be adiabatically eliminated while preserving M_x .

To characterize such mirror-protected loop-like or point-like singularities, we make use of their unique symmetry pattern and define the following *mirror topological charge*:

$$Q_{M_x} = \sum_{k_y=0,\pi} (n_{++}^R - n_{++}^L) \in \mathbb{Z}, \quad (51)$$

where $n_{++}^{R/L}$ counts the number of left and right movers with $\mathcal{S} = M_x = +1$ along the k_y axis. The summation over all high-symmetry k_y restricts our classification to singularities that do not rely on translation symmetry. For a single DDP, this definition implies that $Q_{M_x} = \text{sgn}(v_y)$, as the sign of Q_{M_x} depends on whether the branch with $\mathcal{S} = M_x = +1$ is a left or right mover (see Fig. 9).

Next, we explore the Q_{M_x} of a DDP doublet. Consider a single Dirac node within a DDP doublet, which consists of a pair of mirror-related Weyl nodes. Such a DDP can be effectively described by Hamiltonian (26), and carries a M_x index in the M_x -invariant plane. From Fig. 9, along k_y -axis, the M_x eigenvalues of each branch for this single DDP are: $+v_k k_y$, $M_x = 1$; $+v_k k_y$, $M_x =$

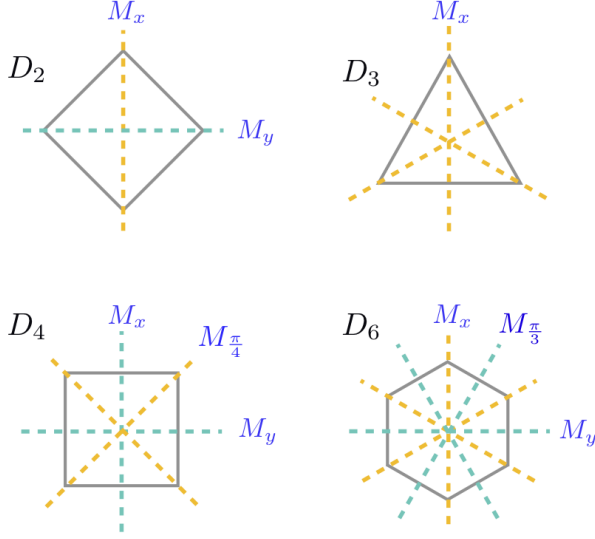


FIG. 11. Mirror planes of the dihedral groups D_2 , D_3 , D_4 and D_6 . Inequivalent mirror planes are drawn in different colors.

-1 ; $-v_k k_y$, $M_x = 1$; $-v_k k_y$, $M_x = -1$. The same is also true for its chiral partner since $[\mathcal{S}, M_x] = 0$, and we depict both DDPs in Fig. 10(a).

The next step is to determine the chiral index for each branch of the DDP doublet. As shown in Fig. 10(a), the chiral symmetry maps one branch of a DDP to a branch in the other DDP with the same M_x eigenvalue and k_y dispersion. Therefore, eigenstates of \mathcal{S} are symmetric and antisymmetric superpositions of these two chiral-related branches, with the same M_x eigenvalue. Namely, two chiral-related branches with $M_x = \pm$ will contribute to two branches with $(+, \pm)$ and $(-, \pm)$. Then it is easy to see that such a DDP doublet always consists of a DDP with $Q_{M_x} = 1$ and another with $Q_{M_x} = -1$. Therefore, we have proved that

- a DDP doublet always carries $Q_{M_x} = 0$.

D. A list of possible topological charges for D_n

We are now ready to present the complete list of possible topological charges for a general D_n group. Summarizing our previous discussions of rotation and mirror charges, the set of nontrivial topological charges will depend on three factors:

1. the commutation relation between M_x and \mathcal{S} ;
2. the commutation relation between the inequivalent mirror $M' = C_n M_x$ and \mathcal{S} ; or, equivalently, the commutation relation between C_n and \mathcal{S} ;
3. $(C_n)^n = +1$ or -1 , i.e. single or double group.

Here, (1)-(3) together lead to $2^3 = 8$ possibilities. We shall label them as $D_{n, \eta_{C_n}, \eta_{M_x}}^s$ for a dihedral group D_n

in the following discussions, where $\eta = -(+)$ when M_x or C_n commutes (anticommutes) with \mathcal{S} , and $s = +(-)$ when $(C_n)^n = +1(-1)$. Besides, we will often denote the mirror M' inequivalent to M_x as M_{θ_n} . Here for D_n group, we have defined

$$\theta_n = \frac{\pi}{2} - \frac{\pi}{n} \quad (52)$$

as the polar angle of the corresponding mirror axis in 2D real space. For example, M_{θ_2} for D_2 group is exactly M_y , since the M_y -axis is labeled by a zero polar angle.

Of all eight possibilities, $D_{n, -, +}^\pm$ contains no nontrivial topological charge, since in this case $\{\mathcal{S}, M_x\} = [C_n, \mathcal{S}] = \{M_{\theta_n}, \mathcal{S}\} = 0$, and hence all rotational and mirror topological charges are trivial. Furthermore, $D_{n, +, +}^\pm$ and $D_{n, +, -}^\pm$ are in fact equivalent, since the former corresponds to $\{\mathcal{S}, M_x\} = [\mathcal{S}, M_{\theta_n}] = \{C_n, \mathcal{S}\} = 0$ and the latter corresponds to $[\mathcal{S}, M_x] = \{\mathcal{S}, M_{\theta_n}\} = \{C_n, \mathcal{S}\} = 0$; hence, they are equivalent upon switching the definition of M_x and M_{θ_n} . Therefore, we are left with only four distinct cases, which we choose to be: $D_{n, +, -}^+$ ($D_{n, +, +}^+$), $D_{n, +, -}^-$ ($D_{n, +, +}^-$), $D_{n, -, -}^+$, and $D_{n, -, -}^-$. Notice that for the D_3 group, there exist only two nontrivial classes $D_{3, -, -}^\pm$, since all of its mirrors are equivalent under C_3 (see Fig. 11).

Now we have the following rules for determining the nontrivial topological charges for each $D_{n, \eta_{C_n}, \eta_{M_x}}^s$ class:

1. rotation charges $Q_J^{(n)}$: nontrivial if $\eta_{C_n} = +$ and the D_n mirror-constrained rotation charge is nontrivial;
2. mirror charge Q_{M_x} : nontrivial if $\eta_{M_x} = -$ and the existence of a single DDP is possible for the corresponding D_n group;
3. both $\{Q_{M_x}, Q_{M_{\theta_n}}\}$ are nontrivial if $\eta_{C_n} = \eta_{M_x} = -$, and a single DDP is possible.
4. If two mirror symmetries M_x and \tilde{M} are equivalent under C_n rotation (e.g. $\tilde{M} = C_n M_x C_n^{-1}$), we necessarily have $Q_{M_x} = Q_{\tilde{M}}$ for $\eta_{M_x} = -$, and only Q_{M_x} will be included in our classification to avoid double counting.

Based on the above rules, we can list all possible nontrivial topological charges for each $D_{n, \eta_{C_n}, \eta_{M_x}}^s$ class as follows:

- D_2 group:

1. $D_{2, +, \pm}^+$: $\{Q_0^{(2)}, Q_{M_x}\}$
2. $D_{2, +, \pm}^-$: trivial
3. $D_{2, -, -}^+$: trivial
4. $D_{2, -, -}^-$: $\{Q_{M_x}, Q_{M_y}\}$

- D_3 group: $D_{3, -, -}^\pm$: Q_{M_x}

- D_4 group:

1. $D_{4,+,\pm}^+ : Q_0^{(4)}$
2. $D_{4,+,\pm}^- : \{Q_{\frac{1}{2}}^{(4)}, Q_{M_x}\}$
3. $D_{4,-,-}^+ : \text{trivial}$
4. $D_{4,-,-}^- : \{Q_{M_x}, Q_{M_{\frac{\pi}{4}}}\}$

- D_6 group:

1. $D_{6,+,\pm}^+ : \{Q_0^{(6)}, Q_1^{(6)}, Q_{M_x}\}$
2. $D_{6,+,\pm}^- : Q_{\frac{1}{2}}^{(6)}$
3. $D_{6,-,-}^+ : \text{trivial}$
4. $D_{6,-,-}^- : \{Q_{M_x}, Q_{M_{\frac{\pi}{3}}}\}$

While the above list exhausts all possible topological charges, there remains one important question: are all the mirror and rotation topological charges for a given D_n group completely independent from one another? To address this question, below we shall first use the D_2 group as a case study. Then we will provide a general prescription allowing us to classify all other D_n groups in a similar fashion.

E. A case study: D_2 group

The D_2 group has two inequivalent mirror planes M_x and M_y that are C_2 -related: $C_2 = M_x M_y$, as shown in Fig. 11. According to our list of topological charges, there are only two nontrivial classes: $D_{2,+,\pm}^+$ and $D_{2,-,-}^-$. While this follows from our general rules, for D_2 group we can alternatively reach this conclusion from a straightforward analysis, which we shall present first.

If there exists only one DDP in D_2 group, it must be invariant under M_y by itself and is thus pinned at a high symmetry position intersected by k_x, k_y and t axes (e.g. the origin of phase space). For DDPs that are not M_y invariant, they must come in M_y -related pairs, forming DDP doublets with a trivial mirror charge. As it turns out, which one of these two scenarios actually happens is completely determined by the commutation relations between M_x, M_y , and \mathcal{S} . Let us take a single DDP at the origin. Since $[\mathcal{S}, M_x] = 0$ is required for a stable DDP, we are left with four possibilities:

1. $[M_x, M_y] = 0, [\mathcal{S}, M_y] = 0$. In this case, the right mover of the DDP with $\mathcal{S} = M_x = +1$ (see Fig. 9) is mapped to a left mover with $\mathcal{S} = M_x = +1$ under M_y . This implies the existence of a mirror-enforced DDP doublet, and the total mirror charge according to Eq. (51) must be $Q_{M_x} = 0$.
2. $[M_x, M_y] = 0, \{\mathcal{S}, M_y\} = 0$. In this case, the right mover of the DDP with $\mathcal{S} = M_x = +1$ is mapped to a left mover with $\mathcal{S} = -1, M_x = +1$, which

is precisely the left mover of the other Weyl node of the same DDP. One can readily check for each left and right mover, and confirm that the DDP is mapped to itself under M_y . Therefore, the DDP in this case is stable.

3. $\{M_x, M_y\} = 0, [\mathcal{S}, M_y] = 0$. In this case, the right mover of the DDP with $\mathcal{S} = M_x = +1$ is mapped to a left mover with $\mathcal{S} = +1, M_x = -1$, which is precisely the left mover of the same Weyl node. One can easily check that the DDP is also mapped to itself under M_y . Therefore, the DDP in this case is also stable.
4. $\{M_x, M_y\} = 0, \{\mathcal{S}, M_y\} = 0$. In this case, the right mover of the DDP with $\mathcal{S} = M_x = -1$ is mapped to a left mover with $\mathcal{S} = M_x = +1$. This implies the existence of a mirror-enforced DDP doublet with trivial mirror charges.

From the above discussions, we find that, out of the four possible scenarios, only the following two cases give rise to a single stable DDP:

1. $[M_x, M_y] = 0, [M_x, \mathcal{S}] = \{M_y, \mathcal{S}\} = 0, \{C_2, \mathcal{S}\} = 0$, and $(C_2)^2 = 1$;
2. $\{M_x, M_y\} = 0, [M_x, \mathcal{S}] = [M_y, \mathcal{S}] = 0, [C_2, \mathcal{S}] = 0$, and $(C_2)^2 = -1$.

These two situations precisely correspond to the two nontrivial classes $D_{2,+,\pm}^+$ and $D_{2,-,-}^-$, respectively. We remark that the above conclusion can also be obtained using an explicit representation of the DDP, as in Hamiltonian (26). As discussed in the previous subsection, there are two different choices of \mathcal{S} and M_x satisfying $[M_x, \mathcal{S}] = 0$. Again, we can take $\mathcal{S} = \gamma_{35}$ and $M_x = \gamma_{14}$ as an example. Given the DDP in Eq. (26), there are two allowed representations for M_y : $M_y = \gamma_{23}$ or $M_y = \gamma_{24}$. One can directly check that these two allowed M_y operations precisely correspond to the above two situations with stable DDPs. In what follows, we will elaborate on the two nontrivial classes and carefully disentangle the relations among the mirror and C_2 topological charges.

1. $D_{2,+,-}^+$

In this case, we have

$$[\mathcal{S}, M_x] = \{\mathcal{S}, M_y\} = 0, \quad \{C_2, \mathcal{S}\} = 0. \quad (53)$$

From the above relations, we conclude that M_y cannot protect stable singularity. Moreover, since $(C_2)^2 = 1$, this corresponds to the D_2 single group with $Q_0^{(2)} \in \mathbb{Z}$. Together with the mirror topological charge $Q_{M_x} \in \mathbb{Z}$, the topological singularities in this case are classified by two integers: $\{Q_0^{(2)}, Q_{M_x}\}$. As it turns out, these two charges are not necessarily equal, but they are not completely independent either.

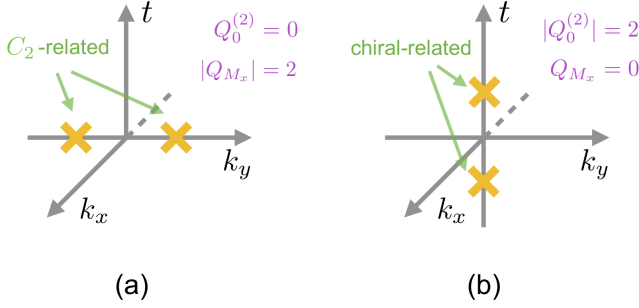


FIG. 12. Relation between $Q_0^{(2)}$ and Q_{M_x} can be seen from inspecting the mobility of a pair of DDPs. (a) A DDP doublet is pinned on the k_y axis by M_x and \mathcal{S} symmetries, but can split along the k_y axis in a C_2 symmetric way. This corresponds to $Q_0^{(2)} = 0$ and $|Q_{M_x}| = 2$. (b) A DDP doublet is pinned on the C_2 -invariant axis, but can split along the t axis in a chiral symmetric way. This corresponds to $|Q_0^{(2)}| = 2$ and $Q_{M_x} = 0$.

To see this, it is instructive to consider two DDPs. While a single DDP must be pinned at the origin by M_x , \mathcal{S} and C_2 symmetries, a pair of DDPs can appear at M_x , chiral, or C_2 -related positions forming a DDP doublet, as shown in Fig. 12. If a pair of DDPs can be symmetrically split along the k_y -axis and yet cannot move along the t -axis as illustrated in Fig. 12(a), it is a C_2 -related DDP doublet. From our previous discussion in Sec. IV, such a group of off-axis DDPs must have $Q_0^{(2)} = 0$. In the meantime, the total mirror charge is nontrivial: $|Q_{M_x}| = 2$, since we essentially have two identical copies of DDP on the k_y axis that are related by C_2 . Similarly, when a pair of DDPs are pinned on the C_2 -invariant axis $k_x = k_y = 0$ and yet can be symmetrically split along the t axis, it forms a chiral-related DDP doublet as illustrated in Fig. 12(b). We instead have $Q_{M_x} = 0$ and $|Q_0^{(2)}| = 2$. Finally, if both DDPs are pinned at the origin, one has $|Q_{M_x}| = |Q_0^{(2)}| = 2$.

Therefore, if a pair of DDPs can be split in some way, we always have $|Q_0^{(2)} + Q_{M_x}| = 2$ and $Q_0^{(2)} Q_{M_x} = 0$. Otherwise, we have $|Q_0^{(2)}| = |Q_{M_x}| = 2$ if no splitting is allowed. This directly leads to the conclusion that

$$Q_{M_x} \equiv Q_0^{(2)} \pmod{2}. \quad (54)$$

Consequently, the set of independent topological charges in this symmetry class is given by

$$\{Q_{M_x}, Q_{M_x} - Q_0^{(2)}\} \in \mathbb{Z} \times 2\mathbb{Z}. \quad (55)$$

$$2. \quad D_{2,-,-}^-$$

In this case, we have

$$[\mathcal{S}, M_x] = [\mathcal{S}, M_y] = 0, \quad [C_2, \mathcal{S}] = 0. \quad (56)$$

This immediately implies that the rotation topological charge is trivial, and that both M_x and M_y can protect stable topological singularities. One can thus assign a pair of mirror topological charges: $\{Q_{M_x}, Q_{M_y}\}$ to characterize the current situation. Moreover, since $(C_2)^2 = -1$, this corresponds to the D_2 double group.

To investigate the relation between Q_{M_x} and Q_{M_y} , let us first notice that for a single DDP, $|Q_{M_x}| = |Q_{M_y}| = 1$, since $Q_{M_x} = \text{sgn}(v_y)$ and $Q_{M_y} = \text{sgn}(v_x)$ for a single DDP taking the form of Eq. (26), as discussed in Sec. VC. For a pair of DDPs, using a similar rationale as in Fig. 12, we find that $Q_{M_x} (Q_{M_y})$ is trivial if the two DDPs can be split symmetrically along the k_x (k_y) axis. Following a similar argument in Sec. VE1, we therefore conclude that

$$Q_{M_x} \equiv Q_{M_y} \pmod{2}. \quad (57)$$

Once again, upon redefining the topological charges as $\{Q_{M_x}, Q_{M_x} - Q_{M_y}\}$, we arrive at the following classification:

$$\{Q_{M_x}, Q_{M_x} - Q_{M_y}\} \in \mathbb{Z} \times 2\mathbb{Z}. \quad (58)$$

F. Classification of D_n -protected topological singularities

Based on the results for D_2 group, we now lay down the following rules for topological charges:

1. For $D_{n,+,-}^\pm$, we always have

$$Q_J^{(n)} \equiv Q_{M_x} \pmod{2}, \quad (59)$$

if $|Q_J^{(n)}|$ indicates the number of DDPs instead of DDP doublets. A similar rule holds for $D_{n,+,+}^\pm$ if we replace M_x with M_{θ_n} .

2. For $D_{n,-,-}^-$, we always have

$$Q_{M_{\theta_n}} \equiv Q_{M_x} \pmod{2} \quad (60)$$

The first rule is based on the observation that a single DDP in class $D_{n,+,-}^\pm$ simultaneously carries rotation and mirror charges with $|Q_{M_x}| = |Q_J^{(n)}| = 1$. This relation can also be understood through a similar argument in Sec. VE1. Therefore, any phase-band singularities that are built from DDPs should always follow the first rule listed above.

The second rule can be intuitively understood for $D_{2,-,-}^-$, since Q_{M_x} and Q_{M_y} of a single DDP explicitly depend on the sign of v_x and v_y , respectively. For $n > 2$, one might naturally expect that $Q_{M_{\theta_n}}$ should exactly equal to Q_{M_x} , given that C_n requires $v_x = v_y$. However, we will argue below that this naive expectation is not true. The simple underlying reason is that for DDPs, the representation of a mirror symmetry sensitively depends on the angular momentum basis.

To see this, we recall that a DDP protected by $D_{n,-,-}^-$ generally admits a phase-band description under the basis $\Psi_J = (|J\rangle, |J+1\rangle, |-J\rangle, |-J-1\rangle)^T$, as shown in Fig. 8(b). For convenience, we now label its rotation and mirror operations as $C_n(J)$ and $M_x(J)$, following the subscript of Ψ_J . In particular, $C_n(J) = \text{diag}(e^{i\frac{2\pi J}{n}}, e^{i\frac{2\pi(J+1)}{n}}, e^{-i\frac{2\pi J}{n}}, e^{-i\frac{2\pi(J+1)}{n}})$. As pointed out in Sec. VB, a single DDP with Ψ_J can exist in $D_{n,-,-}^-$ only when $J = -\frac{1}{2}$ or $J = \frac{n-1}{2}$. As we show in Appendix C, the corresponding mirror symmetries $M_x(-\frac{1}{2})$ and $M_x(\frac{n-1}{2})$ are related by

$$M_x\left(\frac{n-1}{2}\right) = (-1)^{\frac{n}{2}} M_x\left(-\frac{1}{2}\right), \quad (61)$$

On the other hand, since $M_{\theta_n} = C_n M_x$, we have

$$\begin{aligned} M_{\theta_n}\left(\frac{n-1}{2}\right) &= C_n\left(\frac{n-1}{2}\right) M_x\left(\frac{n-1}{2}\right) \\ &= -(-1)^{\frac{n}{2}} C_n\left(-\frac{1}{2}\right) M_x\left(-\frac{1}{2}\right) \\ &= -(-1)^{\frac{n}{2}} M_{\theta_n}\left(-\frac{1}{2}\right), \end{aligned} \quad (62)$$

where we have used the fact that $C_n(\frac{n-1}{2}) = -C_n(-\frac{1}{2})$. This directly leads to

$$\begin{aligned} M_x\left(\frac{n-1}{2}\right) &= (-1)^{\frac{n}{2}} M_x\left(-\frac{1}{2}\right), \\ M_{\theta}\left(\frac{n-1}{2}\right) &= -(-1)^{\frac{n}{2}} M_{\theta}\left(-\frac{1}{2}\right). \end{aligned} \quad (63)$$

Now let us consider two DDPs described by the same effective Hamiltonian (26), under bases $\Psi_{-\frac{1}{2}}$ and $\Psi_{\frac{n-1}{2}}$ respectively. Suppose the DDP under $\Psi_{-\frac{1}{2}}$ carries $Q_{M_x} = Q_{M_{\theta_n}} = 1$. Then the DDP under $\Psi_{\frac{n-1}{2}}$ will instead carry $Q_{M_x} = -Q_{M_{\theta_n}} = (-1)^{\frac{n}{2}}$, based on Eq. (63). This is because the sign of the mirror topological charge as defined in Eq. (51) relies on the explicit representation of the mirror symmetry. Namely, if we add a minus sign to the mirror representation, we also need to flip the corresponding mirror charge. This is why we have the “modulo 2” relation for the mirror charges in Eq. (60), instead of a naive equality.

Equipped with the above principles, it is quite straightforward to read off the classification for phase-band singularities from our list in Sec. VD. In particular, whenever two charges Q and Q' satisfy $Q \equiv Q' \pmod{2}$, we denote their contribution to the classification as $\{Q, Q - Q'\} \in \mathbb{Z} \times 2\mathbb{Z}$. For example, class $D_{4,+,-}^-$ has a classification: $\{Q_{M_x}, Q_{M_x} - Q_{\frac{1}{2}}^{(4)}\} \in \mathbb{Z} \times 2\mathbb{Z}$, and class $D_{6,+,-}^+$ has a classification: $\{Q_{M_x}, Q_0^{(6)}, Q_{M_x} - Q_1^{(6)}\} \in \mathbb{Z}^2 \times 2\mathbb{Z}$. The reason we only include $Q_1^{(6)}$ in the subtraction is that $Q_0^{(6)}$ only accounts for DDP doublets with a trivial mirror charge. Similarly, the second rule requires that class $D_{4,-,-}^-$ has a classification: $\{Q_{M_x}, Q_{M_x} - Q_{M_{\frac{3}{4}}}\} \in$

$\mathbb{Z} \times 2\mathbb{Z}$, and class $D_{6,-,-}^-$ likewise has a classification: $\{Q_{M_x}, Q_{M_x} - Q_{M_{\frac{5}{6}}}\} \in \mathbb{Z} \times 2\mathbb{Z}$.

We are now finally in the position to summarize our full classification of topological singularities for all two-dimensional point groups. We summarize our results in Table I.

VI. BULK-BOUNDARY CORRESPONDENCE & HIGHER-ORDER TOPOLOGICAL INDICES

In this section, we establish a higher-order bulk-boundary correspondence, by relating the bulk phase-band singularities to symmetry-protected corner modes in systems with open boundary, which is a defining boundary signature of 2D AFHOTIs. Such a PBDR procedure extends the idea of dimensional reduction, which was previously developed for classifying static crystalline symmetry-protected topological states. As explained in Sec. IIE, the key step in our PBDR approach is to reduce the original 3D phase-band singularities to 2D singularities characterizing the end modes of the resultant 1D chains after the reduction. This is achieved by introducing globally symmetry-preserving mass domain walls for the original 3D phase-band singularities. The 2D phase-band singularities will thus manifest themselves as domain wall modes after PBDR. The end modes of the resulting 1D AFTI that survive will correspond to robust corner modes in the original 2D system. This allows us to establish the higher-order bulk-boundary correspondence for 2D AFHOTIs protected by point group symmetries.

In what follows, we shall start by classifying general C_n -protected AFHOTIs with rotation topological charges to illustrate our PBDR procedure. This also allows us to construct the corresponding higher-order topological indices. A similar analysis is then performed to D_1 -protected AFHOTIs with a single mirror symmetry. Next, we proceed to consider D_2 group as a case study for the more complicated D_n groups, where the interplay between rotation and mirror charges needs to be carefully disentangled in order to predict the correct boundary features and construct the topological indices. Finally, we provide a general discussion on the classification of AFHOTIs for all D_n groups, as well as the required boundary geometry in order to observe the desired boundary features.

A. Classification of C_n -protected AFHOTIs

1. Dimensional reduction

As discussed in Sec. IV, the topological singularities protected by C_n symmetry are DWPs carrying nontrivial rotation charges. We shall now exemplify our PBDR scheme by coupling a 3D DWP to a spatially-varying mass term that respects C_n symmetry globally, and explicitly solving for the resultant 2D domain wall modes.

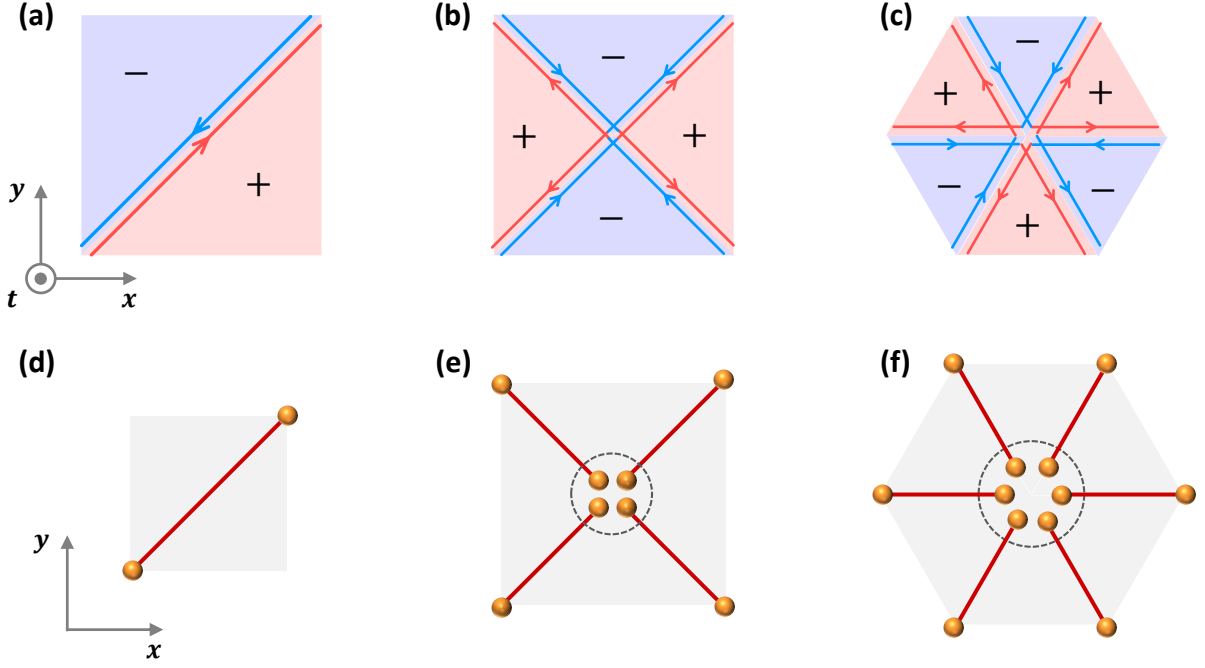


FIG. 13. (a), (b), and (c) show the pattern of mass domain walls to achieve the PBDR for C_2 , C_4 , and C_6 -symmetric systems, respectively. The “ \pm ” labels the sign of the mass term $m(r, \theta)$ in Eq. (65). The colored arrows along the mass domain walls represent the chiral-protected domain wall modes, which are 2D Dirac nodes. (d)-(f) Accordingly, the original 2D Floquet systems are reduced to a collection of symmetry related 1D AFTIs with end modes (depicted as golden dots). End modes residing in the bulk of the system encircled by black dashed lines can be adiabatically eliminated.

Let us recall that a single C_n -protected DWP is described by the following Dirac Hamiltonian:

$$h_d = v_x k_x \gamma_1 - v_y k_y \gamma_2 + v_t t \gamma_5, \quad (64)$$

where the chiral symmetry $\mathcal{S} = \gamma_{45}$, n -fold rotation symmetry $C_n = e^{i\frac{2\pi}{n}\mathcal{J}_z}$ with $\mathcal{J}_z = \text{diag}(J, J+1, J+\frac{n}{2}, J+\frac{n}{2}+1)$, and $v_x = v_y \equiv v_k$ is required for $n > 2$. Under this basis, the rotation charge of this DWP is defined as $Q_J^{(n)} = -\text{sgn}(v_t)$. To gap out this DWP, the only \mathcal{S} -preserving constant mass term is $h_m = m\gamma_3$, which necessarily breaks rotation symmetry since $\{C_n, \gamma_3\} = 0$. Nevertheless, it is possible to add a spatially-varying mass term $h_m(\mathbf{r}) = m(\mathbf{r})\gamma_3$, such that C_n symmetry is preserved globally. For example, we can take $m(\mathbf{r})$ to have the following spatial dependence:

$$m(r, \theta) = m_0 \text{sgn} \left[\cos \left(\frac{n}{2}(\theta + \theta_0) \right) \right], \quad (65)$$

where $\theta = \tan^{-1}(y/x)$ and $r = \sqrt{x^2 + y^2}$ are the polar coordinates, and θ_0 is an arbitrary constant parameter. In particular, $m(r, \theta)$ flips its sign under a C_n operation: $m(r, \theta + \frac{2\pi}{n}) = -m(r, \theta)$, which directly cancels the additional sign flip from $\{C_n, \gamma_3\} = 0$ and leads to $[C_n, h_m(\mathbf{r})] = 0$. Thus, $h_m(\mathbf{r})$ globally preserves C_n symmetry [see Fig. 13(a)-(c)].

However, the singularity in the phase band is not completely eliminated by $h_m(\mathbf{r})$, since the mass term is forced

to vanish when

$$\theta = \theta_m = \frac{(2m+1)\pi}{n} - \theta_0, \quad \forall m \in \mathbb{Z}. \quad (66)$$

From a different perspective, $h_m(\mathbf{r})$ flips its sign across $\theta = \theta_m$, forming a mass domain wall for the DWP at every θ_m , which necessarily binds 2D domain wall modes.

As an example, we consider a single mass domain wall at $\theta = 0$ (i.e. parallel to x -axis) by choosing $\theta_0 = \pi/n$. In the presence of such a domain wall, the Hamiltonian for the DWP now becomes

$$\tilde{h}_d = v_x k_x \gamma_1 - v_y k_y \gamma_2 + v_t t \gamma_5 + m_0 \text{sgn}(y) \gamma_3. \quad (67)$$

The domain wall modes can be analytically solved from the zero-mode equation $\tilde{h}_d |\psi\rangle = 0$ at $k_x = t = 0$. Substituting $k_y \rightarrow -i\partial_y$, this becomes a differential equation:

$$[v_y \partial_y + m_0 \text{sgn}(y) \gamma_{23}] \psi = 0. \quad (68)$$

Consider an ansatz solution $\psi = f(y)\xi_s$, where ξ_s is an eigenstate of γ_{23} with eigenvalue $s = \pm 1$: $\gamma_{23}\xi_s = s\xi_s$. Then, $f(y)$, the spatial part of ψ , can be easily solved as

$$f(y) = \mathcal{N} e^{-s \frac{m_0}{v_y} |y|}, \quad (69)$$

where \mathcal{N} is the normalization factor. To obtain a normalizable solution, we require $m_0 v_y s > 0$, or equivalently, $s = \text{sgn}(m_0 v_y)$. In other words, the choice of eigenstate ξ_{\pm} is determined by the sign of $m_0 v_y$.

By projecting \tilde{h}_d onto the two eigenbases of ξ_s , we obtain the effective Hamiltonian for the domain wall modes

$$h_{\text{dw},s} = v_x k_x \sigma_z + v_t t \sigma_x, \quad (70)$$

which describes a massless 2D Dirac node in (k_x, t) -space, as anticipated. The projected chiral symmetry is given by

$$\tilde{\mathcal{S}}_s = s \sigma_z. \quad (71)$$

This indicates that for whichever choice of $s = \pm 1$, the left and right movers of the domain wall mode (70) always carry opposite chiral eigenvalues. Therefore, this domain wall mode is protected by chiral symmetry and carries a chiral topological charge

$$\mathcal{N}_S = \text{sgn}(m_0 v_x v_y). \quad (72)$$

As discussed in Sec. III, such a nonzero \mathcal{N}_S for the chiral-protected 2D Dirac point is precisely the topological invariant for 1D AFTI in class AIII. This also implies that the resultant 1D chain must carry a single chiral-protected edge mode at each endpoint, when the original 2D system has a single DWP. This result directly applies to other C_n -related domain walls, which indicates that a 2D class AIII Floquet system with C_n -protected phase-band singularities is adiabatically equivalent to C_n -symmetric arrays of 1D class AIII AFTIs.

2. Bulk-boundary correspondence & topological indices

Next, we shall study the number of robust end modes of the 1D chains after dimensional reduction using the chiral winding number \mathcal{N}_S , and establish a bulk-boundary correspondence by relating the corner mode counting to the bulk C_n topological charges. Fig. 13(d)-(f) shows the resultant C_n -invariant arrays after dimensional reduction, along with their end modes. End modes that are close together in the bulk of the system can be adiabatically eliminated due to their finite spatial overlaps in the wavefunctions, whereas those that reside at C_n -related corners correspond to the corner modes of the original 2D systems. Since these corner modes are protected by a nonzero \mathcal{N}_S that arises from bulk singularities and are further distributed spatially in a C_n -symmetric way, they cannot be eliminated by any C_n symmetric perturbations without closing the bulk Floquet gap. We thus conclude that a 2D Floquet system with C_n and chiral symmetry must be an AFHOTI with n C_n -related corner modes, if there is a single phase band DWP.

To examine the robustness of the corners modes when there are multiple DWPs in the system, we now proceed to consider the boundary physics in the presence of two DWPs. We shall work out an explicit example of C_2 -protected AFHOTIs, and the arguments therein apply to C_4 and C_6 symmetries as well. Since the resultant 2D singularity no longer carries any information about the

angular momentum J of the rotation charge $Q_J^{(n)}$, such two DWPs can carry rotation charges $Q_{J_1}^{(n)}$ and $Q_{J_2}^{(n)}$ with either $J_1 = J_2$ or $J_1 \neq J_2$, as long as they do not annihilate one another. Such a double-DWP can be described by the phase-band Hamiltonian

$$h_{d \times 2} = \mu_0 \otimes h_d, \quad (73)$$

where h_d follows the definition in Eq. (64), and $\mu_{0,x,y,z}$ are Pauli matrices for the valley degrees of freedom associated with the two DWPs. The symmetries for this double-DWP system are given by $\mathcal{S} = \mu_0 \otimes \gamma_{45}$, and $C_2 = \mu_0 \otimes \gamma_5$, accordingly. We find four distinct C_2 and chiral symmetric mass terms for the DWPs:

$$h_{m \times 2} = m(\mathbf{r}) \mu_{0,x,y,z} \otimes \gamma_3 \equiv m(\mathbf{r}) M, \quad (74)$$

where $m(\mathbf{r}) = m_0 \text{sgn}[\cos(\theta + \theta_0)]$ describes a mass domain wall at $\theta = \frac{\pi}{2} - \theta_0$. However, as shown in Fig. 14, different choices of the mass matrix M in $h_{m \times 2}$ above lead to distinct domain wall physics, which eventually leads to distinct corner-mode configurations:

- (i) $M = \mu_0 \otimes \gamma_3$: The domain wall modes carry $\mathcal{N}_S = \pm 2$. The sign of \mathcal{N}_S again depends on $\text{sgn}(m_0 v_x v_y)$. The 2D system hosts two corner modes at each of the two C_2 -related corners;
- (ii) $M = \mu_{x,y,z} \otimes \gamma_3$: The domain wall modes have $\mathcal{N}_S = 0$ and thus can be gapped out. The 2D system has no protected corner mode.

Therefore, by two adiabatic deformations of the same Floquet system, we end up with scenarios with either zero or two corner modes. However, these two reduction schemes are both adiabatically connected to the same original 2D system, hence the two seemingly distinct boundary features must correspond to the same bulk phase. In other words, these two different boundary configurations can be converted from one to the other without closing the bulk gap. Indeed, as we demonstrate in Fig. 14 explicitly, the two corner modes in case (i) above can be removed by symmetrically attaching 1D AFTIs on the boundary. This implies that the number of C_2 -protected corner-modes is only well-defined modulo 2 at a single corner. Similar arguments can be directly applied to C_4 and C_6 Floquet systems with double DWPs. Therefore, we have shown that

- 2d C_n -protected AFHOTIs admit a \mathbb{Z}_2 topological classification.

The final step is to construct a topological index that counts the number of robust corner modes. As we have seen from the above examples, the chiral charge \mathcal{N}_S and hence the number of corner modes only cares about the number of net DWPs, but not the explicit values of their topological charges $Q_J^{(n)}$ or the angular momentum J . For example, a spinless C_4 -symmetric system having three DWPs with $Q_0^{(4)} = -1$ and $Q_1^{(4)} = 2$ has

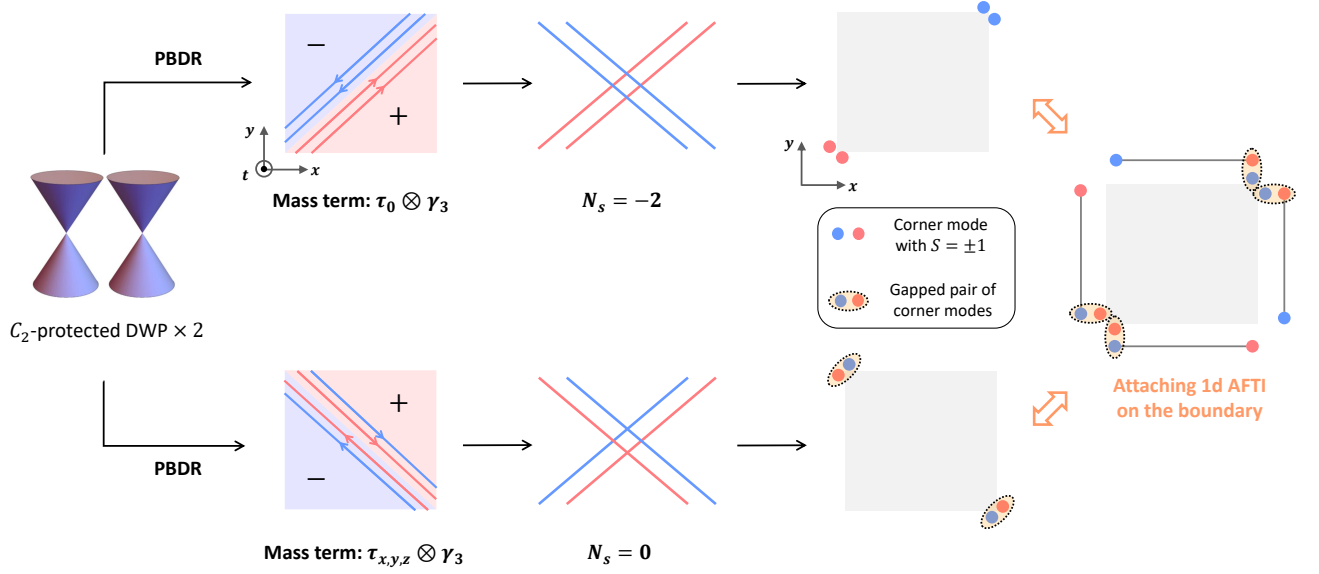


FIG. 14. Starting from two C_2 -protected DWPs, there exist two classes of mass terms in the PBDR procedure giving rise to 2D Dirac nodes carrying different chiral charges \mathcal{N}_S . This further leads to two seemingly distinct corner mode patterns: zero or two corner modes at each corner. These two corner mode patterns correspond to the same bulk phase, and hence can be transformed to one another by symmetrically attaching 1D AFTIs on the boundary, without closing the bulk gap. This demonstrates the \mathbb{Z}_2 classification of general C_n -protected AFHOTIs.

the same boundary feature as any other system with $(Q_0^{(4)}, Q_1^{(4)}) = (l_1, l_2)$, where $l_{1,2} \in \mathbb{Z}$ and $l_1 + l_2 \equiv 1 \pmod{2}$. Therefore, we define the following \mathbb{Z}_2 corner mode index for C_n -symmetric AFHOTIs as the higher-order topological index:

$$\nu_n \equiv \sum_J |Q_J^{(n)}| \pmod{2}, \quad (75)$$

The value of ν_n directly indicates the presence ($\nu_n = 1$) or absence ($\nu_n = 0$) of robust corner mode at each corner. We will provide more examples to illustrate the \mathbb{Z}_2 corner mode index in Sec. VII.

B. Classification of D_1 -protected AFHOTIs

In Sec. VC, we have shown that the phase-band singularity protected by M_x symmetry alone (i.e. D_1 group) is essentially a single Dirac node that can move freely along k_y axis at $(k_x, t) = (0/\pi, \frac{T}{2})$. We show in this subsection how mirror-protected corner modes are related to the mirror topological charge Q_{M_x} , via our PBDR analysis.

1. Dimensional reduction

Consider again the Dirac Hamiltonian (64) now describing a DDP protected by mirror symmetry. As in Sec. VC, we take the chiral symmetry $\mathcal{S} = \gamma_{45}$ and $M_x = \gamma_{13}$, so that $[M_x, \mathcal{S}] = 0$ is satisfied and Q_{M_x} is

nontrivial. Since the $(\mathcal{S}, M_x) = (+, +)$ branch propagates along the $\text{sgn}(v_y)\hat{y}$ direction as shown in Fig. 9, we have $Q_{M_x} = \text{sgn}(v_y)$.

To perform the PBDR, we choose the following M_x -symmetric mass term:

$$h_m(\mathbf{r}) = m_0 \text{sgn}(x)\gamma_3, \quad (76)$$

which creates a mass domain wall along the y -axis. At $k_y = t = 0$, the zero-mode equation is given by

$$[v_x \partial_x - m_0 \text{sgn}(x)\gamma_{13}]\psi = 0. \quad (77)$$

Consider an ansatz solution for the zero-mode wavefunction $\psi = f(x)\xi_s$, where ξ_s is an eigenstate of γ_{13} with eigenvalue $s = \pm 1$: $\gamma_{13}\xi_s = s\xi_s$. Then the spatial part can be solved as $f(x) = \mathcal{N}e^{s\frac{m_0}{v_x}|x|}$, where \mathcal{N} is the normalization factor. The condition for a normalizable wavefunction is given by $m_0 v_x s < 0$, which can be rewritten as

$$s = -\text{sgn}(m_0 v_x). \quad (78)$$

Upon projecting onto the ξ_s basis, we obtain the effective Hamiltonian for the domain wall mode

$$\tilde{h}_{\text{dw},s} = -v_y k_y \sigma_z - v_t t \sigma_x, \quad (79)$$

and the projected symmetries:

$$\tilde{\mathcal{S}}_s = -s\sigma_z, \quad \tilde{M}_x = s\sigma_0. \quad (80)$$

Then the chiral charge for the domain wall fermion is given by

$$\mathcal{N}_S = \text{sgn}(sv_y) = -\text{sgn}(m_0 v_x v_y) = sQ_{M_x}, \quad (81)$$

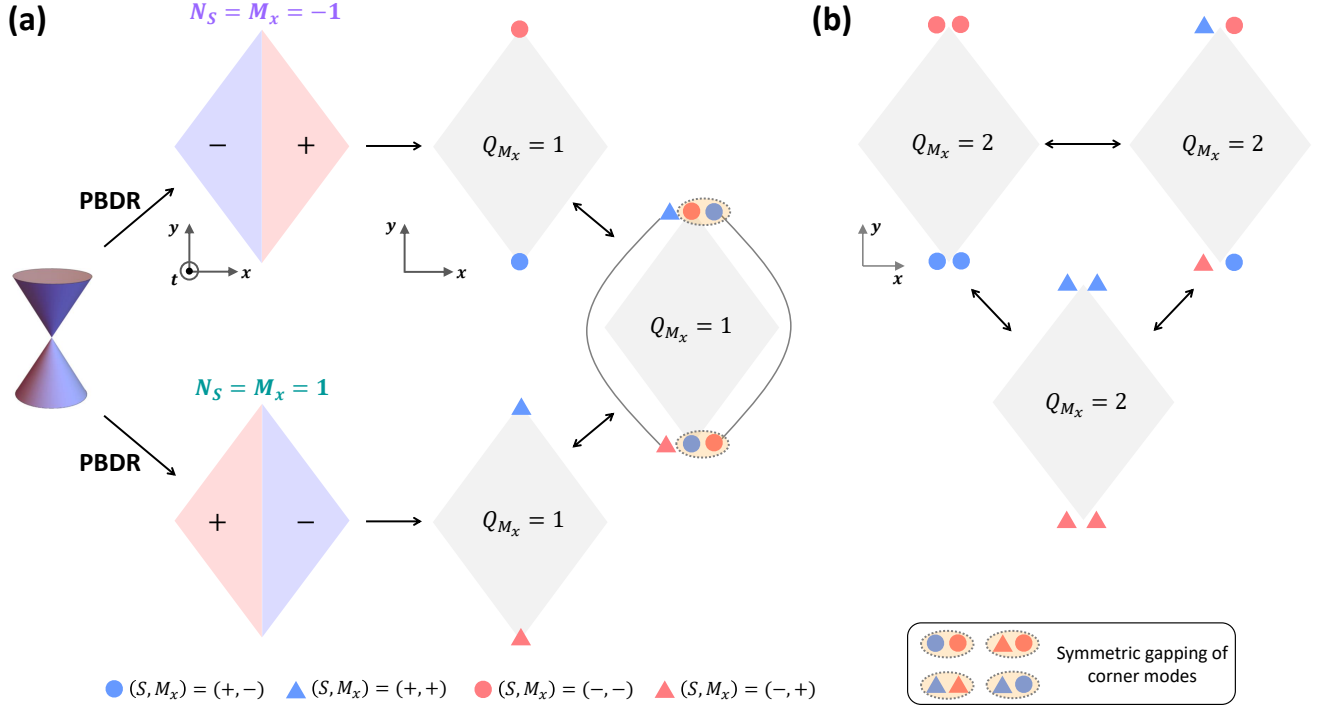


FIG. 15. (a) Starting from a single DDP with $Q_{M_x} = 1$, there exist two distinct corner mode patterns via PBDR (we take $v_x v_y > 0$), which correspond to the same bulk phase and can be connected to one another by symmetrically attaching 1D AFTIs at the boundary. The colors of the corner modes indicate their chiral eigenvalues: $S = +1$ (blue), and $S = -1$ (red). The shapes of the corner modes indicate their mirror eigenvalues: $\tilde{M}_x = +1$ (triangle), and $\tilde{M}_x = -1$ (circle). Pairs of corner modes can annihilate one another if their net mirror charge Q_{M_x} is zero. Since $Q_{M_x} = \mathcal{N}_S \tilde{M}_x$, there are four such possibilities, which we circle in dashed lines. (b) Three topologically equivalent corner mode configurations for $Q_{M_x} = 2$, which can be transformed to one another by symmetrically attaching 1D AFTIs at the boundary.

However, a key difference from the previously discussed C_n case is that, the domain wall mode here carries an additional mirror index. The projected mirror eigenvalue \tilde{M}_x satisfies

$$\tilde{M}_x = s = \mathcal{N}_S Q_{M_x}, \quad (82)$$

which relates the bulk mirror charge to the topological indices of the domain wall mode. This relation is the key to understand the bulk-boundary correspondence for D_1 -protected AFHOTIs.

2. Bulk-boundary correspondence & topological indices

According to Eq. (82), starting from a M_x -protected DDP with $Q_{M_x} = 1$, there are two phenomenologically distinct scenarios for the domain wall modes characterized by different $(\mathcal{N}_S, \tilde{M}_x)$ indices, namely, $(\mathcal{N}_S, \tilde{M}_x) = (+1, +1)$ or $(\mathcal{N}_S, \tilde{M}_x) = (-1, -1)$. Although both cases lead to a single corner mode located at each M_x -invariant corner, the corner modes in these two cases carry distinct S and \tilde{M}_x indices, as shown in Fig. 15(a). However, since these two cases are both adiabatically connected to the same original 2D system, they correspond to the same

bulk phase. As expected, these two corner mode configurations can be transformed from one to the other by symmetrically attaching 1D AFTIs on the boundary without closing the bulk gap, as shown in Fig. 15(a).

Similarly, for two identical M_x -protected Dirac points (i.e. $Q_{M_x} = \pm 2$), there exist three topologically equivalent corner mode configurations that can be generated via the PBDR procedure, as shown in Fig. 15(b). These three configurations correspond to all possible combinations of corner mode configurations shown in Fig. 15(a) for a single DDP. We emphasize that, unlike C_n -protected AFHOTIs, it is not possible to adiabatically eliminate the two M_x -protected corner modes when $Q_{M_x} = \pm 2$. Instead, attaching a pair of mirror-related 1D AFTIs to the system's boundary can only switch among the three corner mode configurations shown in Fig. 15(b).

We have shown that for both single and double DDPs, $|Q_{M_x}|$ directly indicates the number of robust corner modes at each mirror-invariant corner. Systems with $\pm Q_{M_x}$, although harboring the same number of corner modes, are topologically distinct. This is because their corner modes carry distinct S and \tilde{M}_x indices, and hence cannot be adiabatically connected to one another. There-

fore, we conclude that

- $Q_{M_x} \in \mathbb{Z}$ is the topological index for 2D D_1 -protected AFHOTIs.

C. D_2 -protected AFHOTIs

In this subsection, we shall use D_2 -protected AFHOTIs as a case study to demonstrate the general principles for characterizing and classifying D_n -protected AFHOTIs. According to our previous discussions, there are two nontrivial classes with D_2 symmetry: $D_{2,+,\pm}^+$ and $D_{2,-,-}^-$, both having a $\mathbb{Z} \times 2\mathbb{Z}$ classified phase-band singularities.

1. $D_{2,+,\pm}^+$

In Sec. VE 1, we have shown that the phase-band singularities for $D_{2,+,-}^+$ are characterized by a pair of topological charges $\{Q_{M_x}, Q_0^{(2)}\}$ satisfying $Q_0^{(2)} \equiv Q_{M_x} \pmod{2}$. Therefore, the bulk-boundary correspondence here can be directly understood based our results in Sec. IV and Sec. VC for systems with C_2 and M_x symmetries, respectively.

First of all, *any corner mode at a generic, locally M_x -breaking corner can always be gapped out*. To see this, let us consider a system on a rhombus geometry with two x -corners and two y -corners. Assuming the existence of a corner mode with chiral eigenvalue $\mathcal{S} = 1$ at the left x -corner, its mirror partner at the right x -corner must also carry $\mathcal{S} = 1$, since $[M_x, \mathcal{S}] = 0$. However, since $\{C_2, \mathcal{S}\} = 0$, the C_2 -partner of the left x -corner mode gives rise to another corner mode carrying $\mathcal{S} = -1$ at the right x -corner. Therefore, corner modes at every generic corner must come in pairs with opposite \mathcal{S} eigenvalues, which can always be eliminated together.

As a result, the only robust corner modes must reside at M_x -invariant corners, which are solely accounted for by the mirror topological charge, instead of the rotation charges. We conclude that

- the topological index for class $D_{2,+,-}^+$ AFHOTIs is $Q_{M_x} \in \mathbb{Z}$.

The above conclusion can be understood in a formal yet simpler way. Symmetry protected corner modes can only arise from the following topological indices: the C_2 corner mode index $\nu_2 \in \mathbb{Z}_2$ and the mirror charge $Q_{M_x} \in \mathbb{Z}$. Since $\nu_2 \equiv |Q_0^{(2)}| \equiv Q_{M_x} \pmod{2}$, the resulting higher-order topological classification is then

$$(\mathbb{Z}_2 \times \mathbb{Z})/\mathbb{Z}_2 = \mathbb{Z}, \quad (83)$$

which agrees with our previous physical argument. Notably, if we explicitly break M_x while preserving C_2 , the system is now characterized by the C_2 corner mode index ν_2 alone. Therefore, if there were originally an odd number of corner modes before M_x was broken, a single

corner mode at each corner can still survive after breaking M_x . This corner mode can then be symmetrically shifted to generic M_x breaking and C_2 related corners, and remains protected by ν_2 .

Similarly, class $D_{2,+,\pm}^+$ is equivalent to $D_{2,+,-}^+$ with M_x replaced by M_y , and hence is also classified by $Q_{M_y} \in \mathbb{Z}$, hosting robust corner modes at M_y invariant corners.

2. $D_{2,-,-}^-$

Class $D_{2,-,-}^-$ has two nontrivial mirror charges $\{Q_{M_x}, Q_{M_y}\}$ satisfying $Q_{M_x} \equiv Q_{M_y} \pmod{2}$. Therefore, both mirrors can protect their own corner modes at the corresponding mirror-invariant corners. Based on our previous discussions, it is straightforward to conclude that

- AFHOTIs belonging to class $D_{2,-,-}^-$ are characterized by $(Q_{M_x}, Q_{M_x} - Q_{M_y}) \in \mathbb{Z} \times 2\mathbb{Z}$.

The physical meaning of the $\mathbb{Z} \times 2\mathbb{Z}$ classification is that *the number of corner modes at each M_x -invariant corner must equal to that at each M_y -invariant corner, modulo 2*. We shall now demonstrate this classification explicitly following the PBDR procedure.

In Fig. 16(a), we show the possible mass domain wall patterns for a single DDP described by Hamiltonian (64) with $(Q_{M_x}, Q_{M_y}) = (1, 1)$. For example, we again take $\mathcal{S} = \gamma_{45}$, $M_x = \gamma_{13}$, and $M_y = \gamma_{23}$, consistent with $D_{2,-,-}^-$. Then, a globally mirror symmetric mass domain wall can be generated by coupling to a mass term $h_m(\mathbf{r}) = m_0 \text{sgn}(xy)\gamma_3$. We obtain two topologically equivalent corner mode configurations (with $m_0 > 0$ and $m_0 < 0$), hosting one mode at each corner with different \mathcal{S} , M_x/M_y eigenvalues. To further demonstrate that the number of modes at each M_x -invariant corner is equal to that at each M_y -invariant corner modulo two, in Fig. 16(b)&(c) we stack our original system $(Q_{M_x}, Q_{M_y}) = (1, 1)$ with another system with $(Q_{M_x}, Q_{M_y}) = (1, \pm 1)$ respectively. Indeed, we arrive at two different corner mode configurations with two modes at each M_x -invariant corner, which corresponds to $Q_{M_x} = 2$. The number of corner modes at each M_y -invariant corner is either two, indicating $Q_{M_y} = 2$; or zero, indicating $Q_{M_y} = 0$. Therefore, we have demonstrated the $\mathbb{Z} \times 2\mathbb{Z}$ classification for class $D_{2,-,-}^-$ AFHOTIs with two inequivalent mirror charges.

D. Classifying general D_n -protected AFHOTIs

1. Guidelines for classifying D_n -protected AFHOTIs

Now we are ready to summarize the general rules for classifying higher-order topology as well as establishing the bulk-boundary correspondence for all D_n -protected AFHOTIs:

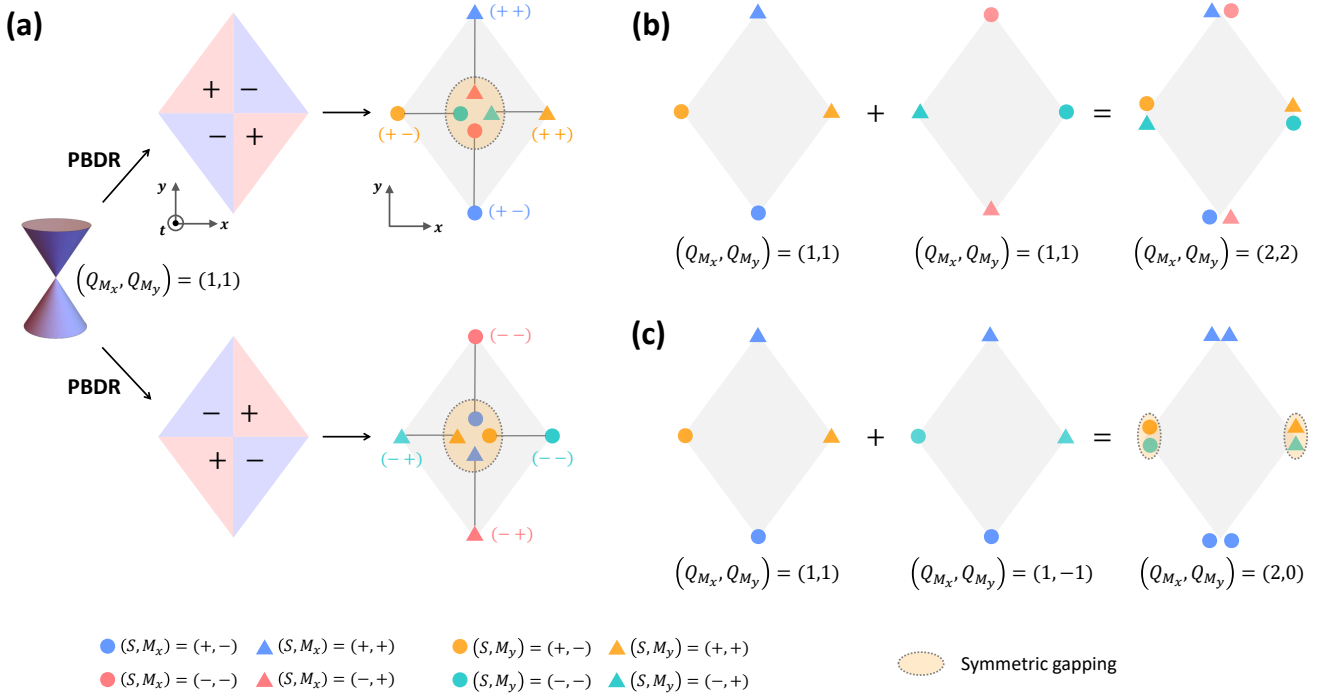


FIG. 16. (a) Two possible domain wall and corner mode patterns generated from a D_2 -protected DDP with $(Q_{M_x}, Q_{M_y}) = (1, 1)$ under PBDR, where we take $v_x v_y > 0$ for definiteness. The chiral and mirror eigenvalues can be read off from the results shown in Fig. 15, and we use the same convention for the shape and color of each corner mode as in Fig. 15. (b) Coupling two systems with $(Q_{M_x}, Q_{M_y}) = (1, 1)$ and $(Q_{M_x}, Q_{M_y}) = (1, 1)$ leads to a net mirror charge of $(Q_{M_x}, Q_{M_y}) = (2, 2)$, which agrees with the presence of two stable corner modes at each M_x or M_y -invariant corner. (c) Coupling two systems with $(Q_{M_x}, Q_{M_y}) = (1, 1)$ and $(Q_{M_x}, Q_{M_y}) = (1, -1)$ leads to a net mirror charge of $(Q_{M_x}, Q_{M_y}) = (2, 0)$. In this case, two robust corner modes only show up at M_x -invariant corners, which is also consistent with the net mirror charges. Similarly to Fig. 15, two corner modes that are close together can be symmetrically gapped out only if they have the same color (chiral eigenvalues) but different shapes (mirror eigenvalues), or vice versa.

- (i) If a C_n topological charge $Q_J^{(n)}$ leads to DDP doublets, it does not contribute to C_n -protected corner modes;
- (ii) If a C_n topological charge $Q_J^{(n)}$ and a mirror topological charge Q_M coexist and satisfy

$$Q_J^{(n)} \equiv Q_M \pmod{2}, \quad (84)$$

they together contribute \mathbb{Z} to the classification, which is solely determined by the value of Q_M ;

- (iii) If two inequivalent mirror topological charges Q_M and $Q_{M'}$ coexist and satisfy

$$Q_M \equiv Q_{M'} \pmod{2}, \quad (85)$$

they together contribute $\mathbb{Z} \times 2\mathbb{Z}$ to the topological classification.

Let us briefly explain the above rules. Based on our discussions of C_n -symmetric AFHOTIs in Sec. VIA, it is straightforward to see that a DDP doublet will always lead to an even number of corner modes at each corner,

which is trivial due to the \mathbb{Z}_2 classification. For the second rule, one can use the argument in Sec. VIC to show that the net contribution from $\{Q_J^{(n)}\}$ and Q_{M_x} to the higher-order topology is $(\mathbb{Z} \times \mathbb{Z}_2)/\mathbb{Z}_2 = \mathbb{Z}$. The third rule directly follows from our results for $D_{2,-,-}$ in Sec. VIC.

2. Higher-order topological indices for D_n -protected AFHOTIs

Combining the above general rules and the classification of phase-band singularities in Sec. V, we are now in place to list our classification results for all D_n -protected AFHOTIs, along with the corresponding topological indices as follows:

- D_1 group: $D_{1,-,-}^\pm$: $Q_{M_x} \in \mathbb{Z}$;
- D_2 group:
 1. $D_{2,+,\pm}^+$: $Q_{M_x} \in \mathbb{Z}$;
 2. $D_{2,+,\pm}^-$: trivial;
 3. $D_{2,-,\pm}^+$: trivial;

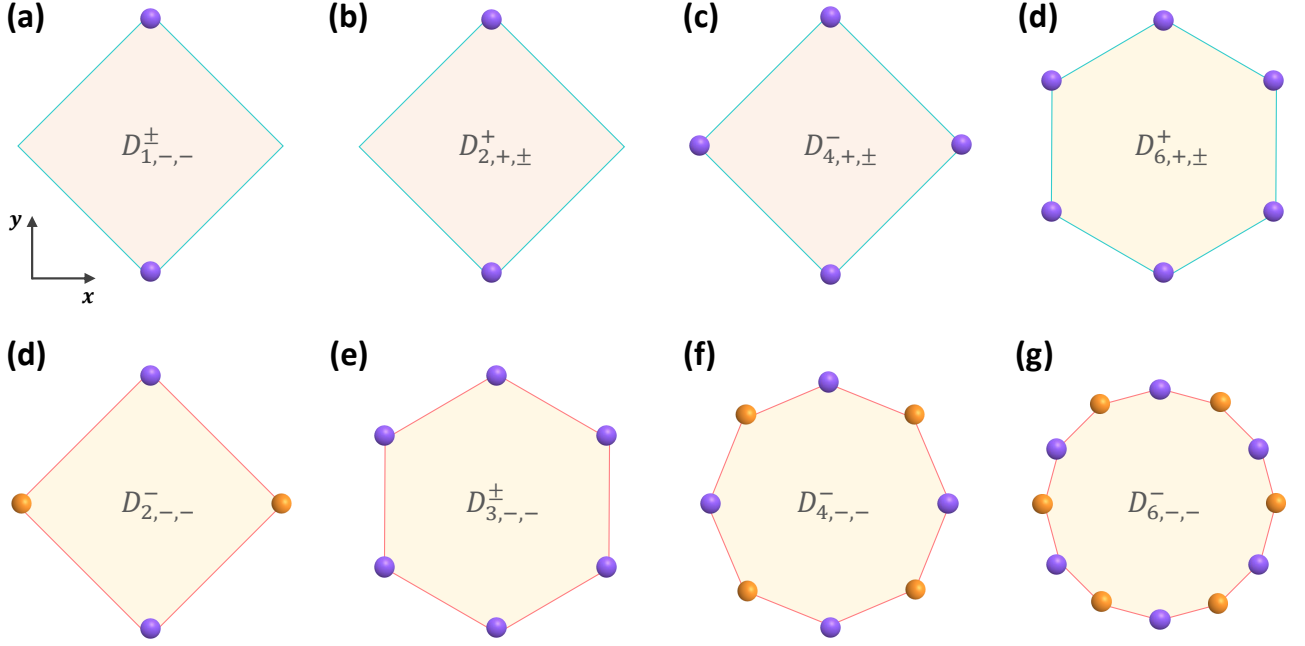


FIG. 17. Schematics of corner mode patterns for all nontrivial D_n classes on appropriately chosen boundary geometries. Corner modes are denoted by spheres, and the different colors denote corner modes protected by two inequivalent mirrors M_x and M' respectively.

- 4. $D_{2,-,-}^-: \{Q_{M_x}, Q_{M_x} - Q_{M_y}\} \in \mathbb{Z} \times 2\mathbb{Z}$;
- D_3 group: $D_{3,-,-}^\pm: Q_{M_x} \in \mathbb{Z}$;
- D_4 group:
 1. $D_{4,+, \pm}^+$: trivial;
 2. $D_{4,+, \pm}^-: Q_{M_x} \in \mathbb{Z}$;
 3. $D_{4,-,-}^+$: trivial;
 4. $D_{4,-,-}^-: \{Q_{M_x}, Q_{M_x} - Q_{M_{\frac{\pi}{4}}}\} \in \mathbb{Z} \times 2\mathbb{Z}$;
- D_6 group:
 1. $D_{6,+, \pm}^+: Q_{M_x} \in \mathbb{Z}$;
 2. $D_{6,+, \pm}^-: \text{trivial}$;
 3. $D_{6,-,-}^+: \text{trivial}$;
 4. $D_{6,-,-}^-: \{Q_{M_x}, Q_{M_x} - Q_{M_{\frac{\pi}{3}}}\} \in \mathbb{Z} \times 2\mathbb{Z}$.

Here we have ignored classes $D_{n,-,+}^\pm$, which do not have any robust topological singularities.

Let us make a few remarks on the above results. First of all, despite having nontrivial rotation charges, $D_{4,+, \pm}^+$ and $D_{6,+, \pm}^+$ admit a trivial topological classification since their rotation topological charges always lead to DDP doublets. Secondly, the higher-order topological classification for $D_{6,+, \pm}^+$ is reduced to \mathbb{Z} , even though the corresponding topological singularities are characterized

by $\{Q_0^{(6)}, Q_{M_x}, Q_{M_x} - Q_1^{(6)}\} \in \mathbb{Z}^2 \times 2\mathbb{Z}$. This is simply because (i) $Q_0^{(6)}$ always leads to DDP doublets; (ii) $Q_1^{(6)} \equiv Q_{M_x} \pmod{2}$. Then based on the second rule listed above, the only topological index in this case is $D_{6,+, \pm}^+$ is $Q_{M_x} \in \mathbb{Z}$.

We summarize the full classification of D_n -protected AFHOTIs in Table II.

3. Boundary geometry for observing all symmetry-protected corner modes

Since all nontrivial D_n -protected AFHOTIs are characterized solely by the mirror topological charges, we conclude that robust corner modes can only live on the mirror-invariant corners of a D_n -protected AFHOTI. Indeed, following a similar argument for D_2 symmetry in Sec. VIC, one can easily show that corner modes appearing on a generic mirror-breaking corner always come in pairs, and thus are unstable for a general D_n group.

As a result, a \mathbb{Z} -classified D_n -protected AFHOTI will host robust corner modes on its M_x -invariant corners, as well as all other corners that are related to the M_x -symmetric corners via C_n rotations. According to our classification in Table II, this includes classes $D_{1,-,-}^\pm$, $D_{2,+, \pm}^\pm$, $D_{3,-,-}^\pm$, $D_{4,+, \pm}^\pm$, and $D_{6,+, \pm}^\pm$ in D_n groups. On the other hand, if the corresponding AFHOTIs admit a $\mathbb{Z} \times 2\mathbb{Z}$ classification, corner modes can appear on geometric corners that are invariant under either M_x or

$M' = C_n M_x$ symmetry, as well as all other corners that are C_n -related. AFHOTIs protected by $D_{2,-,-}^-$, $D_{4,-,-}^-$, and $D_{6,-,-}^-$ fall into this class. Therefore, in order to observe all symmetry protected corner modes, the boundary of the system must be properly chosen so as to possess the appropriate mirror-invariant corners. Below we summarize the geometry needed for each class of D_n -protected AFHOTI in order to observe all boundary features:

- kite: $D_{1,-,-}^\pm$;
- rhombus: $D_{2,+, \pm}^+$, $D_{2,-,-}^-$;
- square: $D_{4,+, \pm}^-$;
- regular hexagon: $D_{3,-,-}^\pm$, $D_{6,+, \pm}^+$;
- regular octagon: $D_{4,-,-}^-$;
- regular dodecagon: $D_{6,-,-}^-$.

One can, of course, choose a geometry with a higher symmetry than listed above to observe the desired corner modes. In Fig. 17, we schematically show the boundary geometry listed above for each class of D_n -protected AFHOTIs.

This completes our higher-order topological classification and bulk-boundary correspondence analysis for D_n -protected AFHOTIs.

VII. MODEL REALIZATIONS AND EXPERIMENTAL DETECTIONS

As a demonstration of our classification scheme, in this section we present two concrete lattice models for C_2 and D_4 -protected AFHOTIs, respectively. We shall analyze the symmetry and topological properties for both models, plot their phase-band spectra to reveal the singularity physics, and explicitly show how the anomalous corner modes are indicated by the corresponding higher-order topological indices defined in Sec. VI. Finally, we will briefly discuss realizations of these AFHOTI models in various experimental platforms and further provide a proposal on accessing the higher-order topological indices in experiment.

A. C_2 -symmetric AFHOTI

Our first model of C_2 -protected AFHOTI starts from a coupled-chain construction of the 1D AFTI model in Sec. IIIB, which is further decorated with a set of interchain dimer bonds u_2 , as shown in Fig. 18(a). Each unit cell now contains four inequivalent atoms, labeled by A_1, A_2, B_1 and B_2 . The time-dependent Hamiltonian is given by:

$$H^{(2)}(\mathbf{k}, t) = \begin{cases} u_0 \sum_{\mathbf{r}, i=1,2} c_{\mathbf{r}, A_i}^\dagger c_{\mathbf{r}, B_i} + \text{h.c.} & 0 < t \leq \frac{T}{4} \quad \text{and} \quad \frac{3T}{4} < t \leq T; \\ u_1 \sum_{\mathbf{r}, i=1,2} c_{\mathbf{r}+\mathbf{a}_x, A_i}^\dagger c_{\mathbf{r}, B_i} + u_2 \sum_{\mathbf{r}} (c_{\mathbf{r}, B_1}^\dagger c_{\mathbf{r}, B_2} + c_{\mathbf{r}+\mathbf{a}_y, A_1}^\dagger c_{\mathbf{r}, A_2}) + \text{h.c.} & \frac{T}{4} < t \leq \frac{3T}{4}, \end{cases} \quad (86)$$

In Appendix E, we provide the matrix representation of $H^{(2)}(\mathbf{k}, t)$ in momentum space. By construction, $H^{(2)}(\mathbf{k}, t)$ respects both C_2 and \mathcal{S} , where

$$\mathcal{S} = \begin{pmatrix} \sigma_z & 0 \\ 0 & -\sigma_z \end{pmatrix}, \quad C_2 = \begin{pmatrix} \sigma_x & 0 \\ 0 & \sigma_x e^{ik_y} \end{pmatrix}, \quad (87)$$

under the basis $\Phi_2 = (|A_1\rangle, |B_1\rangle, |A_2\rangle, |B_2\rangle)^T$. Note that $(C_2)^2 = 1$ and the anti-commutation relation $\{C_2, \mathcal{S}\} = 0$ is satisfied. This model thus corresponds to class $C_{2,+}^+$ in Table II, which has a \mathbb{Z}_2 classification.

As discussed in Appendix E, $H^{(2)}(\mathbf{k}, t)$ has a rather rich phase diagram with the phase boundary determined by

$$u_0 \pm u_1 + u_2 = \frac{2m\pi}{T}, \quad \text{and} \quad u_0 \pm u_1 - u_2 = \frac{2m\pi}{T}, \quad m \in \mathbb{Z}. \quad (88)$$

In Fig. 18(b), we calculate the Floquet quasienergy spectrum with open boundary in both spatial directions for $u_1 = 2u_0 = 4u_2 = 2\pi/T$. As shown in Fig. 18(b), there exists a pair of robust corner-localized 0 and π

modes. To show that these corner modes are protected by irremovable DWPs, we plot the phase band of the return map $\tilde{U}(\mathbf{k}, t)$ along Γ -axis in Fig. 18(c). Indeed, we find a DWP in the phase band featuring the anomalous C_2 -velocity locking effect discussed above and hence is topologically stable. Based on the relation between C_2 eigenvalues and t -directional velocities, it is easy to find that the C_2 corner-mode index $\nu_2 = |Q_0^{(2)}| = 1$, in agreement with the number of corner modes. Therefore, the corner modes in our model is indeed C_2 -protected, and the corresponding higher-order bulk-boundary correspondence also holds.

B. D_4 -symmetric AFHOTI

We now give another example of AFHOTI with D_4 symmetry. Notably, this model was first proposed in Ref. [70] as a Floquet quadrupole insulator, similar to that in Ref. [1], while the key role of D_4 and \mathcal{S} in pro-

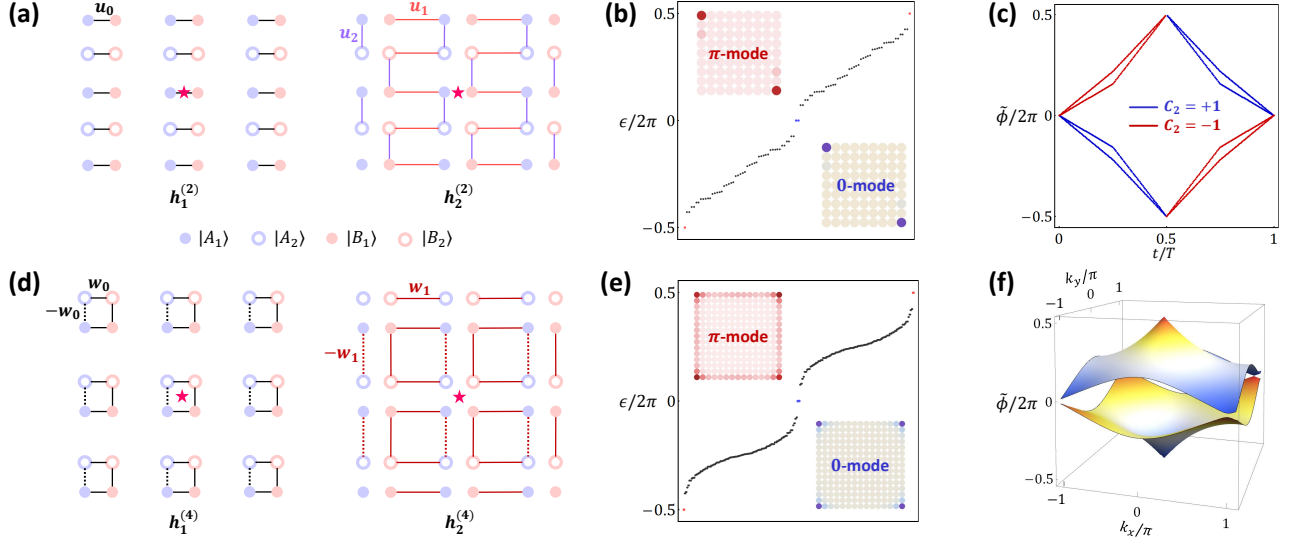


FIG. 18. Schematics of $H^{(2)}$ and $H^{(4)}$ are shown in (a) and (d), where the red stars label the rotation center. Anomalous Floquet corner modes and phase band with C_2 -protected [D_4 -protected] DWP for $H^{(2)}$ [$H^{(4)}$] are shown in (b) and (c) [(e) and (f)], respectively.

testing bulk higher-order topology was overlooked. Here we revisit this model and fully demonstrate its AFHOTI physics based on our theoretical framework.

The D_4 -symmetric AFHOTI model is described by the following time-dependent Hamiltonian

$$H^{(4)}(\mathbf{k}, t) = \begin{cases} h_1^{(4)} & 0 < t \leq \frac{T}{4} \quad \text{and} \quad \frac{3T}{4} < t \leq T; \\ h_2^{(4)} & \frac{T}{4} < t \leq \frac{3T}{4}. \end{cases} \quad (89)$$

Each unit cell for $H^{(4)}$ contains four atoms labeled by $A_{1,2}$ and $B_{1,2}$, following $H^{(2)}$'s convention. Under the basis $\Phi_4 = (|A_1\rangle, |B_1\rangle, |A_2\rangle, |B_2\rangle)^T$, the momentum-space Hamiltonian matrices are

$$\begin{aligned} h_1^{(4)} &= w_0(\gamma_{45} + \gamma_{14}), \\ h_2^{(4)} &= w_1(\cos k_x \gamma_{45} + \cos k_y \gamma_{14} - \sin k_x \gamma_{4} - \sin k_y \gamma_{24}). \end{aligned} \quad (90)$$

The definition of the γ matrices is the same as in Eq. (26). $H^{(4)}$ respects both D_4 and chiral symmetries, where

$$C_4 = \begin{pmatrix} 0 & \sigma_0 \\ -i\sigma_y & 0 \end{pmatrix}, \quad M_x = \gamma_3, \quad \mathcal{S} = \gamma_{34}. \quad (91)$$

Here $(C_4)^4 = -1$ and $\{\mathcal{S}, C_4\} = 0$ is again satisfied. Since $\{M_x, \mathcal{S}\} = 0$, this model corresponds to class $D_{4,+}^-$ in Table II, which has a \mathbb{Z} classification.

When $w_0 = \frac{2}{3}w_1 = \frac{\pi}{\sqrt{2}T}$, $H^{(4)}$ hosts a pair of zero and π modes at each corner of the system, as shown in Fig. 18(e). We further scan the phase band of the return map $\tilde{U}(\mathbf{k}, t)$ within one period and identify the existence of a DDP located at the Γ -axis, as shown in Fig. 18(f). The D_4 -symmetric model is analytically tractable, and

we derive the effective Hamiltonian of this DDP in appendix F. The effective Hamiltonian has a block-diagonal form up to $\mathcal{O}(k^2)$, corresponding to the two Weyl points that form this DDP,

$$H_{\text{eff}} = \begin{pmatrix} v_t t & e^{i\frac{\pi}{4}} v_k k_+ & 0 & 0 \\ e^{-i\frac{\pi}{4}} v_k^* k_- & -v_t t & 0 & 0 \\ 0 & 0 & v_t t & e^{i\frac{\pi}{4}} v_k k_+ \\ 0 & 0 & e^{-i\frac{\pi}{4}} v_k^* k_- & -v_t t \end{pmatrix}, \quad (92)$$

where $v_t = \frac{w_1 T}{\sqrt{2}}$, $v_l = (-i/\sqrt{2})e^{i[\frac{w_0 T}{2\sqrt{2}}]} \sin \frac{w_0 T}{2\sqrt{2}}$. We find that the j_z eigenvalues of the four bands form the basis $\Psi = (|\frac{1}{2}\rangle, |\frac{3}{2}\rangle, |-\frac{1}{2}\rangle, |-\frac{3}{2}\rangle)^T$, corresponding to the previous $\Psi_{d,+}$ with $n = 4$ and $J = \frac{1}{2}$. Indeed, such a DDP is stable, and can be analytically shown to carry a C_4 topological charge $Q_{\frac{1}{2}}^{(4)} = -\text{sgn}(v_t)$. The mirror topological charge can only be defined for $M_{\frac{\pi}{4}} = C_4 M_x$, since $[M_{\frac{\pi}{4}}, \mathcal{S}] = \{M_x, \mathcal{S}\} = 0$, where we numerically find $|Q_{M_{\frac{\pi}{4}}}^{\frac{1}{2}}| = 1$ for our choice of parameters, in agreement with the corner mode configuration depicted in Fig. 18(e). This unambiguously demonstrates D_4 -protected anomalous Floquet higher-order topology in this system. Furthermore, if M_x is broken, the higher-order topology is still C_4 -protected, as the DDP might split into a DWP yielding $|Q_{\frac{1}{2}}^{(4)}| = 1$.

C. Experimental realization and detection of phase-band singularities

Besides serving as a proof of concept, both models can be feasibly realized in various state-of-the-art experimen-

tal platforms, such as cold atoms [83], photonic waveguides [84–87], ring resonators [88], and acoustic platforms [89], where their first-order cousin (i.e. 2D AFTIs) has been successfully demonstrated. In particular, we also note a recent experiment on Floquet SSH model with anomalous π mode in photonic waveguides [90], which, upon some slight modifications, can be directly coupled to achieve our C_2 AFHOTI phase.

Besides detecting the corner modes at both quasienergies 0 and π , one can instead prove the higher-order topological nature by directly measuring the phase-band singularities in the bulk. To achieve this, we propose to design a path shown in Fig. 2 that connects an AFHOTI phase to the high frequency limit by slowly increasing the driving frequency ω , until ω is much larger than the band width of the static Hamiltonian. During this process, there exists a topological critical point that closes the π quasienergy gap and further separates the AFHOTI phase from a static limit, which is exactly our proposed phase-band singularity. Namely, by simply tuning the system to its high frequency limit, one can directly extract our proposed higher-order topological index by measuring the properties of the topological critical point in the Floquet spectrum. It should be noted that a similar measurement of the monopole charge for Weyl singularities has already been achieved for 2D class A AFTIs in a cold atom system [83]. Therefore, the boundary signal of corner modes, together with the bulk measurement of the higher-order topological index, will demonstrate the anomalous Floquet higher-order topological physics in an unambiguous way.

VIII. DISCUSSIONS

To conclude, we have established a long-sought theoretical framework to diagnose and classify anomalous Floquet higher-order topological phenomena, which is completely beyond any known topological diagnostic for static crystalline systems. Our approach is based on the concept of symmetry-protected phase-band singularities, which manifest themselves as exotic Dirac/Weyl singularities featuring unconventional dispersion relations that can only occur on the surface of higher-dimensional TCIs. To prove the higher-order bulk-boundary correspondence between phase-band singularities and Floquet corner modes, we develop the method of phase-band dimensional reduction, which provides a direct mapping between 2D AFHOTIs to 1D AFTIs. With the 1D AFTIs as the topological building blocks, we manage to extract the higher-order topological indices for all point-group symmetry protected 2D AFHOTIs, which thus accomplishes both the topological classification and characterization.

We mention that there are still several intriguing open questions for Floquet topological matters, waiting to be explored within our proposed framework. For example, we have limited our discussion in the present work to “strong” topological phenomena. In principle, a finer

topological classification with translation symmetries can be achieved similarly, where we expect the weak anomalous Floquet topological phases to be indicated by line-node-like phase-band singularities. Featuring flat-band-like 0 and π edge modes, an example of such weak AFTI is simply a “trivial” stacking of 1D AFTIs, which is already contained in the phase diagram of our C_2 -AFHOTI model (see Appendix E for details).

On the other hand, it is straightforward to apply our framework to classify anomalous Floquet higher-order topological phenomena in other tenfold-way symmetry classes. Nonetheless, switching from the chiral symmetry \mathcal{S} to other internal symmetries (e.g. particle-hole symmetry) could lead to completely distinct topological classification and boundary physics. For example, we have demonstrated that \mathcal{S} strictly prohibits any anomalous chiral edge modes, since the net phase-band Weyl charge must vanish. In contrast, such a constraint is relaxed when we consider driven systems with particle-hole symmetry. Namely, a 2D driven superconductor could be 1st-order topological with anomalous chiral Majorana edge modes, or 2nd-order topological with anomalous corner Majorana modes at both quasienergies 0 and π [91].

Beyond spatial crystalline symmetries, 2D AFHOTIs can also be protected by nonsymmorphic space-time crystalline symmetries [65, 68, 92], e.g. a time-glide mirror that combines both spatial mirror reflection and a half-period translation along the time direction. Note that such a time-glide AFHOTI has been proposed to admit a winding-number-based topological index, similar to a 1D class AIII AFTI discussed in Sec. III. Therefore, the topological winding number for time-glide AFHOTIs is also expected to indicate the existence of certain topological singularities in the phase bands, which fits well into our classification framework.

The present classification scheme is also readily generalized to 3D AFHOTIs with either (i) anomalous chiral/helical hinge modes traversing the Floquet band gap or (ii) robust 0 and π corner modes. The phase bands now live in a four-dimensional (\mathbf{k}, t) space, and hence exhibits new types of phase-band topological singularities that are related to the surface states of 5D TCIs.

Last but not least, it is also desirable to reformulate our proposed higher-order topological indices into more accessible topological invariants for \tilde{U} , perhaps similar to those homotopy invariants for 1D and 2D AFTIs. We leave this interesting topic to future works [93].

ACKNOWLEDGMENTS

We thank Sheng-Jie Huang, DinhDuy Vu, Yi-Ting Hsu, and in particular S. Das Sarma and Jiabin Yu for helpful discussions. We also thank Biao Huang and Haiping Hu for useful exchanges regarding Ref. [1]. R.-X. Z. acknowledges support from a JQI Postdoctoral Fellowship. Z.-C. Y. is supported by MURI ONR N00014-20-1-2325, MURI AFOSR, FA9550-19-1-0399, and Simons

Foundation. Z.-C. Y. also acknowledges support from the NSF PFCQC program.

Appendix A: C_2 -protected 4D topological crystalline insulators

In this section, we present a general theory of C_2 -protected 4D TCIs that are characterized by a new 4D topological invariant, the rotation Chern number. We will construct the corresponding minimal model, define the rotation Chern number, and further solve analytically for the 3D topological surface states. We will show that the surface states of such a C_2 -protected 4D TCI are precisely Weyl nodes exhibiting the C_2 -velocity locking as in the C_2 -protected DWPs.

1. Minimal model and rotation Chern number

We start by presenting a minimal model of C_2 -protected 4D TCI, following the construction scheme in Ref. [78]. Consider the following γ matrices

$$\begin{aligned}\gamma_1 &= \tau_x \otimes \sigma_z, \quad \gamma_2 = \tau_y \otimes \sigma_z, \quad \gamma_3 = \tau_0 \otimes \sigma_x, \\ \gamma_4 &= \tau_0 \otimes \sigma_y, \quad \gamma_5 = \tau_z \otimes \sigma_z,\end{aligned}\quad (\text{A1})$$

with which all other γ matrices can be generated as $\gamma_{ij} = [\gamma_i, \gamma_j]/(2i)$. Then for a general 4D Dirac system with $h = \sum_{i=1}^5 d_i \gamma_i$, its second Chern number is given by [94]

$$\mathcal{C}^{(2)} = \frac{3}{8\pi^2} \int d^4 k \epsilon^{abcde} \hat{d}_a \partial_{k_x} \hat{d}_b \partial_{k_y} \hat{d}_c \partial_{k_z} \hat{d}_d \partial_{k_w} \hat{d}_e, \quad (\text{A2})$$

which is defined in the 4D momentum space (k_x, k_y, k_z, k_w) . Here $\hat{d}_i = d_i / \sqrt{\sum_i d_i^2}$. Our minimal model consists of two 4D Chern insulators with opposite $\mathcal{C}^{(2)}$ values, which can be achieved by the following Hamiltonian,

$$h_{\text{TCI}}(\mathbf{k}) = \begin{pmatrix} h_+(\mathbf{k}) & 0 \\ 0 & h_-(\mathbf{k}) \end{pmatrix}, \quad (\text{A3})$$

where $h_{\pm}(\mathbf{k}) = v[\sin k_x \gamma_1 \pm \sin k_y \gamma_2 + \sin k_z \gamma_3 + \sin k_w \gamma_4] + m(\mathbf{k}) \gamma_5$. In particular, $m(\mathbf{k}) = A_0 + A_1[\cos k_x + \cos k_y + \cos k_z + \cos k_w]$ and the matrix block h_{\pm} hosts $\mathcal{C}^{(2)} = \pm 1$ when $-4A_1 < A_0 < -2A_1$.

We now consider a two-fold rotation symmetry $C_2 = s_0 \otimes \gamma_{12}$ that transforms h_{TCI} as,

$$C_2 h_{\text{TCI}}(k_x, k_y, k_z, k_w) C_2^{-1} = h_{\text{TCI}}(-k_x, -k_y, k_z, k_w) \quad (\text{A4})$$

On the C_2 -invariant plane with $k_{x,y} = 0$ spanned by (k_z, k_w) , h_{TCI} becomes four decoupled 2×2 matrix blocks,

$$h_{\text{TCI}} = \bigoplus_{i=1}^4 h_i, \quad (\text{A5})$$

Here, we have

$$\begin{aligned}h_1 &= h_3 = v(\sin k_z \sigma_x + \sin k_w \sigma_y) + \tilde{m}(k_z, k_w) \sigma_z, \\ h_2 &= h_4 = v(\sin k_z \sigma_x + \sin k_w \sigma_y) - \tilde{m}(k_z, k_w) \sigma_z,\end{aligned}\quad (\text{A6})$$

with $\tilde{m}(k_z, k_w) = A_0 + 2A_1 + A_1(\cos k_z + \cos k_w)$. Therefore, when $-4A_1 < A_0 < -2A_1$, we find $h_{1,3}$ has a first Chern number $\mathcal{C}^{(1)} = 1$, while the first Chern number for $h_{2,4}$ is -1 . According to the representation of C_2 , $h_{1,3}$ and $h_{2,4}$ live in the $C_2 = +1$ and $C_2 = -1$ subspaces, respectively. Although the net $\mathcal{C}^{(1)}$ is zero for all h_i s, following Ref. [78], we can define a new C_2 -protected topological invariant dubbed the rotation Chern number $\mathcal{C}_{\mathcal{R}}$, where

$$\mathcal{C}_{\mathcal{R}} \equiv \frac{\mathcal{C}^{(1)}(C_2 = 1) - \mathcal{C}^{(1)}(C_2 = -1)}{2} \in \mathbb{Z}. \quad (\text{A7})$$

For h_{TCI} with $-4A_1 < A_0 < -2A_1$, the rotation Chern number $\mathcal{C}_{\mathcal{R}} = 1$.

2. Surface state and C_2 -velocity locking

The nontrivial value of $\mathcal{C}_{\mathcal{R}}$ directly implies the C_2 -protected 4D crystalline topology in h_{TCI} , despite a vanishing second Chern number. To explore the corresponding topological boundary modes for this class of 4D TCI, we consider a 4D slab with periodic boundary conditions in x, y, z -directions but an open boundary condition along the w -direction. Expanding h_{TCI} around $k_x = k_y = k_z = 0$ to $\mathcal{O}(k)$, we have

$$h_{\pm} = v(k_x \gamma_1 \pm k_y \gamma_2 + k_z \gamma_3) - iv \partial_w \gamma_4 + M_0 \gamma_5, \quad (\text{A8})$$

where $M_0 = A_0 + 4A_1 > 0$. Then both h_{\pm} admit the same zero-mode equation at $k_x = k_y = k_z = 0$,

$$(-iv \partial_w \gamma_4 + M_0 \gamma_5) \psi(w) = 0, \quad (\text{A9})$$

which can be rewritten as

$$(\partial_w - \frac{M_0}{v} \gamma_{45}) \psi(w) = 0. \quad (\text{A10})$$

We now consider a trial wavefunction

$$\psi(w) = f(w) \xi_s, \quad (\text{A11})$$

where the spatial part $f(w) = \mathcal{N} e^{-\lambda w}$ and the spinor part $\gamma_{45} \xi_s = s \xi_s$ for $s = \pm$. It is easy to solve that $\lambda = -\frac{m_0 s}{v}$, which is required to be positive for a normalized wavefunction. Then for $v > 0$, we have $s = -1$ and thus have two choices for ξ_s ,

$$\xi_-^{(1)} = \frac{1}{\sqrt{2}}(0, 0, 1, 1)^T, \quad \xi_-^{(2)} = \frac{1}{\sqrt{2}}(-1, 1, 0, 0)^T. \quad (\text{A12})$$

By projecting h_{\pm} onto the zero-mode basis, we obtain the effective Hamiltonians for the corresponding surface state

$$h_{\text{surface}} = v \begin{pmatrix} k_z & -k_+ & 0 & 0 \\ -k_- & -k_z & 0 & 0 \\ 0 & 0 & k_z & -k_- \\ 0 & 0 & -k_+ & -k_z \end{pmatrix}, \quad (\text{A13})$$

while the projected C_2 symmetry is

$$\tilde{C}_2 = \begin{pmatrix} -1 & & & \\ & 1 & & \\ & & -1 & \\ & & & 1 \end{pmatrix}. \quad (\text{A14})$$

From Eq. (A13) and Eq. (A14), it is easy to see that

- the surface state consists of two 3D Weyl nodes with opposite monopole charges;
- the surface state features C_2 -velocity locking effect along the C_2 -invariant axis ($k_x = k_y = 0$) in the surface Brillouin zone.

Therefore, the surface state of a 4D C_2 -protected TCI with $\mathcal{C}_R = 1$ exactly reproduces the key features of the dynamical Weyl pair found in a C_2 -protected 2D AFHOTI.

Appendix B: Topological charges of D_n single groups with $(C_n)^n = 1$

In this section, we derive the topological charges for D_n single groups with $(C_n)^n = 1$. As discussed in the main text, M_x maps a phase band eigenstate with $j_z = J$ to another eigenstate at the same location with $j_z = -J$. When J takes integer values, however, not all possible J leads to a two-dimensional irrep. In particular, when $-J = J \bmod n$, the corresponding eigenstate remains to be a one-dimensional irrep. of C_n . Below we list the irreps for each D_n single group:

- D_2 : only 1-d irreps for $J = 0, 1$;
- D_4 : two 1-d irreps for $J = 0, 2$, and one 2-d irrep $\{J = 1, J = 3\}$;
- D_6 : two 1-d irreps for $J = 0, 3$, and two 2-d irreps $\{J = 1, J = 5\}, \{J = 2, J = 4\}$.

First, the condition for an unstable Dirac point: $J + 1 = -J \bmod n$, which leads to $Q_{\frac{n-1}{2}}^{(n)} = 0$, places no constraint for integer-valued J 's. Second, since D_2 shares the same irreps as C_2 , mirror symmetry does not introduce further constraints in this case. So the classification for D_2 single group is still $Q_0^{(2)} \in \mathbb{Z}$. For D_4 , there is only one 2-d irrep, so there will be a three-fold degenerate Dirac point formed by the phase band states $(|J = 1\rangle, |J = 2\rangle, |J = 3\rangle)^T$. This leads to the constraint $Q_0^{(4)} = Q_1^{(4)}$, which reduces the classification to $Q_0^{(4)} \in \mathbb{Z}$. For D_6 , there are two 2-d irreps, which form a four-fold degenerate Dirac point under the basis $(|J = 1\rangle, |J = 2\rangle, |J = 4\rangle, |J = 5\rangle)^T$. This leads to the constraint $Q_1^{(6)} = -Q_4^{(6)}$ which is identical to that from the chiral symmetry. However, it is also possible to form a three-fold degenerate Dirac point under $(|J = 0\rangle, |J = 1\rangle, |J = 5\rangle)^T$, which imposes

$Q_0^{(6)} = -Q_5^{(6)} = Q_2^{(6)}$. Therefore, the classification for D_6 single group reduces to $\{Q_0^{(6)}, Q_1^{(6)}\} \in \mathbb{Z}^2$. We summarize the results below:

- D_2 : $Q_0^{(2)} \in \mathbb{Z}$;
- D_4 : $Q_0^{(4)} \in \mathbb{Z}$;
- D_6 : $\{Q_0^{(6)}, Q_1^{(6)}\} \in \mathbb{Z}^2$.

Appendix C: Angular momentum basis and mirror symmetry

We now prove the relation between $M_x(\frac{n-1}{2})$ and $M_x(-\frac{1}{2})$ in Eq. (61) of Sec. V F.

Recall that a single DDP compatible with $D_{n,-,-}^-$ is described by the basis $\Psi_J = (|J\rangle, |J+1\rangle, |-J\rangle, |-J-1\rangle)^T$, where $J = -\frac{1}{2}$ or $J = \frac{n-1}{2}$. In particular, an even n requires $\frac{n-1}{2}$ to be a half-integer, which agrees with the double group nature of $D_{n,-,-}^-$.

For spinful fermions, an angular momentum state can be formally written as

$$|j_z\rangle = |l_z, s_z\rangle \quad (\text{C1})$$

where $l_z \in \mathbb{Z}$ and $s_z = \uparrow, \downarrow$ denote the orbital and spin contributions to j_z . As a result, a state $|J\rangle$ can come from the following two microscopic possibilities:

$$|J\rangle = |J - \frac{1}{2}, \uparrow\rangle, \text{ or } |J\rangle = |J + \frac{1}{2}, \downarrow\rangle, \quad (\text{C2})$$

according to Eq. C1. We note M_x flips the spin as a π rotation around y axis, and further flips l_z with an additional factor of $(-1)^{l_z}$. Therefore, we have

$$M_x \begin{pmatrix} |l_z, \uparrow\rangle \\ |-l_z, \downarrow\rangle \end{pmatrix} = (-1)^{l_z} i \sigma_y \begin{pmatrix} |l_z, \uparrow\rangle \\ |-l_z, \downarrow\rangle \end{pmatrix}. \quad (\text{C3})$$

Consequently, we find that for $|J\rangle$,

$$M_x \begin{pmatrix} |J\rangle \\ |-J\rangle \end{pmatrix} = (-1)^{J-\frac{1}{2}} i \sigma_y \begin{pmatrix} |J\rangle \\ |-J\rangle \end{pmatrix} \quad (\text{C4})$$

always holds, in spite of the choices in Eq. C2. Then it is easy to show that

$$\begin{aligned} M_x(-\frac{1}{2}) &= -i \tau_z \otimes \sigma_y, \\ M_x(\frac{n-1}{2}) &= -i(-1)^{\frac{n}{2}} \tau_z \otimes \sigma_y, \end{aligned} \quad (\text{C5})$$

leading to

$$M_x(\frac{n-1}{2}) = (-1)^{\frac{n}{2}} M_x(-\frac{1}{2}) \quad (\text{C6})$$

as shown in Eq. (61).

Appendix D: Fragility of dynamical Weyl quadrupole in Ref. [1]

We will show in this section that the “dynamical Weyl quadrupole” introduced in Ref. [1] as a characterization for the anomalous quadrupole phase is in fact unstable. The model studied in Ref. [1] is similar to the D_4 -symmetric model discussed in the main text as well as in Ref. [70], but only has D_2 symmetry. The time dependent Hamiltonian of Ref. [1] is given by:

$$\begin{aligned} H(t) &= h_0, \quad t \in T_1; & H(t) &= h_y, \quad t \in T_2; \\ H(t) &= h_x, \quad t \in T_3; & H(t) &= h_0, \quad t \in T_4; \end{aligned} \quad (D1)$$

where $T_s = [(s-1)T/4, sT/4]$. The Hamiltonian in each time duration is given by: $h_0 = t_0(\tau_1\sigma_0 + \tau_2\sigma_2)$, $h_x = t_x(\cos k_x\tau_1\sigma_0 - \sin k_x\tau_2\sigma_3)$, and $h_y = t_y(\cos k_y\tau_2\sigma_2 + \sin k_y\tau_2\sigma_1)$, where τ, σ are Pauli matrices, and the choice of basis is the same as in the D_4 symmetric model in the main text. The important symmetries for our purpose are:

$$M_x = i\tau_1\sigma_3, \quad M_y = i\tau_1\sigma_1. \quad (D2)$$

Despite the similarity with the D_4 symmetric model discussed in the main text, this model does not have C_4 rotation symmetry, nor does it have chiral symmetry. Ref. [1] claims that the phase band Weyl nodes form a quadrupole pattern protected by M_x and M_y , and defines the total Weyl charge within the first quadrant of the Brillouin zone mod 2 as a topological invariant for the corner mode at quasienergy π/T . However, since there is no chiral symmetry in this model, mirror symmetry alone cannot protect dynamical singularities, according to our discussions in Sec. VC. Therefore, one can adiabatically move the quadruplet of Weyl nodes altogether such that they coincide at one point in (\mathbf{k}, t) space, and gap them out with symmetry-preserving perturbations. We now show this explicitly for this model.

We choose $t_x = t_y = \pi/T$ as in Ref. [1], and take $t_0 = \sqrt{2}\pi/T$ for which the model hosts corner modes at quasienergy π/T . As shown in Fig. 19(a), the phase band exhibits a four-fold degenerate Dirac singularity at $(k_x = k_y = 0, t = \frac{T}{2})$. Slightly changing t_0 will split this Dirac node and form the Weyl quadrupole configuration as discussed in Ref. [1]. Therefore, the situation shown in Fig. 19(a) corresponds to smoothly deforming the quadrupole pattern such that they coincide at one point. Next, we introduce the following perturbation to Hamiltonian (D1):

$$h_0 \rightarrow h_0 - \delta(\tau_2\sigma_2 + \cos k_x\tau_3\sigma_2 + \sin k_y\tau_3\sigma_1). \quad (D3)$$

One can easily check that this perturbation respects D_2 symmetry. However, upon adding this perturbation, the singularity is gapped out, as shown in Fig. 19(b). Therefore, we conclude that the dynamical Weyl quadrupole configuration introduced in Ref. [1] is unstable under generic D_2 -symmetric perturbations, consistent with our previous general discussions.

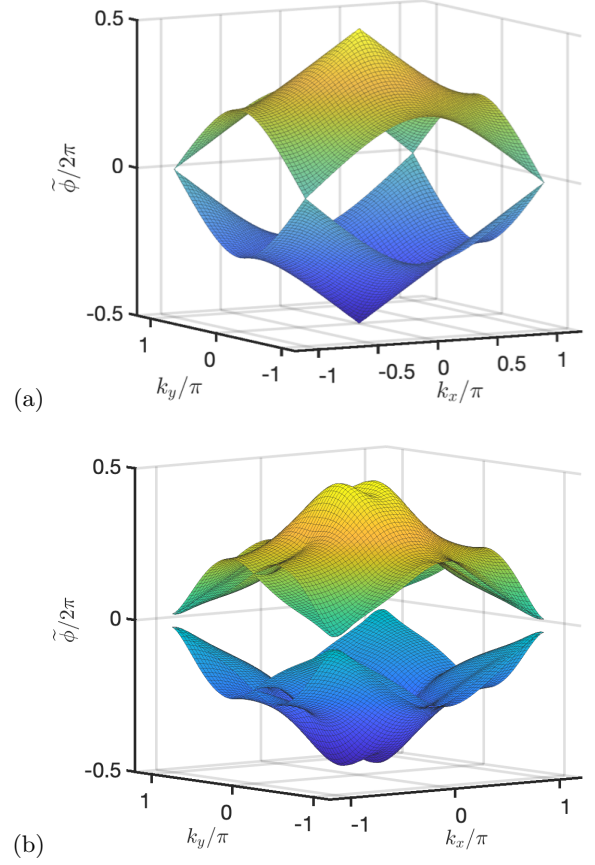


FIG. 19. (a) Phase band $\tilde{U}(\mathbf{k}, \frac{T}{2})$ of the D_2 model (D1). We choose $t_x = t_y = \pi/T$, $t_0 = \sqrt{2}\pi/T$, in accordance with Ref. [1], and the model hosts corner mode at quasienergy π/T . The phase band shows a four-fold Dirac singularity at the Γ point. (b) The singularity is gapped out upon adding a perturbation (D3) that respects D_2 symmetry. We choose $\delta = 0.4\pi/T$. Although only the phase band at $t = \frac{T}{2}$ is shown here, we have also checked the phase band at arbitrary t and confirmed that there is no singularity anywhere for $0 < t < T$.

Appendix E: Phase diagram of the C_2 -symmetric model

We first present the matrix representation of $H^{(2)}$ in momentum space,

$$\begin{aligned} h_1 &= u_0\tau_0 \otimes \sigma_1, \\ h_2 &= \begin{pmatrix} 0 & u_1e^{ik_x} & u_2 & 0 \\ u_1e^{-ik_x} & 0 & 0 & u_2e^{ik_y} \\ u_2 & 0 & 0 & u_1e^{ik_x} \\ 0 & u_2e^{-ik_y} & u_1e^{-ik_x} & 0 \end{pmatrix} \end{aligned} \quad (E1)$$

The analytical expression for $U(\mathbf{k}, t)$ at a general (\mathbf{k}, t) is difficult to obtain, which nonetheless is indeed solvable for each rotation-invariant axis. We further note that the Floquet quasienergy gap can close only at $\mathbf{k} = (0, 0)$ or

$\mathbf{k} = (\pi, 0)$. Then the phase boundaries are found to be

$$u_0 \pm u_1 + u_2 = \frac{2m\pi}{T} \text{ and } u_0 \pm u_1 - u_2 = \frac{2m\pi}{T} \quad (\text{E2})$$

for $m \in \mathbb{Z}$. These phase boundaries lead to a rich topological phase diagram, as shown in Fig. 20. In particular, the blue and red phase boundaries in Fig. 20 denote the Floquet gap closing at quasienergies 0 and π , respectively. Here are the meaning of each phase in Fig. 20

- *Trivial*: A topologically trivial phase with no boundary feature.
- *0-weak or π -weak*: A weak topological insulator which hosts 1d flat edge band at 0 or π energy.
- *0-HOTI or π -HOTI*: A higher-order topological insulator with 0 or π corner modes.
- *0-nodal or π -nodal*: A gapless system with point nodes at energy 0 or π .
- *0-line or π -line*: A gapless system with line nodes at energy 0 or π .

For example, a π -HOTI only hosts π -corner modes instead of 0-corner modes. On the other hand, a 0-HOTI & π -HOTI hosts both 0 and π corner modes, which is exactly the AFHOTI phase in the main text. For our purpose, we focus on the AFHOTI phase in the phase diagram. A full topological characterization of the other exotic Floquet phases is left for future work.

Appendix F: Analytical details of D_4 -symmetric AFHOTI

1. Analytical expression of $U(\mathbf{k}, t)$

We are interested in the time-evolution operator $U(\mathbf{k}, t)$ for $t \in (\frac{T}{4}, T]$, since $U(\mathbf{k}, t < \frac{T}{4})$ cannot host any DDP. For convenience, we define $U_2 = U(\mathbf{k}, \frac{T}{4} < t \leq \frac{3T}{4})$ and $U_3 = U(\mathbf{k}, \frac{3T}{4} < t \leq T)$. In what follows, we will set $T = 1$ for simplicity. We switch to a rotation-symmetric basis by finding a unitary matrix V , s.t.

$$VC_4V^\dagger = \begin{pmatrix} e^{i\frac{\pi}{4}} & 0 & 0 & 0 \\ 0 & e^{-i\frac{\pi}{4}} & 0 & 0 \\ 0 & 0 & e^{i\frac{3\pi}{4}} & 0 \\ 0 & 0 & 0 & e^{-i\frac{3\pi}{4}} \end{pmatrix} = e^{i\frac{\pi}{2}J_z}, \quad (\text{F1})$$

where $J_z = \text{diag}[\frac{1}{2}, -\frac{1}{2}, \frac{3}{2}, -\frac{3}{2}]$. Therefore, the Hamiltonian $\hat{H}^{(4)}(\mathbf{k}, t) = VH^{(4)}(\mathbf{k}, t)V^\dagger$ is under the following new basis

$$\Psi = \left(\left| \frac{1}{2} \right\rangle, \left| -\frac{1}{2} \right\rangle, \left| \frac{3}{2} \right\rangle, \left| -\frac{3}{2} \right\rangle \right)^T. \quad (\text{F2})$$

We expand U_{2t} and U_{3t} around Γ and find that they have a universal form,

$$U_i(\mathbf{k}, t) = \begin{pmatrix} a_i & 0 & b_i & 0 \\ 0 & a_i & 0 & c_i \\ -b_i^* & 0 & a_i^* & 0 \\ 0 & -c_i^* & 0 & a_i^* \end{pmatrix}, \text{ for } i = 2, 3, \quad (\text{F3})$$

where

$$\begin{aligned} a_2 &= e^{-\frac{i}{2\sqrt{2}}[w_0 + w_1(4t-1)]}, \\ b_2 &= -\frac{1+i}{2} \sin \left[\sqrt{2}w_1(t - \frac{1}{4}) \right] e^{\frac{iw_0}{2\sqrt{2}}k_+}, \\ c_2 &= -\frac{1-i}{2} \sin \left[\sqrt{2}w_1(t - \frac{1}{4}) \right] e^{\frac{iw_0}{2\sqrt{2}}k_-}, \end{aligned} \quad (\text{F4})$$

and

$$\begin{aligned} a_3 &= e^{-\frac{i}{\sqrt{2}}[w_1 + w_0(2t-1)]}, \\ b_3 &= -\frac{1+i}{2} \sin \left[\frac{w_1}{\sqrt{2}} \right] e^{i\sqrt{2}w_0(1-t)k_+}, \\ c_3 &= -\frac{1-i}{2} \sin \left[\frac{w_1}{\sqrt{2}} \right] e^{i\sqrt{2}w_0(1-t)k_-}. \end{aligned} \quad (\text{F5})$$

When a DDP occurs at (\mathbf{k}_0, t_0) , we expect the time-evolution operator

$$U(\mathbf{k}_0, t_0) = -\mathbb{1}_4 \quad (\text{F6})$$

Take $\mathbf{k}_0 = \Gamma$, the condition for a DDP to occur in U_i is simply

$$a_i = -1. \quad (\text{F7})$$

2. Condition for DDP

Let us first check U_2 . When imposing $a_2 = -1$, we have

$$w_0 + w_1(4t - 1) = 2\sqrt{2}\pi, \quad \frac{T}{4} \leq t \leq \frac{3T}{4}, \quad (\text{F8})$$

which is only possible when

$$2w_1 + w_0 \geq 2\sqrt{2}\pi. \quad (\text{F9})$$

We have focused on the parameter regime where $w_0, w_1 \in [0, \sqrt{2}\pi]$, due to the periodicity of the phase diagram [70].

When DDP exists in U_3 , we have $a_3 = -1$, leading to

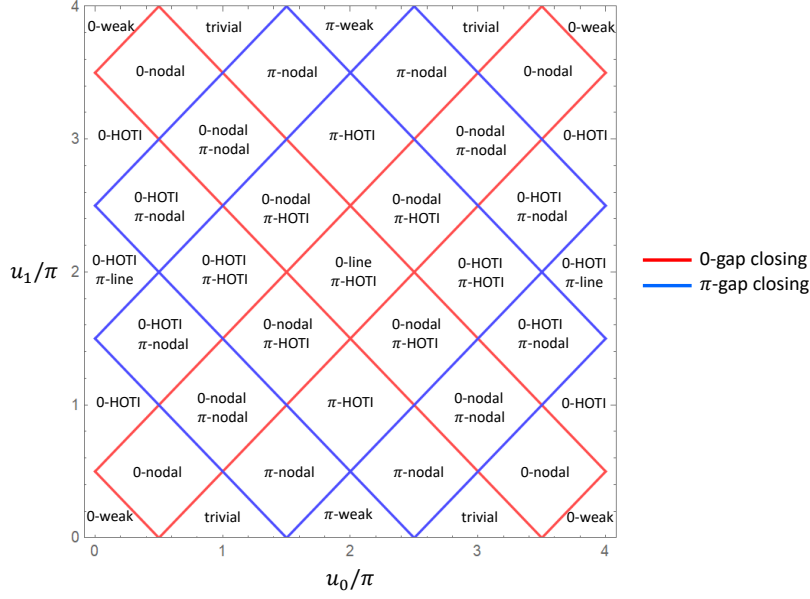
$$\sqrt{2}(w_1 + w_0(2t - 1)) = 2\pi, \quad \frac{3T}{4} \leq t \leq T. \quad (\text{F10})$$

By solving the above inequalities, we arrive at the DTS condition for U_3 as

$$\begin{aligned} 2w_1 + w_0 &\leq 2\sqrt{2}\pi \\ w_1 + w_0 &\geq \sqrt{2}\pi. \end{aligned} \quad (\text{F11})$$

Together with the condition for U_2 , we conclude that the DDP always exists when $w_0 + w_1 \geq \sqrt{2}\pi$. As shown in Ref. [70], $w_0 + w_1 = \sqrt{2}\pi$ is exactly the phase boundary separating the phases with and without π corner modes for $H^{(4)}$. Thus, we have proved for $H^{(4)}$ that

- the DDP occurs *if and only if* the system hosts symmetry-protected π corner modes.

FIG. 20. Phase diagram of $H^{(2)}$ for $u_2 = 0.5\pi$

3. Effective Hamiltonian of D_4 -protected DDP

Now we show that the topological singularity found above by is indeed a D_4 -protected four-fold-degenerate Dirac point. As an example, we consider the singularity

at $t = t_0 \in (\frac{T}{4}, \frac{3T}{4}]$ for U_2 . Following Eq. F8, we have

$$w_0 + w_1(4t_0 - 1) = 2\sqrt{2}\pi \quad (\text{F12})$$

By expanding $U_2(\mathbf{k}, t)$ around t_0 with $t = t_0 + \Delta t$, and denote $\Delta t \equiv t$, we arrive at

$$U_2(\mathbf{k}, t) \approx -\mathbb{1}_4 + \begin{pmatrix} iv_t t & 0 & -e^{i\frac{\pi}{4}} v_k k_+ & 0 \\ 0 & iv_t t & 0 & -e^{-i\frac{\pi}{4}} v_k k_- \\ e^{-i\frac{\pi}{4}} v_k^* k_- & 0 & -iv_t t & 0 \\ 0 & e^{i\frac{\pi}{4}} v_k^* k_+ & 0 & -iv_t t \end{pmatrix} \quad (\text{F13})$$

where

$$v_t = \frac{w_1}{\sqrt{2}}, \quad v_k = \frac{1}{\sqrt{2}} e^{i\frac{w_0}{2\sqrt{2}}} \sin \frac{w_0}{2\sqrt{2}}. \quad (\text{F14})$$

This immediately leads to

$$h_D = i \log U_2(\mathbf{k}, t) = \begin{pmatrix} v_t t & 0 & -ie^{i\frac{\pi}{4}} v_k k_+ & 0 \\ 0 & v_t t & 0 & -ie^{-i\frac{\pi}{4}} v_k k_- \\ ie^{-i\frac{\pi}{4}} v_k^* k_- & 0 & -v_t t & 0 \\ 0 & ie^{i\frac{\pi}{4}} v_k^* k_+ & 0 & -v_t t \end{pmatrix}, \quad (\text{F15})$$

which is exactly a 3d Dirac point in the (\mathbf{k}, t) parameter space.

[1] H. Hu, B. Huang, E. Zhao, and W. V. Liu, “Dynamical singularities of floquet higher-order topological insulators,” *Phys. Rev. Lett.* **124**, 057001 (2020).

[2] D. J. Thouless, M. Kohmoto, M. P. Nightingale, and M. den Nijs, “Quantized hall conductance in a two-dimensional periodic potential,” *Phys. Rev. Lett.* **49**,

- 405–408 (1982).
- [3] F. D. M. Haldane, “Model for a quantum hall effect without landau levels: Condensed-matter realization of the ”parity anomaly”,,” *Phys. Rev. Lett.* **61**, 2015–2018 (1988).
 - [4] C. L. Kane and E. J. Mele, “ Z_2 topological order and the quantum spin hall effect,” *Phys. Rev. Lett.* **95**, 146802 (2005).
 - [5] B. A. Bernevig and S.-C. Zhang, “Quantum spin hall effect,” *Phys. Rev. Lett.* **96**, 106802 (2006).
 - [6] M. Z. Hasan and C. L. Kane, “Colloquium: Topological insulators,” *Rev. Mod. Phys.* **82**, 3045–3067 (2010).
 - [7] X.-L. Qi and S.-C. Zhang, “Topological insulators and superconductors,” *Rev. Mod. Phys.* **83**, 1057–1110 (2011).
 - [8] B. Bradlyn, L. Elcoro, J. Cano, M. G. Vergniory, Z. Wang, C. Felser, M. I. Aroyo, and B. A. Bernevig, “Topological quantum chemistry,” *Nature* **547**, 298–305 (2017).
 - [9] H. C. Po, H. Watanabe, and A. Vishwanath, “Fragile topology and wannier obstructions,” *Phys. Rev. Lett.* **121**, 126402 (2018).
 - [10] L. Elcoro, B. J. Wieder, Z. Song, Y. Xu, B. Bradlyn, and B. A. Bernevig, “Magnetic topological quantum chemistry,” *arXiv preprint arXiv:2010.00598* (2020).
 - [11] L. Fu, “Topological crystalline insulators,” *Phys. Rev. Lett.* **106**, 106802 (2011).
 - [12] C.-X. Liu, R.-X. Zhang, and B. K. VanLeeuwen, “Topological nonsymmorphic crystalline insulators,” *Phys. Rev. B* **90**, 085304 (2014).
 - [13] R.-X. Zhang and C.-X. Liu, “Topological magnetic crystalline insulators and corepresentation theory,” *Phys. Rev. B* **91**, 115317 (2015).
 - [14] Y. Ando and L. Fu, “Topological crystalline insulators and topological superconductors: From concepts to materials,” *Annual Review of Condensed Matter Physics* **6**, 361–381 (2015).
 - [15] Z. Wang, A. Alexandradinata, R. J. Cava, and B. A. Bernevig, “Hourglass fermions,” *Nature* **532**, 189–194 (2016).
 - [16] P.-Y. Chang, O. Erten, and P. Coleman, “Möbius kondo insulators,” *Nature Physics* **13**, 794–798 (2017).
 - [17] B. J. Wieder, B. Bradlyn, Z. Wang, J. Cano, Y. Kim, H.-S. D. Kim, A. M. Rappe, C. Kane, and B. A. Bernevig, “Wallpaper fermions and the nonsymmorphic dirac insulator,” *Science* **361**, 246–251 (2018).
 - [18] T. H. Hsieh, H. Lin, J. Liu, W. Duan, A. Bansil, and L. Fu, “Topological crystalline insulators in the snite material class,” *Nature communications* **3**, 1–7 (2012).
 - [19] Y. Tanaka, Z. Ren, T. Sato, K. Nakayama, S. Souma, T. Takahashi, K. Segawa, and Y. Ando, “Experimental realization of a topological crystalline insulator in snite,” *Nature Physics* **8**, 800–803 (2012).
 - [20] W. A. Benalcazar, B. A. Bernevig, and T. L. Hughes, “Quantized electric multipole insulators,” *Science* **357**, 61–66 (2017).
 - [21] W. A. Benalcazar, B. A. Bernevig, and T. L. Hughes, “Electric multipole moments, topological multipole moment pumping, and chiral hinge states in crystalline insulators,” *Phys. Rev. B* **96**, 245115 (2017).
 - [22] J. Langbehn, Y. Peng, L. Trifunovic, F. von Oppen, and P. W. Brouwer, “Reflection-symmetric second-order topological insulators and superconductors,” *Phys. Rev. Lett.* **119**, 246401 (2017).
 - [23] Z. Song, Z. Fang, and C. Fang, “ $(d - 2)$ -dimensional edge states of rotation symmetry protected topological states,” *Phys. Rev. Lett.* **119**, 246402 (2017).
 - [24] F. Schindler, A. M. Cook, M. G. Vergniory, Z. Wang, S. S. Parkin, B. A. Bernevig, and T. Neupert, “Higher-order topological insulators,” *Science advances* **4**, eaat0346 (2018).
 - [25] E. Khalaf, “Higher-order topological insulators and superconductors protected by inversion symmetry,” *Phys. Rev. B* **97**, 205136 (2018).
 - [26] Q. Wang, C.-C. Liu, Y.-M. Lu, and F. Zhang, “High-temperature majorana corner states,” *Phys. Rev. Lett.* **121**, 186801 (2018).
 - [27] Z. Yan, F. Song, and Z. Wang, “Majorana corner modes in a high-temperature platform,” *Phys. Rev. Lett.* **121**, 096803 (2018).
 - [28] C.-H. Hsu, P. Stano, J. Klinovaja, and D. Loss, “Majorana kramers pairs in higher-order topological insulators,” *Phys. Rev. Lett.* **121**, 196801 (2018).
 - [29] R.-X. Zhang, W. S. Cole, and S. Das Sarma, “Helical hinge majorana modes in iron-based superconductors,” *Phys. Rev. Lett.* **122**, 187001 (2019).
 - [30] G. van Miert and C. Ortix, “Higher-order topological insulators protected by inversion and rotoinversion symmetries,” *Phys. Rev. B* **98**, 081110 (2018).
 - [31] Y. Wang, M. Lin, and T. L. Hughes, “Weak-pairing higher order topological superconductors,” *Phys. Rev. B* **98**, 165144 (2018).
 - [32] B. J. Wieder and B. A. Bernevig, “The axion insulator as a pump of fragile topology,” *arXiv preprint arXiv:1810.02373* (2018).
 - [33] R.-X. Zhang, W. S. Cole, X. Wu, and S. Das Sarma, “Higher-order topology and nodal topological superconductivity in fe(se,te) heterostructures,” *Phys. Rev. Lett.* **123**, 167001 (2019).
 - [34] X. Wu, X. Liu, R. Thomale, and C.-X. Liu, “High- t_c superconductor fe (se, te) monolayer: an intrinsic, scalable and electrically-tunable majorana platform,” *arXiv preprint arXiv:1905.10648* (2019).
 - [35] Z. Yan, “Higher-order topological odd-parity superconductors,” *Phys. Rev. Lett.* **123**, 177001 (2019).
 - [36] W. A. Benalcazar, T. Li, and T. L. Hughes, “Quantization of fractional corner charge in C_n -symmetric higher-order topological crystalline insulators,” *Phys. Rev. B* **99**, 245151 (2019).
 - [37] F. Schindler, M. Brzezińska, W. A. Benalcazar, M. Iraola, A. Bouhon, S. S. Tsirkin, M. G. Vergniory, and T. Neupert, “Fractional corner charges in spin-orbit coupled crystals,” *Phys. Rev. Research* **1**, 033074 (2019).
 - [38] R.-X. Zhang, J. D. Sau, and S. D. Sarma, “Kitaev building-block construction for higher-order topological superconductors,” *arXiv preprint arXiv:2003.02559* (2020).
 - [39] P. Zhu, K. Loehr, and T. L. Hughes, “Identifying C_n -symmetric higher-order topology and fractional corner charge using entanglement spectra,” *Phys. Rev. B* **101**, 115140 (2020).
 - [40] S.-B. Zhang, W. B. Rui, A. Calzona, S.-J. Choi, A. P. Schnyder, and B. Trauzettel, “Topological and holographic quantum computation based on second-order topological superconductors,” *Phys. Rev. Research* **2**, 043025 (2020).
 - [41] Y.-T. Hsu, W. S. Cole, R.-X. Zhang, and J. D. Sau, “Inversion-protected higher-order topological superconductivity in monolayer wte₂,” *Phys. Rev. Lett.* **125**,

- 097001 (2020).
- [42] D. Vu, R.-X. Zhang, and S. D. Sarma, “Time-reversal-invariant c_2 -symmetric higher-order topological superconductors,” [arXiv preprint arXiv:2005.03679](#) (2020).
 - [43] E. Khalaf, H. C. Po, A. Vishwanath, and H. Watanabe, “Symmetry indicators and anomalous surface states of topological crystalline insulators,” *Phys. Rev. X* **8**, 031070 (2018).
 - [44] H. C. Po, A. Vishwanath, and H. Watanabe, “Symmetry-based indicators of band topology in the 230 space groups,” *Nature communications* **8**, 1–9 (2017).
 - [45] F. Schindler, Z. Wang, M. G. Vergniory, A. M. Cook, A. Murani, S. Sengupta, A. Y. Kasumov, R. Deblock, S. Jeon, I. Drozdov, et al., “Higher-order topology in bismuth,” *Nature physics* **14**, 918–924 (2018).
 - [46] Y. Xu, Z. Song, Z. Wang, H. Weng, and X. Dai, “Higher-order topology of the axion insulator euin_2as_2 ,” *Phys. Rev. Lett.* **122**, 256402 (2019).
 - [47] Z. Wang, B. J. Wieder, J. Li, B. Yan, and B. A. Bernevig, “Higher-order topology, monopole nodal lines, and the origin of large fermi arcs in transition metal dichalcogenides xte_2 ($x = \text{Mo}, \text{W}$),” *Phys. Rev. Lett.* **123**, 186401 (2019).
 - [48] B. J. Wieder, Z. Wang, J. Cano, X. Dai, L. M. Schoop, B. Bradlyn, and B. A. Bernevig, “Strong and fragile topological dirac semimetals with higher-order fermi arcs,” *Nature communications* **11**, 1–13 (2020).
 - [49] R.-X. Zhang, F. Wu, and S. Das Sarma, “Möbius insulator and higher-order topology in $\text{mnbi}_{2n}\text{te}_{3n+1}$,” *Phys. Rev. Lett.* **124**, 136407 (2020).
 - [50] T. Oka and H. Aoki, “Photovoltaic hall effect in graphene,” *Phys. Rev. B* **79**, 081406 (2009).
 - [51] T. Kitagawa, E. Berg, M. Rudner, and E. Demler, “Topological characterization of periodically driven quantum systems,” *Phys. Rev. B* **82**, 235114 (2010).
 - [52] N. H. Lindner, G. Refael, and V. Galitski, “Floquet topological insulator in semiconductor quantum wells,” *Nature Physics* **7**, 490–495 (2011).
 - [53] L. Jiang, T. Kitagawa, J. Alicea, A. R. Akhmerov, D. Pekker, G. Refael, J. I. Cirac, E. Demler, M. D. Lukin, and P. Zoller, “Majorana fermions in equilibrium and in driven cold-atom quantum wires,” *Phys. Rev. Lett.* **106**, 220402 (2011).
 - [54] J. Cayssol, B. Dóra, F. Simon, and R. Moessner, “Floquet topological insulators,” *physica status solidi (RRL)–Rapid Research Letters* **7**, 101–108 (2013).
 - [55] M. C. Rechtsman, J. M. Zeuner, Y. Plotnik, Y. Lumer, D. Podolsky, F. Dreisow, S. Nolte, M. Segev, and A. Szameit, “Photonic floquet topological insulators,” *Nature* **496**, 196–200 (2013).
 - [56] Y. H. Wang, H. Steinberg, P. Jarillo-Herrero, and N. Gedik, “Observation of floquet-bloch states on the surface of a topological insulator,” *Science* **342**, 453–457 (2013).
 - [57] G. Usaj, P. M. Perez-Piskunow, L. E. F. Foa Torres, and C. A. Balseiro, “Irradiated graphene as a tunable floquet topological insulator,” *Phys. Rev. B* **90**, 115423 (2014).
 - [58] T. Oka and S. Kitamura, “Floquet engineering of quantum materials,” *Annual Review of Condensed Matter Physics* **10**, 387–408 (2019).
 - [59] M. Nakagawa, R.-J. Slager, S. Higashikawa, and T. Oka, “Wannier representation of floquet topological states,” *Phys. Rev. B* **101**, 075108 (2020).
 - [60] F. Harper, R. Roy, M. S. Rudner, and S. Sondhi, “Topology and broken symmetry in floquet systems,” *Annual Review of Condensed Matter Physics* **11**, 345–368 (2020).
 - [61] R.-X. Zhang and Z.-C. Yang, “Tunable fragile topology in floquet systems,” [arXiv preprint arXiv:2005.08970](#) (2020).
 - [62] M. S. Rudner, N. H. Lindner, E. Berg, and M. Levin, “Anomalous edge states and the bulk-edge correspondence for periodically driven two-dimensional systems,” *Phys. Rev. X* **3**, 031005 (2013).
 - [63] R. Roy and F. Harper, “Periodic table for floquet topological insulators,” *Phys. Rev. B* **96**, 155118 (2017).
 - [64] S. Yao, Z. Yan, and Z. Wang, “Topological invariants of floquet systems: General formulation, special properties, and floquet topological defects,” *Phys. Rev. B* **96**, 195303 (2017).
 - [65] Y. Peng and G. Refael, “Floquet second-order topological insulators from nonsymmorphic space-time symmetries,” *Phys. Rev. Lett.* **123**, 016806 (2019).
 - [66] M. Rodriguez-Vega, A. Kumar, and B. Seradjeh, “Higher-order floquet topological phases with corner and bulk bound states,” *Phys. Rev. B* **100**, 085138 (2019).
 - [67] S. Chaudhary, A. Haim, Y. Peng, and G. Refael, “Phonon-induced floquet second-order topological phases protected by space-time symmetries,” [arXiv preprint arXiv:1911.07892](#) (2019).
 - [68] Y. Peng, “Floquet higher-order topological insulators and superconductors with space-time symmetries,” *Phys. Rev. Research* **2**, 013124 (2020).
 - [69] R. W. Bomantara and J. Gong, “Measurement-only quantum computation with floquet majorana corner modes,” *Phys. Rev. B* **101**, 085401 (2020).
 - [70] B. Huang and W. V. Liu, “Floquet higher-order topological insulators with anomalous dynamical polarization,” *Phys. Rev. Lett.* **124**, 216601 (2020).
 - [71] R. W. Bomantara, L. Zhou, J. Pan, and J. Gong, “Coupled-wire construction of static and floquet second-order topological insulators,” *Phys. Rev. B* **99**, 045441 (2019).
 - [72] R. Seshadri, A. Dutta, and D. Sen, “Generating a second-order topological insulator with multiple corner states by periodic driving,” *Phys. Rev. B* **100**, 115403 (2019).
 - [73] K. Plekhanov, M. Thakurathi, D. Loss, and J. Klinovaja, “Floquet second-order topological superconductor driven via ferromagnetic resonance,” *Phys. Rev. Research* **1**, 032013 (2019).
 - [74] W. Zhu, Y. Chong, and J. Gong, “Floquet higher order topological insulator in a periodically driven bipartite lattice,” [arXiv preprint arXiv:2010.03879](#) (2020).
 - [75] M. Fruchart, “Complex classes of periodically driven topological lattice systems,” *Phys. Rev. B* **93**, 115429 (2016).
 - [76] X. Liu, F. Harper, and R. Roy, “Chiral flow in one-dimensional floquet topological insulators,” *Phys. Rev. B* **98**, 165116 (2018).
 - [77] F. Nathan and M. S. Rudner, “Topological singularities and the general classification of floquet–bloch systems,” *New Journal of Physics* **17**, 125014 (2015).
 - [78] R.-X. Zhang and C.-X. Liu, “Topological invariants for three dimensional dirac semimetals and four dimensional topological rotational insulators,” [arXiv preprint arXiv:1605.04451](#) (2016).
 - [79] H. Song, S.-J. Huang, L. Fu, and M. Hermele, “Topological phases protected by point group symmetry,” *Phys.*

- [Rev. X **7**, 011020 \(2017\).](#)
- [80] H. Isobe and L. Fu, “Theory of interacting topological crystalline insulators,” [Phys. Rev. B **92**, 081304 \(2015\).](#)
 - [81] W. P. Su, J. R. Schrieffer, and A. J. Heeger, “Solitons in polyacetylene,” [Phys. Rev. Lett. **42**, 1698–1701 \(1979\).](#)
 - [82] W. P. Su, J. R. Schrieffer, and A. J. Heeger, “Soliton excitations in polyacetylene,” [Phys. Rev. B **22**, 2099–2111 \(1980\).](#)
 - [83] K. Wintersperger, C. Braun, F. N. Ünal, A. Eckardt, M. D. Liberto, N. Goldman, I. Bloch, and M. Aidelsburger, “Realization of an anomalous floquet topological system with ultracold atoms,” [Nature Physics **16**, 1058–1063 \(2020\).](#)
 - [84] S. Mukherjee, A. Spracklen, M. Valiente, E. Andersson, P. Öhberg, N. Goldman, and R. R. Thomson, “Experimental observation of anomalous topological edge modes in a slowly driven photonic lattice,” [Nature communications **8**, 1–7 \(2017\).](#)
 - [85] L. J. Maczewsky, J. M. Zeuner, S. Nolte, and A. Szameit, “Observation of photonic anomalous floquet topological insulators,” [Nature communications **8**, 1–7 \(2017\).](#)
 - [86] S. Mukherjee, H. K. Chandrasekharan, P. Öhberg, N. Goldman, and R. R. Thomson, “State-recycling and time-resolved imaging in topological photonic lattices,” [Nature communications **9**, 1–6 \(2018\).](#)
 - [87] S. Mukherjee and M. C. Rechtsman, “Observation of floquet solitons in a topological bandgap,” [Science **368**, 856–859 \(2020\).](#)
 - [88] S. Afzal, T. J. Zimmerling, Y. Ren, D. Perron, and V. Van, “Realization of anomalous floquet insulators in strongly coupled nanophotonic lattices,” [Phys. Rev. Lett. **124**, 253601 \(2020\).](#)
 - [89] Y.-G. Peng, C.-Z. Qin, D.-G. Zhao, Y.-X. Shen, X.-Y. Xu, M. Bao, H. Jia, and X.-F. Zhu, “Experimental demonstration of anomalous floquet topological insulator for sound,” [Nature communications **7**, 1–8 \(2016\).](#)
 - [90] Q. Cheng, Y. Pan, H. Wang, C. Zhang, D. Yu, A. Gover, H. Zhang, T. Li, L. Zhou, and S. Zhu, “Observation of anomalous π modes in photonic floquet engineering,” [Phys. Rev. Lett. **122**, 173901 \(2019\).](#)
 - [91] D. Vu, R.-X. Zhang, Z.-C. Yang, and S. Das Sarma, in preparation.
 - [92] T. Morimoto, H. C. Po, and A. Vishwanath, “Floquet topological phases protected by time glide symmetry,” [Phys. Rev. B **95**, 195155 \(2017\).](#)
 - [93] J. Yu, R.-X. Zhang, and Z.-D. Song, in preparation.
 - [94] X.-L. Qi, T. L. Hughes, and S.-C. Zhang, “Topological field theory of time-reversal invariant insulators,” [Phys. Rev. B **78**, 195424 \(2008\).](#)